A 5G Communication System based on Flexible Spectrum Technology for the SKA

R.S. KAREMBERA

2022

A 5G Communication System based on Flexible Spectrum Technology for the SKA

By

Reinhard Siwombe Karembera

Submitted in fulfilment of the requirements for the degree

of

Philosophiae Doctor

To be awarded at the Nelson Mandela University

April 2022

Promoter

Prof. Timothy Gibbon

Co-Promoter

Dr. Shukree Wassin

NELSON MANDELA UNIVERSITY

PERMISSION TO SUBMIT FINAL COPIES

OF TREATISE/DISSERTATION/THESIS TO THE EXAMINATION OFFICE

Please type or complete in black ink

FACULTY: Science

SCHOOL/DEPARTMENT: Physics

I, (surname and initials of supervisor) Prof Tim Gibbon

and (surname and initials of co-supervisor) Dr Shukree Wassin

the supervisor and co-supervisor respectively for (surname and initials of candidate) Karembera, R

(student number) s221376593 a candidate for the (full description of qualification) PhD in Physics

with a treatise/dissertation/thesis entitled (full title of treatise/dissertation/thesis):

A 5G Communication System based on Flexible Spectrum Technology for the SKA

It is hereby certified that the proposed amendments to the treatise/dissertation/thesis have been effected and that **permission is granted to the candidate to submit** the final copies of his/her treatise/dissertation/thesis to the examination office.

T Sibbon — 16 March 2022

SUPERVISOR **DATE**

And

pp T Sibbon — 16 March 2022

CO-SUPERVISOR **DATE**

Declaration

I, *Reinhard Siwombe Karembera*, student number *221376593*, hereby declare that the above *treatise/ dissertation/ thesis* for *PhD Physics* is my own work and that it has not previously been submitted for assessment or completion of any postgraduate qualification to another University or for another qualification.

…….

Reinhard Siwombe Karembera

Dedication

This PhD thesis is dedicated to my family.

Acknowledgement

I would like to give my sincere thanks to my heavenly father Jehovah God for empowering me with the “power beyond normal” to be able to complete this work. Without Jehovah, I probably would have not been able to submit this thesis on time.

Secondly, to my supervisor Professor Timothy Gibbon. Prof., you have been very helpful throughout my PhD course. You did not only become my supervisor, but you became a brother, a motivator, and a Samaritan that looked out for me both academically and physically. Thank you, Prof., and may your good spirit continue to empower and motivate those whom your life will come across.

To my family – my wife and my son. You were the reason I worked so hard to come to this stage. Every time I thought of you, I had the reason to push myself to conduct an experiment, write a paper, and make a publication. Your existence in my life gave me a purpose to work hard.

To my lab mates, you really motivated me to work hard. Each and every one of you motivated me to be a better person in my research. George Isoe, I remember when you suggested me to look into numerical analysis and modelling. Those suggestions gave birth to numerous publications which brought me to this point of writing my thesis. Thank you so much, George. To Ketshabile Nfanyana, you have no idea how much you motivated and inspired me. Your enthusiasm helped me to become and a go-getter. Thank you so much Ketshabile. I wish you all the best in your future endeavors. To Shukree Wassin, you left us with good knowledge of the lab equipment, and you were always ready to help me carry out my experiments. I am very grateful, and I wish you all the best. Mr. James Jena. We became spiritual brothers during our last year. Our discussion was always very encouraging and motivating. Throughout my research you stood by me, and you gave me brotherly support. I remember most times; you had to leave your own work and pay attention to my work. I am very grateful. I wish you all the best as you progress in your life journey.

To Nelson Mandela University, and especially the physics department, I am very thankful for giving me the opportunity to do my PhD with you. SARAO, your financial support made this study possible. I will always be grateful for your support.

Finally, I would like to extend my appreciation to everyone -- my spiritual brothers, friends, and family for constantly looking out for me and encouraging me to work hard to realize this milestone.

List of figures

Table of contents

Abstract

Radio astronomy research is rapidly expanding across the African continent. At the same time, the fifth generation (5G) of mobile communication systems are also being researched and developed. Throughout history, mobile communication networks are known to affect the activities of radio astronomy. If not carefully managed, radio frequencies from mobile communication devices can severely affect radio astronomy observations. To that end, many techniques have been proposed to protect the radio astronomer from RFIs coming from radio communication networks.

Some of the proposed techniques such as RFI quite zones and spectrum assignment by regulatory authorities will not be convenient during the implementation of 5G mobile networks. This is because 5G radio communication systems are expected to support spectrum-hungry application such as video-on-demand, augmented realities, high-definition television and so on. To realize this, the 5G networks will be forced to have access to protected radio spectrum, including those at which radio astronomy activities are being researched. To facilitate this, the 5G radio communication networks should have the intelligence to coexist within such protected spectrums without the consequences of radio frequency interferences (RFI) to the primary user.

In this thesis, we present novel 5G networks with the intelligence that allow them to coexist within radio astronomy areas without introducing RFIs to the primary user. We proposed a photonic solution, keeping in mind the characteristic requirements for future 5G radio communication networks.

The thesis begins by reviewing the current trend of radio astronomy research in Africa. It was found that radio astronomy research in Africa is growing rapidly. Many African countries such as South Africa and Ghana are at advanced stages when it comes to radio astronomy research. Therefore, the finding and proposal of this thesis will be valuable to such countries.

In order to develop a radio access network (RAN) that can coexist within radio astronomy areas, the thesis reviewed past and present state-of-the-art RANs. Each access network was analyses for its feasibility to be implemented within radio astronomy areas to realize mobile communication without the consequences of RFIs to the astronomer. It was motivated that the current centralized radio access network (C-RAN) the best solution to be developed for radio communication within radio astronomy areas. This is because the C-RAN architecture is centralized by pooling network resources to a common point. From such pool, network resources can be controlled and shared among 5G network user, including radio astronomers and the surrounding communities.

The next chapters reviewed photonic RF transmitters and their associated lasers currently being proposed to be used within C-RANs. The review showed that photonic RF transmitters based on optical heterodyning of two independent laser and those using optical frequency combs are feasible and attractive to be used within radio astronomy areas to realize radio communications services. This is due to their simplicity and flexibility, both in their designed and the generation of RF carrier signals. In the same review, it was found that vertical cavity surface emitting lasers (VCSELs) will offer the possibility of realizing simple and cost-effective C-RANs within radio astronomy areas.

In the experiment of chapter 5, we investigated the transmission characteristics of a photonic RF transmitter based on optical heterodyning of two independent VCSELs. It was reported that VCSELs are able to provide high data rates to astronomical users by adopting high-level pulse amplitude modulation (PAM) formats. In our demonstration, we transmitted 17 Gbps 4-pulse amplitude modulation (PAM-4) data over 24 km of optical fiber. These results highlighted the potential of adopting VCSEL-based heterodyning to realize advanced 5G radio services within radio astronomy. According to our knowledge, this was the first time that this cost-effective and high-bandwidth 5G C-RAN was reported.

In the same chapter 5, we investigated the transmission performance of a VCSEL-based optical frequency comb as the photonic RF transmitter for 5G C-RANs within radio astronomy areas. The VCSEL was gain switched with an electrical signal to generate the needed optical comb. More than 10 coherent comb lines were obtained using such a low-power optical device. From the generated comb, up to 16 Gbps of binary data were transmitted across a photonically-generated radio carrier frequency of 56 GHz. Bit error rates of 10^{-9} were recoded after 20.5 km standard single mode fiber with optical powers below -15 dBm. These results gave guidelines toward a future were low-cost VCSELs can be used to realize coherent and high data rate 5G networks within radio astronomy areas.

Many proposed techniques use complex configuration to realize flat optical frequency combs for 5G radio communication. The reasons and motivations for using such complicated architectures is not yet validated. Chapter 6 of this thesis reports on novel results suggesting that low-cost non-flat optical frequency combs can find application in 5G radio networks to achieve similar performance as those using complicated flat optical comb generators. It was found that no-flat optical frequency combs reduce the 5G network cost by using low-loss optical modulator while enhancing the quality of serves to both wireless and the fixed users. By carefully controlling the power ratio between two optical lines form a non-flat frequency comb, the 5G network could support both fixed and wireless user with error-free data.

The generated optical frequency comb of chapter 5 was used in chapter 7 to demonstrated novel and exciting results. In the current radio astronomy areas, both the observed data and the reference clock signals for telescope synchronization are transmitted over optical fibers using independent lasers. In our numerical demonstration of chapter 7, we used a single VCSEL to transmit both data and reference clock signals for radio astronomy applications. The reported configuration is attractive as it reduces the management of independent laser sources. It also reduces the cost of purchasing individual lasers for each network transmission scenario.

Chapter 8 of this thesis numerically demonstrated a novel fixed-wireless 5G C-RAN. The optical comb of chapter 5 was also used in chapter 8 to realize the fixed-wireless 5G radio communication network. The technique of frequency reuse was used for optimal uses of the local oscillator power. The optical local oscillator signal was used for downlink, uplink, and for photonic up-conversion to RF carriers. To our knowledge, it was for the first time this type of network was demonstrated. In both case, the network was able to deliver error-free data to the intended users. This network will be attractive for application within radio astronomy areas as both fixed and wireless users seek to connect to the internet without any threat of RFI to the observing telescopes.

While chapters 5, 6, 7, and 8 demonstrated the feasibility of photonic 5G C-RANs to support the radio astronomer with advanced communication services, their ability to mitigate RFI was not shown even though comments were made to highlight how such networks will avoid interferences. In chapter 9 of this thesis, we have reported a novel 5G networks where the RFI effects are mitigated as soon as they are detected. The network adopted the optical heterodyning scheme as the photonic transmitter. The system was shown to maneuver across the assigned spectrum to avoid any frequency collision with the primary user. The systems response was measured to be around 3 microseconds. This result, together with the data transmission results reported in the previous chapters, showed that radio communication services can coexist with radio astronomy without the consequences of RFIs, thanks to the flexibility associated with the photonic generation of RF carrier signals.

List of acronyms

RFI – Radio Frequency Interference

ELT – Extremely Larger Telescope

FBG – Fiber Bragg Grating

SKA – Square Kilometer Array

5G – Fifth Generation

VCSEL – Vertical Cavity Surface Emitting Laser

WDM – Wavelength Division Multiplexing

PAM-4 – 4 Level Pulse Amplitude Modulation

16-QAM – 16 Quadrature Amplitude Modulation

VLBI – Very Long Baseline Interferometry

SKA-SA – Square Kilometer Array South Africa

ITU-R – International Telecommunication Union

IF – Intermediate Frequency

RAN – Radio Access Network

GPRS – General Packet Radio Services

UMTS - The Universal Mobile Telecommunications System (UMTS)

LTE – Long Term Evolution

PSTN – Public Switched Telephone Network

UTRAN - UMTS Terrestrial Radio Access Network

QoS – Quality of Service

RNC – Radio Network Controller

BS(s) – Base Station(s)

WCDMA - Wideband Code Division Multiple Access

RRM – Radio Resource Management

CNs – Core Networks

WIMAX – Worldwide Interoperability for Microwave Access

GSM – Global System for Mobile Communications

HSPA – High Speed Packet Access

IEEE – Institute for Electrical and Electronic Engineers

SNR – Signal to Noise Ratio

E-UTRAN – Evolved UMTS Terrestrial Radio Access Network

BSS – Base Station Subsystem

MIMO – Multiple Input Multiple Output

RATs – Radio Access Terminals

D-RAN – Distributed Radio Access Network

RRH – Remote Radio Head

BBU – Baseband Unit

DU – Data Unit

C-RAN – Cloud Radio Access Network

CAPEX – Capital Expenses

OPEX – Operational Expenses

MNO – Mobile Network Operator

CD-RAN – Centralized Distributed Radio Access Network

eMBB – Enhance Mobile Broadband

DSP – Digital Signal Processing

DFB – Distributed Feedback

TEC – Thermoelectric Cooler

CW – Continuous Wave

CWL – Continuous Wave Laser

LD – Laser Diode

LDC – Laser Diode Controller

RHD – Remote Heterodyning Detection

OFDM – Orthogonal Frequency Division Multiplexing

SMF – Single Mode Fiber

SSMF – Standard Single Mode Fiber

OOK – On-Off Keying

DML – Dual Mode Laser

MZM – Mach Zehnder Modulator

PD – Photodiode

BER – Bit Error Rate

NZ-DSF – Non-Zero Dispersion Shifted Fiber

OFC – Optical Frequency Comb

PPG – Pulse Pattern Generator

BERT – Bit Error Rate Tester

WSS – Wavelength Selective Switch

B2B – Back-to-Back

LPF – Low Pass Filter

VOA – Variable Optical Attenuator

EDFA – Erbium Doped Fiber Amplifier

EVM – Error Vector Magnitude

REC – Radio Equipment Controller

RNC – Radio Network Controller

Chapter 1: Introduction

The subject of photonics is well-understood by researchers to be a key enabling technology for overcoming the limitations imposed by its electronic counterpart. Photonics is defined as 'The technology of generating and harnessing light and other forms of radiant energy whose quantum unit is the photon.' [1]. This is realized through light generation, detection, manipulation, processing, and amplification, if necessary. Photonics finds application in areas such as communication systems, radar systems, radio astronomy (Astrophotonics), optical spectroscopy, medical, and computing to name but a few. Even though photonics covers a wide range of technical applications over the whole spectrum, most applications are in the range of visible and near-infrared light. This thesis is focused on the application of photonics in radio astronomy within the 1550nm wavelength region.

1.1 Astrophotonics – application of photonics in radio astronomy

Astrophotonics bridges the subject of astronomy and photonics. It is defined simply as the application of photonics to astronomical instrumentation [2]. The field of Astrophotonics has emerged over the past decade in order to address the ever-increasing demand with astronomical research. Early years have seen a successful application of photonics in astronomy. Worth-mentioning include but not limited to: (i) photonic waveguides to combine signals from widely spaced telescopes in stellar interferometry [3], (ii) frequency combs for ultra-high precision spectroscopy to detect planets around nearby stars (dual-comb spectroscopy) [4], (iii) ultra-broadband fiber Bragg gratings (FBG) to suppress unwanted background noise, (iv) photonic lanterns that allow single-mode behaviour within a multimode fiber, (v) planar waveguides to miniaturize astronomical spectrographs [5], (vi) large mode area fibers to generate artificial stars in the upper atmosphere for adaptive optics correction, and (vii) liquid crystal polymers in optical vortex chronographs and adaptive optics systems. Astrophotonics, a field that has already created new photonics capabilities, is now extending its reach down to the Rayleigh scattering limit at ultraviolet wavelengths, and out to mid infrared wavelengths beyond 2500nm. We review some state-of-the-art applications of Astrophotonics in the following paragraphs.

Several fiber channels are installed on existing facilities and provide routine astronomical observations. The attenuation due to the propagation through the fibers is negligible when compared to the transmitted optical signal. The flexibility of optical fibers has enabled a set of existing telescopes to be integrated into an interferometric [6]. This flexibility also allows more advanced optical dissemination of data and clock signals to the telescopes [7].

For extremely large telescopes (ELT) to attain their full diffraction limit, the distortion induced by the turbulent atmosphere should be corrected. Adaptive optics has now been demonstrated successfully on existing telescopes and is already integrated into the design of ELTs [8]. This change in telescope flexibility is expected to provide a major gain in sensitivity. It will also lead to greatly improved coupling of photonic devices at the telescope core point.

Review on recent developments in Astrophotonics open the doors to many possible adaptations of photonics to assist with the issue of radio frequency interference. Adaptive photonics can be used not only to correct for the distortion cause by external turbulences, but also to realize full co-existence of these turbulence within the observation spectrum. Coexistence will accelerate the realization of communication systems within radio astronomical areas. The restriction of mobile services in radio astronomy borders is a subject of great concern especially now that mobile service has become an integral part of every

astronomer. This can be addressed by Astrophotonics. This thesis will act as a guideline toward that exciting future.

1.2 The outline of the thesis

Before developing systems for radio astronomy application, it is important to analyze and get an understanding of Africa's current interest in radio astronomy. Chapter 2 will briefly discuss radio astronomy in Africa. Special emphasis will be given to the background and relevance of radio astronomy in Africa. There has been a great interest in radio astronomy within the African continent. South Africa is one of the African countries that embraced the field of radio astronomy and it continues to do so. The Square Kilometer Array (SKA) telescope currently under operation in South Africa is evidence of the nation's interest in the field. In section 2.1.2, we will briefly introduce and discuss the SKA South Africa (SKA-SA) project. Like any other big scale scientific projects, the SKA-SA project has brough about both positive and negative developments. The economy of people, especially those within the identified observation areas have seen good economic developments. At the same time, measure was to be taken to mitigate radio frequency interference to telescope observations. These could be caused by mobile services providers and mobile users within these areas. As a result, mobile service in these areas is limited, affecting the indigenous farmers and the local community.

In the last section of chapter 2, we will review the existing RFI mitigation techniques proposed by different literatures. The section highlights a need to introduce innovative solutions to avoid RFI distortions. In this thesis, we propose a novel solution to realize mobile communication services within radio astronomy areas. This proposed solution brings radio communication services within astronomical facilities without the effects of RFI. The proposed solution is photonic and innovative. In the experimental chapters, we will demonstrate our own novel photonic solution for RFI mitigations. This can ultimately relax the mobile communication restriction currently imposed on radio astronomy communities.

In chapter 3, the thesis reviews the history of radio communication systems. The review will cover from the third generation (3G) of mobile communication networks to the currently-researched fifth generation (5G) radio communication systems. This review is necessary to identify and address some of the challenges which made it difficult to combine radio astronomy and mobile communication systems. The review will also assist with identifying a radio access network architecture of the communication system which offers the best possibility of getting integrated within astronomical areas without the effects for RFIs.

Based on convincing evidence presented in chapter 3, the thesis identified and proposed a 5G communication system with its radio access architecture as the best solution to be intergraded within radio astronomy areas. A 5G communication systems is based on the application of photonic RF transmitters to realize high RF carriers to support high data rate transmission. Chapter 4 will review some of the laser technologies used to design photonic RF transmitters, the basic subsystem of a radio access network (RAN). This review is necessary to identify suitable lasers that can be used to design our proposed photonic solution to realize mobile services while radio astronomy while mitigating RFI. Discussion will be focused on edge emitting continuous lasers such as distributed feedback laser (DFB) and other lasers such as fiber lasers and dual-mode laser as they continue to find applications in 5G radio communication systems. Chapter 4 also identifies the recently-developed vertical cavity surface emitting lasers (VCSELs) as ideal optical source to be used in mobile commutation systems, especially those requiring low-cost photonic RF transmitters with improved power

efficiency. Chapters 5-9 are experimental chapters, where the implementation and results of our proposed VCSEL-based 5G radio communication systems are presented and discussed. In section 4.2, we will review the proposed design techniques to realize photonic RF transmitters using the lasers reviewed in section 4.1. This review will prove useful as we present and demonstrate our proposed photonic RF transmitter design that offers the possibility of being adopted within radio astronomy areas.

Most reported works on the application of microwave photonics for 5G radio communication uses high-power semiconductor lasers such as distributed semiconductor or fiber lasers. These lasers are power-hungry and bulky to be used in future 5G systems requiring system integration. In Chapter 5, we will experimentally demonstrate the application of VCSELs in 5G radio communication systems. The first demonstration involves a novel application of independent low-power VCSELs for optical heterodyning to generate high-frequency RF signals for application in 5G networks. In the same chapter, we will also demonstrate a novel 5G radio communication system using a VCSEL-based optical frequency comb as the photonic RF transmitter.

In chapter 6, the thesis will experimentally-demonstrate and discuss important results about the effects of optical local oscillator power in VCSEL-based optical comb on the generated RF carrier signal and on the transmitted baseband information. The effects are analyzed using bit error rates (BERs) of the baseband signal and RF power analysis for the wireless signal. The findings of this chapter clarify the general theory where flat optical frequency combs are believed to necessary for application in 5G radio communication systems.

Chapter 7 numerically-demonstrate a VCSEL-based optical frequency comb for application in wavelength division multiplexing (WDM) 5G radio communication systems. The chapter demonstrate the unreported capabilities of a VCSEL-based optical frequency comb for application in WDM-based 5G radio communication systems where both clock and data signals are transmitted simultaneously. The results of the chapter will also be useful for designing economical optical networks in radio astronomy where both reference clock and astronomical data are transmitted simultaneously through optical fibers. Current systems use different lasers to achieve this. In our proposed solution, a novel technique is demonstrated using a single low-cost VCSEL carrier.

Multilevel modulation formats are important to maximize the spectral efficiency of the network. In chapter 8, we will demonstrate a VCSEL-based 5G radio communication network where multilevel modulation formats are used to achieved improved spectral efficiency. This will be demonstrated by using 4 pulse amplitude modulation (PAM-4) and 16 quadrature-amplitude modulation (16-QAM) modulation formats.

Chapter 9 will experimental demonstrate a novel and intelligent 5G radio communication system to be used within radio astronomy areas without introducing RFI. The emphasis is on the application of photonic RF transmitters, regardless of the type of lasers used, to realize a flexible 5G radio communication systems with RFI mitigation capability in astronomical areas. Chapter 10 will summarize and give concluding remarks.

Chapter 2: Radio Astronomy

Radio astronomy is the study of celestial objects emitting at radio frequencies. Radio astronomy uses either single telescope or several telescopes that are linked together and utilizes the techniques of radio interferometry [9]. The field of radio astronomy have observed radiation coming from the Milky Way. Subsequent observations have identified several different sources of radio emission. These include stars and galaxies, as well as entirely new classes of objects, such as radio galaxies, quasars, pulsars, and masers. The discovery of the cosmic microwave background radiation, regarded as evidence for the Big Bang theory, was made through radio astronomy. Therefore, radio astronomy is a field of science that explores the universe to have a good understanding of the space. Like any other scientific research, radio astronomy comes with its own challenges. The most common problem to radio astronomy is RFI due to radio emitting devices such as mobile cellular units. To continue the exploration and the discovery of the hidden treasures of the universe through radio astronomy, the RFI challenge associated with this field needs to be addressed using innovative techniques. This thesis present one of such innovative solutions. The use of the interferometry technique allows radio astronomers to achieve high resolution images. At the same time, this increases the base line and consequently makes the telescope prone to RFI.

2.1 Radio astronomy in Africa

Africa, like any other continents, have embraced the subject of astronomy at radio frequencies. In the next section, we highlight some of the African countries that have welcomed the field of radio astronomy. In the same discussion, we will list some note-worthy astronomical research projects pursued by each of these countries. In section 2.1.2, we will take a closer look at the SKA South Africa (SKA-SA), an exciting astronomical research project that South Africa as country has embarked on.

2.1.1 African countries undertaking astronomy research

South Africa is one country that has embrace the study of the universe through radio astronomy. This is evident when looking at the number of radio astronomy research facilities available in the country. The Hartebeesthoek Radio Astronomy Observatory (HartRAO) is one of South Africa's oldest radio astronomy facility, and it is estimated to be about 30 years old [10]. The country continues to make developments in radio astronomy related facilities with its current seven-dish MeerKAT precursor array (KAT-7) [11]. The 64-dish MeerKAT, part of the large SKA, is another exciting radio astronomy research facility in south Africa. Together with SKA, it will be used for transformational radio astronomy research. The baseline and the square size of this telescope is large. This ultimately means exposing this large array of telescopes to a vast majority of RFIs. The effect due to RFI becomes a serious concern. Therefore, the SKA telescope at large is of most interest as far as this thesis is concern. In south Africa for example, an enlarged area of approximately 135 000 ha was obtained [12]. It is understood that this area will be declared a protected area in order to mitigate the negative effects due to RFI. We seek to replicate these efforts by designing and establishing novel photonic 5G communication solutions that can coexist within the SKA telescope array without introducing any further RFI effects. Additionally, in the Karoo region, the Hydrogen Intensity and Real Time Analysis eXperiment (HIRAX) telescope will be established, co-existing with the SKA-SA site. This project is expected to have an important synergy with the 64-dish MeerKAT, thus experiencing the same type of RFI [13].

Ghana is another example of an African partner country to the SKA. The country has been

mentored by South Africa over the past six years and will soon emerge as a leading partner in the field of radio astronomy. Ghana is expected to have a science-quality 32m dish converted from a redundant satellite communication antenna to a radio astronomy research facility. Initially, it will be fitted with 5 GHz and 6.7 GHz receivers to be followed later by a 1.4-1.7 GHz receiver [14]. We notice that these are the same frequencies proposed for 4G and 5G communication systems [15]. This means that the radio telescope is expected to face serious RFI from 5G radio communication services if novel RFI mitigation solutions are not implemented. The telescope is being designed for use as a single dish observatory and for participation in the developing African Very Long Baseline Interferometry (VLBI) Network (AVN) and the European VLBI Network. Ghana is expected to host a remote station during a possible SKA Phase 2. The location of the country on 5 degree north of the Equator gives it the distinct advantage of viewing the entire plane of the Milky Way galaxy and nearly the whole sky. Evidently, the RFI effect due radio communication is expected to expand and will affect any partner country to the SKA. The novel RFI mitigations solutions presented by this thesis will thus benefit countries such as Ghana.

In 1992, Mauritius also appeared on the scene with its meter-wave Fourier Synthesis T-shaped array, the Mauritius Radio Telescope (MRT) [16]. The radio telescope was designed to study the southern sky for point sources at 151.6 MHz in the declination of -70° to -10° and sensitivity of 200mJy [16]. The MRT survey produced a southern sky equivalent of the Sixth Cambridge Catalog (6C) of bright radio sources [17].

Different aspects have contributed to the accelerated development of radio astronomy in Africa. For example, more efficient and cheaper undersea fiber optic cables for telecommunication signal transport are already submerged in the Indian and Atlantic Ocean of the African continent. The KAT-7 [18] and the recent 64-dish MeerKAT all became successful astronomical projects. Due to all these factors, and with the decision that Africa would host a large part of the SKA, many redundant satellite communication antennas were converted to assets for radio astronomy research. Ghana has such an asset converted to radio astronomy observatory as can be seen in figure 2.1b below [19]. This was a redundant satellite communication antenna at its Kuntunse Intelsat Satellite Communication Earth Station.

In the mid-2000's, Botswana, Ghana, Kenya, Madagascar, Mauritius, Mozambique, Namibia, and Zambia were all invited to partner with South Africa in its bid to host the SKA. This produced new motivation for countries on the continent to accelerate their efforts in embracing radio astronomy studies and research.

Figure 2.1a shows SKA's footprint across Africa, showing how the continent is accelerating the study of radio astronomy research. Therefore, parallel research needs to be taken to support such developments by providing innovative solutions to potential challenges expected from such scientific developments. As the majority of the expected RFI will come from radio communication devices, the solution proposed in this thesis will facilitated a significant reduction in RFI to radio astronomers across the African continent. It will also give the regulation authorities across the African continent, the opportunity to embrace a full utilization of the already-scarce spectrum resource.

2.1.2 The SKA-SA telescope array – The South African component of the SKA

The SKA will be one of the telescopes probing the entire electromagnetic spectrum ranging from radio to gamma-rays and even beyond. It will be studying subterrestrial spectrums such as gravitational waves, cosmic rays, and neutrinos. The SKA project will be a radio telescope

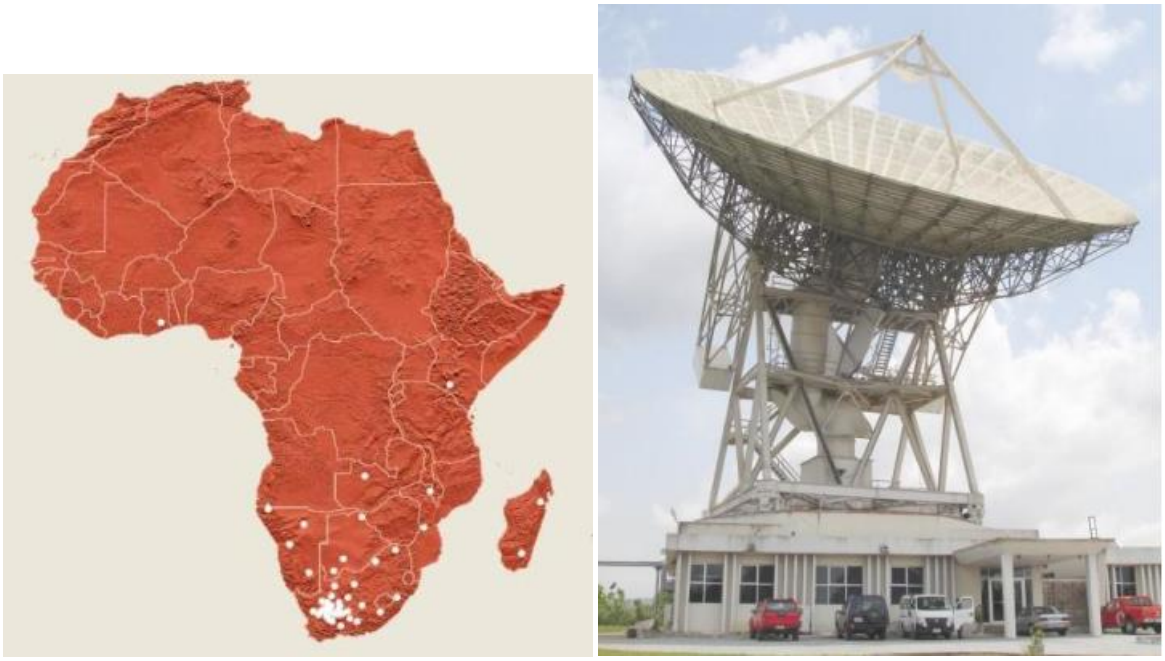

(a) **(b)**

Figure 2.1 SKA footprint across Africa (a) [20] and The Ghana's Kuntunse 32m converted telecommunication antenna (b) [19].

with an apertures above 1000 square meters [21]. With such a large aperture size, this telescope will be subjected to millions of people connected to different types of radio networks. As a result, it will have to deal with great RFI from people across the globe. The project was formulated from the very beginning by a team of international bodies, institution, and astronomers. After a thorough process, two sites, one in the Karoo region of central South Africa and the other in the state of Western Australia, were identified as suitable for most of the SKA's intended wavelength range. Fifteen funding agencies now regularly discuss SKA development and funding options [22]. The project timeline has the telescope operational below 10 GHz by 2022. Although the precise range of wavelengths has not yet been determined, the SKA will eventually produce images and other data over wavelengths from ~4.3 m (70 MHz) to ~1 cm (30 GHz) [23], the same frequency of interest as far as 5G radio communication networks are concern. Innovative solutions are needed to be established to mitigate the anticipated challenges of realizing parallel developments these two important fields of science.

The operational centre for the SKA-SA is being established on two farms that the government bought in the early 2000s. These are namely the KAT-7 that South Africa built as part of its bid to host the SKA and the 64-receptor array known as MeerKAT which is nearing completion [24]. In 2007 the South African parliament passed a legislation to advance and protect areas in which astronomy and related scientific projects of national strategic importance can be undertaken. Any activity which interferes in any other way with astronomy and related scientific project in those areas should be avoided. This includes activities which could cause radio frequency interference (RFI), the major threat to radio astronomy.

One of these issues is evidently RFI due to radio communication services. Regulation have tried to protect a few windows in the radio spectrum, but many applications now need to have

Table 1. Frequency bands which SKA-SA operates in

Bands	Frequency
1	50 – 850 MHz
2	900 – 1670 MHz
3	1750 – 3500 MHz

access to parts of the spectrum within the reserved regions. The SKA spectral domain is given in table 1. Much of the frequency ranges in table 1 are shared with the communications industry, an industry that is critical to the modern society. The key point is therefore the definition of interference from the perspective of both the consumer and the astronomer. What an astronomer considers an interference the consumer considers it as a useful signal. We propose a novel photonic-assisted 5G communication system, aiming to introduce a new mutual definition of the term "interference" to both the astronomer and the radio consumer. Before such a solution is technically demonstrated, we deem it necessary to review some of the existing and proposed RFI mitigation techniques for astronomical areas such as the SKA-SA. It is important to note that the solutions to be review in section 2.2 are those intendent to avoid RFI due radio communication devices, the same RFI that this thesis seeks to address.

2.2 RFI mitigation techniques for astronomical areas such as SKA-SA

Every use of the radio frequency spectrum – broadcast radio and TV, cell phones communication, navigation satellites, as well as all the wireless control and monitoring systems, has the potential to affect radio astronomy observations. Cell phones and satellites communication contribute mostly to the RFIs that affect the astronomer. To that end, different RFI mitigation techniques to protect radio astronomy from cell phones and satellites communication have been proposed in recent years. RFI mitigation is a well-established research topic in other areas [25], but it is relatively recent in radio astronomy. This section presents a review on recent developments in RFI mitigation strategies for the radio astronomer. The review focuses on strong local RFI that is not coherent over the telescope array. This type of RFI plays a damaging role because telescope antennas subject to a local RFI have a high system noise, which ultimately reduces the signal-to-noise ratio of astronomical data. This is likely to be the case in modern telescope arrays like the SKA. The SKA is expected to extend over large baseline distances where the RFI is likely to be local to a subset of the array's antennas or local to just a single antenna within the array.

2.2.1 Proactive Mitigation Strategies

2.2.1.1 Regulations

Proactive strategies provide the best defense of all, keeping the spectrum clean by removing the sources of RFI. One of such strategies is regulation. Through the International Telecommunication Union (ITU-R), the international community has made a great effort to balance the need of the community for wireless communication service with the interest of the radio astronomers through the allocation of reserved spectral bands. The ITU-R Recommendation ITU-R RA-769 [26] outlines the protection criteria and defines the harmful limits. The CRAF Handbook for Radio Astronomy [27] and the ITU Handbook on Radio Astronomy [28] provides a good discussion.

Regulations as an RFI mitigation solution probably offers the easiest way to protect

astronomers from RFI but have some note-worthy disadvantages. The obvious disadvantage is the static assignment of spectrum resource to a single application, avoiding other applications from accessing the same spectrum. In [29], the authors proposed a policy where regulations can put in place a solution which allow astronomers to occupy a certain spectral band for given period of time, leaving the spectrum open to different applications when the observation time has collapsed. Our proposed solution seeks to support this conveniency by allowing mobile radio communication systems have access to the same spectrum resources when the astronomer is not observing at that particular frequency. This remove the inconveniency of static spectrum assignment as it is currently being done by different international regulatory bodies.

2.2.1.2 Radio Quiet Zones

The second proactive strategy is the creation of radio astronomy sites free of any RFI sources. This is made possible through a number of ways. Firstly, natural topographies can be used for protection of astronomical activities against any RFI. For example, the National Radio Astronomy Observatory (NRAO) Green Bank Observatory is in a shielded valley in West Virginia, USA [30]. The Dominion Radio Astrophysical Observatory (DRAO) Penticton observatory is also in a protected valley in British Columbia, Canada [30]. Radio quite zones can also be realized through some national licensing authorities, those who have the power to declare "Radio Quiet Zones" around specific observatories. The South African government has taken similar steps to protect the Karoo region by declaring it a radio quite zone [31]. Australian government has also implemented the same solution to protect the radio astronomy park set up by the state government of Western Australia [32].

The radio quite zone RFI mitigation strategy has several disadvantages. Firstly, to create such radio quiet zones, the existing community have to be migrated far away from the identified sites. This causes many inconveniences as many tend to lose their ancestral land and culture. Secondly, existing radio communication infrastructures have to be removed completely, resulting in a loss of capital, revenue, and employment. Additionally, this strategy can provide no protection from satellite downlinks, nor from airborne radar systems. The solution proposed and presented in this thesis seeks to address these challenges. For example, when a new astronomical site is identified where some communication systems already exist, the radio astronomer can coexist with the existing radio infrastructures as these systems does not offer any RFI threat to the astronomer. The community does not have to move from their lands for reason of having mobile radio devices. Ultimately, the country experiences a true parallel development in both astronomy and telco services.

2.2.1.3 The observatory community

Some authors [33] have pointed out that observatories themselves could be the cause for a significant fraction of RFI. These local RFI sources include modem computers and high-speed electronics within the observatory receiver systems. Solutions to this include eternal vigilance and serious monitoring of all new equipment for sound design and RFI-containment practices [33]. The main control complex could be designed to have extensive RFI shielding. For example, the Karoo Array Processor Building (KAPB) that hosts the storage and computing for the radio instrumentation and the correlator for the KAT-7 and MeerKAT arrays is designed with high RFI-attenuation capabilities [34]. Furthermore, visitors accessing the site could be screen of any potential RF sources within their possession. This is also the case when visiting the Hartebeesthoek of South Africa, the oldest observatory in the country.

Similar to the radio quite zone mitigation strategy, restricting radio devices, especially

mobile cellphones could be a cause for serious inconveniences. This is especially true in this era where astronomers need to have their mobile internet handy for reasons such as personal research and developments. In this thesis, we have proposed a novel photonic solution to mitigate inherent RFI due to mobile radio devices. This thesis seeks to bridge the gap by innovatively designing intelligent radio communication system that does not possess any danger to radio astronomy research. The photonic part of the solution also addresses the natural RFIs due to electronic systems and accelerate the idea of coexistence [35].

2.2.2 Reactive Mitigation Strategies

With these mitigation strategies, the assumption governing the receiver's response is that it is linear. This puts a requirement on the receiver designers to provide adequate reserve against overloading with excessive power that can drive the electronics into nonlinearity [36-38]. When the receiver is driven into nonlinearity, high-order harmonics are generated which can cause serious ambient RFI to the radio astronomer. This will render the design solution ineffective.

2.2.2.1 RFI Blanking in Time or Frequency

Modern digital signal processing makes it possible to perform quite sophisticated blanking. The incoming data stream can be processed in blocks of samples to derive the noise characteristics. The blanking window can also be tailored to remove low-level RFI on bursts of RFI [39-40]. Blanking can be applied in a radio telescope arrays. However, there is a possibility of identifying the RFI that is coherent between antennas. This makes it necessary to refine the process of identifying the RFI. An impressive RFI mitigation tool on the Westerbork Array was described [41]. The effectiveness of this process was achieved by setting the interference-to-noise ratio to an extend where the RFI dominated the system noise. Low-level RFI do not possess a serious issue. In some experiments, it was required that long integrations time was needed in order to detect weak objects. These weak objects only showed up at the end of the setup or the integration time. The post-correlation technique was proposed in [42] to address this long integration time needed to monitor these weak RFIs.

2.2.2.2 The Adaptive Filter

The canonical adaptive filter [43] was introduced to the radio-astronomical community as a powerful tool for removing RFI in 1998. To date the design of the filter has improved. In a recent paper [44], the filter was designed by developing a real-time, digital adaptive filter implemented on a Field Programmable Gate Array (FPGA) capable of processing 4096 spectral channels in a 1 GHz of instantaneous bandwidth. The filter was able to cancel a broad range of interference signals and quickly adapted to changes on the RFI source. This minimized the data loss without any assumption on the astronomical or interfering signal properties. The correction speed was measured to be 208.1 μs for a broadband noise-like RFI signal and 125.5 μs for a multiple-carrier RFI signal. In chapter 9, we developed a RFI mitigation system that adapt to the observing spectrum. The response time was recorded to be approximately 3 μs.

In some cases, it is not avoidable to blank the receiving system when the RFI exceeds a given threshold. The outcome will not be as good as in the RFI-free case. This is because there could be a reduction in signal-to-noise ratio, and possibly a reduction in the imaging fidelity. Other techniques make the science goals achievable. In some of these techniques, this is achieved by designing a system that does not have to rely on the signal-to-noise ratio [45].

2.2.2.3 RFI Excision

A powerful set of cancellation schemes is available if the RFI signal can be identified. The identification key for the RFI could be its location, its power, its trajectory, its statistical properties, or its detailed properties. A number of successful RFI excision strategies operate within its physical implementation. This means the strategy identifies the potential RFI source, performs an automated task to mitigate the potential risk. The potential reduction in computer processing power using the pre-correlation scheme, when compared to mitigation strategies such as those operating on raw data streams (post-correlation), makes these strategies attractive options. In addition, they extend the effectiveness of their RFI mitigation to much lower ranges of interference-to-noise ratio systems [46]. In chapter 9, we will demonstrate how a novel RFI excision strategy can be adopted to realize mobile communication in astronomy areas. A novel RFI cancellation scheme that automatically detect and correct for interference will be demonstrated based on a simple photonic RF transmitter technique. This was made possible by designing a radio access network (RAN) that have a photonic RF system as its transmitter. The following sections will review different mobile communication RANs. The review is necessary to guide the reader toward the choice of RAN implemented in this thesis that can coexist within radio astronomy areas without the consequences of RFI.

Chapter 3: Mobile Communication RAN Systems

In chapter 2, we have discussed how radio astronomy research is expanding across the African continent. We have also identified that RFI due to mobile communication devices will negatively affect the progress in radio astronomy research. We reviewed some of the proposed solutions to mitigate RFI from radio communication systems. We established that the present solutions are rather unscalable and ineffective to support future developments where networks will be converged and the spectrum resource will be shared among different applications.

In this thesis, we propose an RFI mitigation solution by designing a wireless communication network which is flexible and able to coexist within radio astronomy areas without introducing RFI. Our solution is unique because at the moment, radio communication networks do not exist within radio astronomy observatory areas. Our solution will also support network convergence and spectrum sharing.

In order to propose a radio communication system that can coexist within radio astronomy borders, it is necessary to review past and existing radio communication technologies. Many radio communication systems were proposed in the 1990s [47]. In the following sections, we will briefly review the evolution of radio communication systems. This review will focus on radio access network (RAN) architectures for each generation. This is necessary to identify a RAN architectures that can be integrated into radio astronomy areas. Criteria such as RAN flexibility, RAN scalability, data transmission speed, and their associated systems and subsystems will be used to motivate the RAN of choice proposed in this thesis.

3.1 The third-generation mobile networks

We start our review with the third generation (3G) of mobile communication networks. 3G is the upgrade for 2.5G General Packet Radio Service (GPRS) [48] and 2.75G Enhanced Data Rates for The Global System for Mobile Communications GSM Evolution (EDGE) mobile networks [49]. It was proposed for faster data transfer. Later 3G releases 3.5G and 3.75G provided mobile broadband access of several Mbit/s to smartphones and modems in laptop computers. This allowed these standards to be applied to wireless voice telephony, mobile internet access, fixed-wireless internet access, video calls, and mobile TV technologies. This makes 3G a potential candidate to be integrated within radio astronomy areas. For this network to be integrated within radio astronomy areas however, the RAN scalability, network speed, and other important criteria should outperform latest generations such as the fourth generation (4G) and fifth generation (5G) mobile networks. We take a review on RAN architecture for 3G networks and discuss it potential for integration within radio astronomy facilities.

3.1.1 RAN architecture for 3G mobile networks

In order to meet the traffic demand, to build cost-efficient networks, and to provide enhanced quality of service (QoS) to the end user, numerous RAN architectures and technologies have been proposed for radio communication networks of each generation. Figure 3.1 shows a RAN architecture for 3G radio communication network. The 3G RAN is also known as the Universal Mobile Telecommunications System (UMTS) Terrestrial RAN (UTRAN). The UTRAN is built up on the previously existing 2G standard. It is therefore strongly influenced by this RAN architectures.

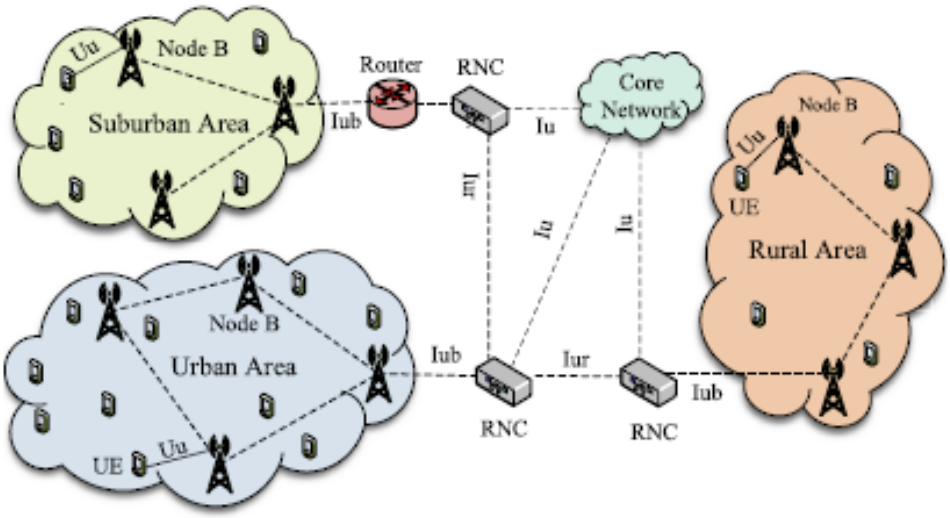

Figure 3.1 The UTRAN architecture for 3G RAN [50].

As illustrated in figure 3.1, the UTRAN consists of one or more Radio Network Subsystems (RNSs), each having at least one Radio Network Controller (RNC) and a number of base stations [50,51]. The RNC communicates with Node B and the core network (CN) over two transmission links known as the Iub interface and the Iu interface, respectively. There are two types of Iu interfaces: one for circuit-switching core networks (CNs) and the other for packet-switching CNs. The base station and air interface in the UTRAN are called Node B and Uu, respectively.

UTRAN uses Wideband Code Division Multiple Access (WCDMA), which is based on Direct Sequence Spread Spectrum (DSSS) and Code Division Multiple Access (CDMA) [52]. Both WCDMA and CDMA are used in 3G networks in order to achieve higher speed and support more simultaneous user links. What is attractive about the CDMA aspect of UTRAN is the fact that a single frequency is used for each base station. If this RAN is to be implemented for radio communication in astronomical areas, it will be relatively easy to control a number of base station from a central station as they both use the same radio transmitter. This is in contrast with the Time Division Multiple Access (TDMA) and the Frequency Division Multiple Access (FDMA) technologies which were previously adopted for 2G systems.

The RNC is the central element of the UTRAN, which is responsible for mobility management of user equipment (UE) and Radio Resource Management (RRM) of all attached cells. Moreover, the RNC is also responsible for the setup, release, and maintenance of Radio Barriers (RBs) [53]. With the RNC controlling a number of base stations, it is easy to manage network resources from a central point. The RFI mitigation algorithm is also simplified and centralized. The control algorithm can be extended to all other connected base stations without designing a different solution for each subsystem. This makes the 3G RAN scalable. For example, when government wants to extend the radio observatory area. They might occupy new areas with existing base stations. Instead of designing a different control system for the new radio astronomy area, the same control circuits from the previous RNC can be used to mitigate RFI at the new radio astronomy site. Spectrum efficiency is also improved when using the CDMA because all the BSs are using the same RF carrier frequency.

The most common 3G standards are the universal mobile telecommunications service (UMTS), standardized by the 3rd Generation Partnership Project (3GPP) [54]. UMTS standards are used mostly in Africa and other regions predominated by infrastructure used by

GSM of the second generation (2G) [54]. It will therefore be economical to use existing 2G resources and expertise to integrate the existing 3G RAN infrastructures within radio astronomy areas.

However, we notice that the use of a single frequency to support a number of base stations could make the integration of 3G RAN architecture within radio astronomy areas difficult. The reason is that in the case of RFI at a certain radio astronomy observatory area. Shifting the 3G radio carrier frequency will result into a shift in the radio spectrum for all the base stations connected to that RNC. An RFI affecting only one particular local point will be interpreted as affecting the entire radio network (RN). This can be a source for inconvenience.

Another drawback for the 3G RAN architecture is that they are mostly designed using legacy electronic RF transmitters. Even if an electronic 3G RAN can be designed with some intelligence to control RFI due to the RF carrier frequency, the constituting electronic devices of the RF transmitter system can cause ambient RFIs which could be very difficult to control. This will initiate other control mechanism for these weak electronic signals, ultimately making the RAN costly and bulky. In our proposed design, we used photonic systems to avoid these challenges.

3.1.2 Data transmission performance for 3G

To meet the International Mobile Telecommunication 2000 (IMT-2000) standards, a 3G system is required to provide peak data rates of at least 200 kb/s [55]. However, many 3G systems are designed to offer higher data rates than the minimum technically required for a 3G service. In particular, 3.5G and 3.75G releases provide mobile broadband access of several Mb/s to smartphones and laptop mobile modems [56]. Depending on the capacity and the population of people surrounding the radio astronomy area, this data rate can be reasonable to be implemented within radio astronomy areas. Of course, with the current demand for high bandwidth, the end user is expected to have some degree of bandwidth inefficiency. However, it is worth remembering that this will be the first step toward realizing radio communication services within radio astronomy areas. Therefore, it is expected that the 3G network bandwidth will be acceptable to the radio astronomer.

The 3G RAN can support data rates up to 2 Mb/s for stationary/walking users and 348 kb/s for moving vehicles [57]. The high-speed packet access (HSPA) technology specifications, representing an intermediate phase toward the fourth generation (4G), initially supported an increased peak data rates of up to 14 Mb/s in the downlink and 5.76 Mb/s in the uplink [57]. The predecessors for 4G technology are 3GPP Long Term Evolution (LTE) offering 100 Mbit/s in the downlink and 50 Mbit/s in the uplink over 20 MHz carrier frequency in the radio access network [57]. The 20 MHz RF carrier frequency used in LTE are within the SKA spectrum given in table 1. Thus, the 3G RAN architecture could be a feasible solution to be designed within radio astronomy areas as far as the network speed is concerned. Before that, it will be reasonable to look at other RAN technologies after them. In the next section, we review the RAN architecture and the data transmission performance for 4G networks.

3.2 The fourth-generation mobile networks

The fourth generation (4G) of broadband cellular networks is the technologys succeeding 3G. A 4G system must provide capabilities defined by ITU in IMT Advanced [58]. These requirements include coverage, data rates, allowable error rates, and delay [58]. Potential and current applications include amended mobile web access, IP telephony, gaming services, high-definition mobile TV, video conferencing, and 3D television. These applications will be needed

within radio astronomy as they continue to contribute toward personal and organizational developments. The 4G network is commercialized upon the first two standards.

The first is called the long-term evolution (LTE) standard. It was commercially deployed in countries such as Sweden in 2009. In telecommunications, LTE is a standard for wireless broadband communication for mobile devices and data terminals. The standard is based on the GSM/EDGE and UMTS/HSPA technologies. It increases the capacity and speed using a different radio interface together with core network improvements. To date, the LTE standard has since been deployed throughout most parts of the world, including Africa. As a matter of fact, the study in [59] showed that 97% of the African society is supported by 4G LTE network infrastructure. Most of the RFI which will be experienced by the African radio astronomers can therefore be assumed to come from the LTE radio communication infrastructures. Few of these networks can be re-engineered to novel radio communication systems which can automatically avoid RFI to radio astronomers. The work demonstrated in this thesis is a commitment toward that era.

The second standard is called the mobile Worldwide Interoperability for Microwave Access (WiMAX) standard [60] which was commercially deployed in South Korea in 2006 and has since been deployed in most parts of the world. Even though the mobile WiMAX standard exists within some part of Africa, they are rather very uncommon and does not possess a great risk of RFI to radio astronomy research.

3.2.1 RAN architecture for 4G mobile networks

The RAN architecture for 4G radio communication networks is based on the Evolved UTRAN (E-UTRAN). It was standardized together with the LTE in Rel. 8 and Rel. 9 [61,62]. Compared with the base station subsystem (BSS) and UTRAN for 2G RAN and 3G RAN, respectively, the E-UTRAN have no centralized controller but only base stations which are called eNodeB, as illustrated in figure 3.2 [61]. The eNodeBs are interconnected with each other through X2 interface, and to the Evolved Packet Core (EPC) through S1 interface. Additionally, every eNodeB is connected to the Mobility Management Entity (MME) and the Serving Gateway (S-GW) through S1-MME and S1-U interfaces, respectively. The interface that connects eNodeB with the UEs is known as LTE-Uu [63].

Unlike previous RANs, the E-UTRAN for the 4G RAN integrates all functions including radio resource management (RRM), header comparison, security, etc., into the eNodeBs, which leads to a reduced latency and an improved efficiency [64]. We also notice the difference of 4G RAN with the 3G RAN architecture. While the RNC in 3G RAN acts as the main system and controls a number of base stations in a centralized manner, the 4G RAN empowers each base station to act as a single and independent entity called the eNodeB. This empowerment of the base station comes with some advantages. When the base station is design to control its own network resources, it can then be redesigned to mitigate RFI independently of the other base stations outside the radio astronomical areas. This means that when RFI occurs which is local to a specific base station, the other base stations do not have to change their RF carrier frequency. This is because they are completely independent from the base station experiencing RFI. Only the base station with RFI can act to mitigate the effects.

The disadvantage of the 4G RAN is that it is not scalable. Since the base stations are independent from each other, integrating them into new radio astronomy areas will require the design of new base stations for each location. Each base station will require its own RFI mitigation system. This can be costly.

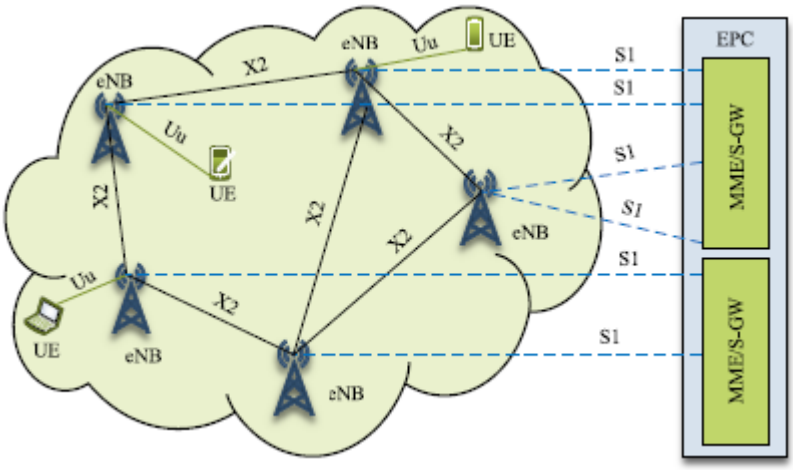

Figure 3.2 The E-UTRAN architecture for 4G RAN [61].

In the 4G RAN, multiple enhanced packet core (EPC nodes), i.e., MME/S-GW in figure 3.2 supports a single eNodeB through the S1 interface. This scheme allows load sharing and eliminates the risk of single-point failure for the EPC nodes. This could be a good reason to select 4G RAN over 3G RAN when using them within radio astronomy areas. Similar to the 3G RAN, the 4G RAN is also build using electronic devices. Even if the current 4G RAN can be re-design with the intelligence for mitigating RFI at their operational frequency, the constituting electronic devices of the transmitter system can cause ambient RFIs which could be very difficult to control. This will initiate other control mechanism for these weak electronic signals, ultimately making the RAN costly and bulky.

3.2.2 Data transmission performance requirements for 4G

4G radio communication technologies provide a comprehensive and secure all-IP-based solution. ITU-R specified in March 2008 the set of requirements for 4G standards and IMT-Advanced specification [65]. The peak speed requirements for 4G service are 100 Mbit/s for high-mobility communication links (such as from trains and cars) [65]. The data rate is 1 Gbit/s for low-mobility communication links (such as pedestrians and stationary users) [65]. The LTE Advanced is essentially an enhancement to LTE. The LTE advanced comes with the coordinated multipoint transmission that allows for higher system capacity and helps handling the enhanced data speeds. The peak download data rate is 1 Gb/s, while the peak upload data rate is 500 Mb/s [65]. On the other hand, the IEEE 802.16m represents the evolution of 802.16e offering 1 Gb/s data rate for stationary reception and 100 Mb/s for mobile reception. Together with the advantages for the 4G RAN discussed above, the data rates for this radio communication technology makes it an attractive solution for integration within radio astronomy areas. Principal 4G technologies can be summarized as follows:

(i) Multi-antenna and multiuser concept.
(ii) Frequency-domain equalization and frequency-domain statistical multiplexing.
(iii) Turbo codes are used as channel codes to reduce the required signal to noise ratio (SNR) at receiver side.
(iv) Channel-dependent scheduling is used to utilize the time-varying channel.
(v) Link adaptation is used based on adaptive modulation and error-correcting codes.
(vi) Relaying is used including fixed relay networks and the cooperative relaying concept.

3.3 State of the art 3G/4G RAN architecture

The 3G RAN and 4G RAN discussed above have both been improved into a new configuration [66]. In this new RAN, the radio and signal processing units of the UTRAN and the E-UTRAN are separated from each other. This new RAN architecture is shown in figure 3.3 and is called the distributed RAN (D-RAN). In fact, the 5G RAN to be discussed next is a slight improvement to the D-RAN. In D-RAN, the radio unit is set close to the 3G/4G macro-BS. It is called the Remote Radio Head (RRH) or Remote Radio Unit. The baseband signal processing unit is located in a convenient and easily accessible location. It is called the Baseband Unit (BBU) or the Data Unit (DU). The BBU dynamically allocates network resources to its corresponding RRHs with respect to the network requirements [66]. The D-RAN on figure 3.3 is attractive for deployment in radio astronomy areas. This is because it retains the advantages of 3G RANs discussed in section 3.1.1. It also improves both the 3G and 4G RANs in many ways. For example, each RRH is interconnected to its corresponding BBU through a transport network known as the Common Protocol Radio Interface (CPRI). This new development allows the transmission of In-phase and Quadrature (IQ) radio frequency (RF) signal as well as baseband digital signals. Both optical fiber and microwave can be deployed for the link between RRH and BBU, which is called the fronthaul. The use of optical fiber allows these newly developed RANs to be converted into photonic systems. Photonic systems will eliminate the inherent RFI noise from electronic transmitters. According to [67], the distance between BBU and RRH can reach up to 40 km, which leads to processing and propagation delays. A white-paper published by EXPO suggests that the length of optical fiber connecting RRH and BBU should be limited to 15-25 km [68], which is therefore the recommended length limit of fronthaul links. The use of optical fibers will also allow these RANs to be more flexible and facilitate for high data transmission. To the best of our knowledge, the D-RAN is one of the efficient RAN solutions for realizing radio communication services within a radio astronomy facilities.

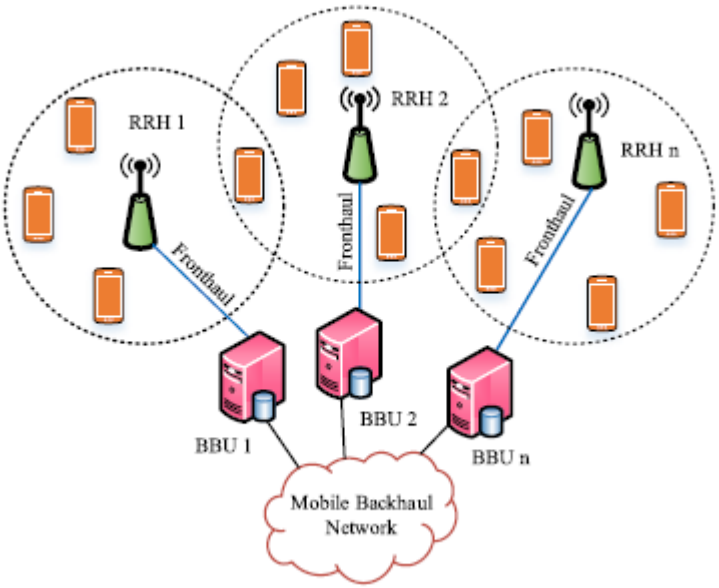

Figure 3.3 New D-RAN architecture for 3G/4G, where RRHs and BBUs are separated, however, every RRH is connected to its own dedicated BBU through fronthaul [66].

The inherent capability for each BBU to control its own RRH means that a solution can be implemented within that BBU for RFI mitigation independently without affecting any other RRHs outside the radio astronomy facility. The use of optical fibers as fronthaul links allow for high-speed data transmission. Nevertheless, the D-RAN for 4G/3G is neither scalable, nor efficient enough to deliver the high bandwidth, low latency and cost-efficient services expected by 5G mobile applications. The fifth generation (5G) RAN offers an exciting opportunity to be implemented within radio astronomy areas. It will be discussed in the following sections.

3.4 The fifth-generation mobile networks

The fifth-generation (5G) of radio communication networks have been deployed by mobile network operators worldwide since 2015 [69]. It is the planned successor to the 4G networks which is widely deployed network to date. 5G radio communication networks are expected to support more than 1.7 billion subscribers worldwide by 2025, according to [70]. To the astronomer, this is a very serious concern for RFI, unless innovative measures are taken to mitigate such interferences. The RFI mitigation techniques discussed in chapter 2 will not be able to protect the astronomers from 5G-related interferences. This is because 5G networks will support spectrum-hungry applications, forcing these radio communication networks to share spectrum with other telco and big data science projects such as radio astronomy. This thesis proposes a novel solution to solve this challenge. We propose a photonic 5G RAN which is flexible enough to coexist within radio astronomy areas. Our proposed RAN is photonic and is designed to share spectrum with radio astronomy observatories in order to support the spectrum efficiency required by these 5G services. We propose a centralized RAN architecture. Contrary to the latest RAN for 3G and 4G discussed in section 3.3, our proposed RAN groups all the BBUs into a centralized and cloudified BBU pool.

3.4.1 Centralized RAN architecture for 5G mobile networks

As the amount of user-data continues to increase due to various QoS requirements, network operators are forced to fulfill these requirements through centralization and cloudification of the D-RAN architecture, either by centralizing only the BBUs or the BBUs and their corresponding RRHs. This new centralized and cloudified RAN, where network resources are pooled in a centralized BBU pool, is known as centralized RAN (C-RAN) [71,72]. C-RAN was first proposed by IBM using the name Wireless Network Cloud (WNC) [73]. A detailed review in [74] showed the viability of C-RAN. This includes the integration of advanced technologies such as common public radio interface compression, single fiber bidirectional, and wavelength-division multiplexing. As given in figure 3.4, the main basic concept behind C-RAN is to remove all BBUs from their corresponding RRHs, and to pool them into a centralized, cloudified, shared, and virtualized BBU pool [75]. Each RRH is then connected through a fronthaul link to this centralized BBU pool. Each BBU pool is able to support up to tens of RRHs and connected through a backhaul link with the core network. To the best of our knowledge, C-RAN is an excellent RAN solution for realizing mobile communication services within radio astronomy borders. The C-RAN will be scalable, and efficient enough to deliver the high bandwidth, low latency and cost-efficient services expected by 5G mobile applications. The C-RAN architecture decreases the capital expenditure (CAPEX) and operational expenditure (OPEX) of mobile network operators (MNO). It will reduce the energy consumption, increases the network scalability, and simplify RFI management and maintenance. The centralization aims to optimize network control performance, improves the spectral efficiency, and decrease energy consumption.

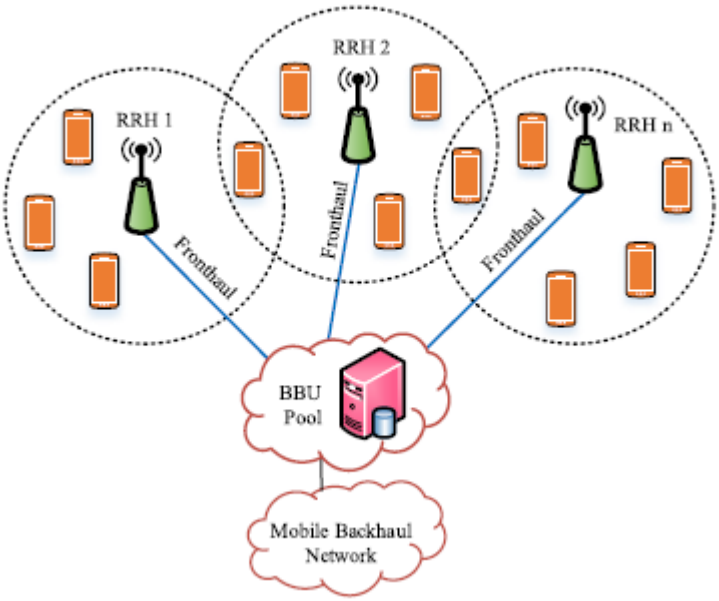

Figure 3.4 The C-RAN architecture, where RRHs and BBU are separated, however, all RRHs are connected to a shared and centralized baseband processing unit in a virtualized BBU pool through fronthaul [75]

The C-RAN can be divided into two subcategories, depending on the splitting of functions between RRH and BBU. The two categories are Fully-Centralized C-RAN and Partially-Centralized C-RAN. In a fully-centralized C-RAN, all functions related to layer 1, layer 2, and layer 3 are all located in the BBU. In this architecture, the RRH remains only a passive unit, having only the antenna to radiate the wireless radio signal. Both fully and partially centralized C-RANs are discussed at detail in [76]. To our knowledge, a fully centralized C-RAN brings advantage to 5G mobile network for expansion into radio astronomy areas as they can support multi-standard operation, independent of the air interface [77].

Both fully- and partially-centralized RANs have been studied and developed from the perspective of 5G radio communication networks. The deployment of both or either of them depends on the radio network characteristics. For example, if the service provider is willing to expand their network coverage or split the cell in order to improve the capacity, it will be easy to deploy new RRHs in the fully-centralized RAN. This can be done by connecting the newly deployed RRHs with the BBU pool. On the contrary, if the service provider notices an increase in the network load, it will only be required to upgrade the hardware in the BBU pool of a partially-centralized RAN so as to increase the processing capacity without investing on the upgrading of the RRH.

In this thesis, we propose a fully centralized C-RAN based on photonics technologies. A typical configuration of a photonic and fully centralized C-RAN is given in figure 3.5. Similar to the fully-centralized RAN in figure 3.4, our proposed RAN also have all its functions integrated into the BBU pool. In our proposed design, this is defined as the central office (please see figure 3.5). Using this network configuration, it is possible to avoid RFI to the astronomer by controlling the photonic RF transmitter without affecting any other 5G radio communication networks connected to a different central office. The C-RAN of this thesis is also scalable as it centralizes all the network function into the central office. Our proposed C-RAN supports the current trends for 5G networks where photonic techniques are being used to facilitate the generation of high-frequency RF carriers in the mmW range.

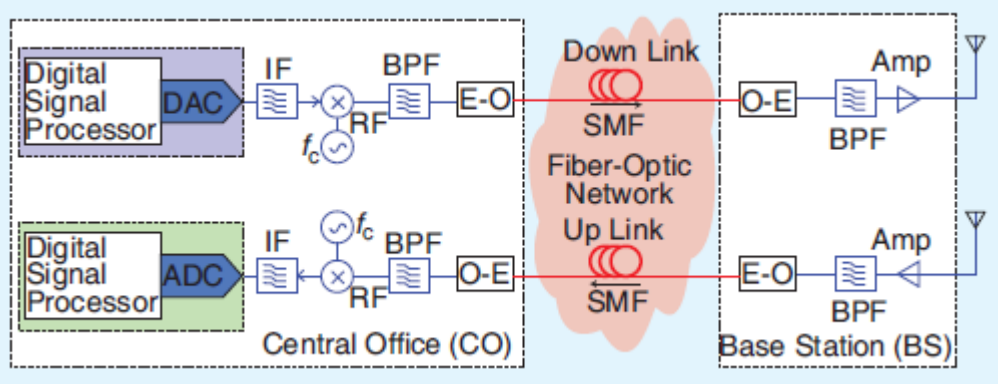

Figure 3.5 A fully-centralized photonics C-RAN [77]

The mmW range proposed for 5G radio communication networks is necessary to support the high data rates expected from 5G radio access networks. These high frequency signals are difficult to generate electronically. In the next section, we look at the data transmission performance requirements expected for 5G radio access networks. Our proposed C-RAN is also expected to meet these requirements. In chapters 5, 7, 8, we will numerically and experimentally demonstrate how our proposed 5G C-RAN meets the data transmission requirements.

3.4.2 Data transmission performance requirements for 5G

The main advantage for 5G radio communication networks is that they will have a greater wireless bandwidth, giving higher download speeds, approximately up to 10 Gbit/s [78]. The increase in speed will be enabled by using additional higher-frequency radio waves in addition to the low and medium band frequencies used in 3G and 4G networks.

A 5G radio communication network will be an Ultra-Dense Heterogeneous Network, consisting up to three different types of cells [79]. Each cell will require specific antenna designs and will provide tradeoff between download speed, distance, and service area. Mid-band 5G will operates at microwaves frequencies (2.5–3.7 GHz). These frequencies allow speeds up to 100–900 Mbit/s and provide service up to several kilometers in radius. 5G networks operating at microwave frequencies are the most anticipated to be deployed in many African countries by 2023. We notice immediately that these are the same frequencies under which the SKA telescope will operates as given in table 1. On the positive side, this means that a single cell tower will be able to provide 5G radio communication services to different radio astronomy areas. This will save both implementation and maintenance costs. It will also means subjecting the radio astronomer to less radio base stations, consequently less RFI. On the negative side however, this will also mean that the present spectrum under which the SKA operates will be subjected to a greater 5G radio communication interferences. Hence the need to develop novel solutions to mitigate these effects.

5G speeds will range from about 50 Mb/s to over 1 Gb/s. The fastest 5G speeds would be realized in the mmWave bands and is expected to reach > 20 Gb/s using carrier aggregation and multiple-input and multiple-output (MIMO) technology [80]. Sub-6 GHz 5G band (mid-band 5G) is by far the most common. This band is expected to deliver between 100 and 4400 Mb/s, and have a longer reach than mmWave, especially in outdoors [81]. The Low-band spectrum offers the greatest range, thereby a greater coverage area for a given site. Its speeds however are lower than the mid and high bands. The full 5G networks are expected to fulfill the following Next Generation Mobile Networks Alliance requirements [82,83]:

(i) Supporting tens of thousands of users with data rates of tens of Mb/s.
(ii) For metropolitan areas data rates of 100 Mb/s should be supported.
(iii) The workers located on the same floor should get 1 Gb/s simultaneously.
(iv) For wireless sensors networks, we should be able to establish several hundreds of thousands of simultaneous connections.
(v) Significantly higher spectral efficiency compared to 4G.
(vi) The coverage must be improved significantly.
(vii) Latency must be reduced significantly compared to LTE.
(viii) The signalling efficiency must be improved.

At high frequencies, data rates in 5G radio communication networks will certainly be limited by propagation conditions such as multi-path etc. [81]. The primary constraining factor however is the terminal transmitter power, which increases linearly with the bandwidth. This implies that to cover a large area at high data rates, dense infrastructures need to be deployed. This will cause an increase in the number of terminal transmitters. When multiple radio transmitter terminals are used within the same spectrum means, the radio link will be subjected to internal interferences from other RATs, possibly in an uncoordinated manner. Reliably estimating, for instance, the carrier to interference ratio (C/I) as a basis for RRM decisions will considerably be more difficult. In chapter 9 of this thesis, we will propose a simple and cost effective RRM algorithm for future 5G C-RAN operating at high frequency signals. This will include mechanisms for dynamically reallocating and/or sharing the spectrum between astronomers and radio access terminals (RATs).

Chapter 4: Photonics-assisted 5G C-RAN

This thesis proposes, for the first time, the use of photonic-assisted 5G C-RANs to realize 5G radio communication networks within astronomy areas. However, the design of photonic-assisted 5G C-RANs for general 5G radio communication started about two decades ago and continues to be studied to date. For example, researchers have been proposing the use of photonic-assisted RF transmitters to be used in 5G C-RANs for generation of higher frequency RF carriers to realize the eMBB requirement [84-86]. High frequency RF carriers will be very challenging to generate using electronic means.

In this chapter, we will review some latest developments in the design of photonic-assisted 5G C-RAN architectures. The main component of a photonic 5G C-RAN is the photonic RF transmitter. When designing a photonic 5G C-RAN to coexist within radio astronomy areas without causing RFI, the flexibility at the photonic RF transmitter plays a major role. These photonic RF transmitters are designed using lasers. Different laser types have been proposed to implement photonic RF transmitters. In the following sections, we will discuss some of these laser technologies. Section 4.2 will review some of the latest photonic RF transmitter configurations proposed for application in 5G C-RANs. Section 4.3 will study the flexibility of photonic RF transmitters to enable them for RFI mitigation in photonic 5G C-RAN.

4.1 Lasers for photonic-assisted 5G C-RAN

Millimeter-wave signals for 5G C-RANs are generated using commercially available single- and dual-frequency laser sources. We will review some of these lasers in the following sections. For each laser type, we will discuss its design, advantage, and disadvantages.

4.1.1 Fabry Perot Lasers

The simplest laser technology is the Fabry-Perot light source [87]. The typical configuration of Fabry Perot laser is shown in figure 4.1. In this laser technology, there are two broad-band reflectors (mirrors) at the two ends of the lasing optical cavity. The light resonates between these two mirrors and forms the dominant mode of the laser device [88]. The back reflector is generally having a higher reflectivity while the front mirror has lower reflectivity. The light that escapes at the front mirror forms the output of the laser device. Due to the broadband nature of the mirrors, the laser normally supports multiple longitudinal modes or standing waves at the same time. This causes the spectrum to be broad and unstable. At the optical communication wavelengths between 1.55 um and 1.3 um, over unspecified temperatures, it was noted in [188] that the peak gain typically moves about 0.4 nm to the longer wavelengths as the temperature increases, and the longitudinal modes shift about 0.1 nm to the longer wavelengths. With this type of wavelength shifting, the photonic RF transmitter designed using these lasers will becomes unstable. For example, when applying this laser type in radio astronomy for photonic 5G communication systems while avoiding RFI, the photonic RF transmitter cannot stay at the intended RF frequency. The RF spectrum will shift rapidly across the observing spectrum, causing even more RFI to the astronomer.

In Fabry Perrot lasers, frequency or wavelength tuning is realized by varying the distance between the two mirrors. With this frequency tuning mechanism, it will be difficult to apply this laser in the design of flexible RF transmitter for application in radio astronomy areas. This is because when RFI occurs, the mirrors have to be shifted mechanically in order to generate a new RF frequency at which the 5G C-RAN can now operate. Ultimately, this will make the

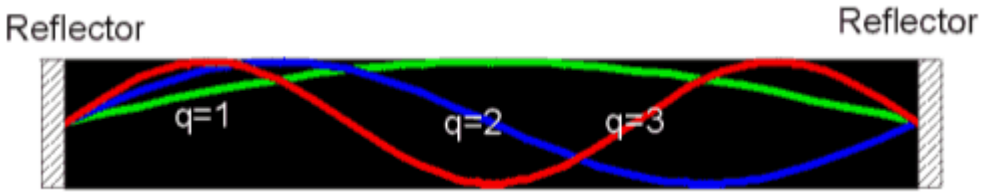

Figure 4.1 A typical configuration of Fabry Perot laser [88].

whole transmitter system complex, bulk, and costly. Due to their broad spectrum and their mechanical nature, Fabry Perot laser hardly find application in areas such optical communication and microwave photonics. Another drawback for this laser technology is the broad optical spectrum they possess. Our proposed 5G C-RAN, intendent to be deployed within radio astronomy areas, will use optical fibres to transport the photonically-generated RF signals to the RRH (see figure 3.5). When each wavelength propagates through the fiber at slightly different velocity, the resulting optically generated RF carrier will have a large linewidth due to chromatic dispersion in the fiber [89], affecting the overall performance of the 5G C-RAN.

4.1.2 Distributed Feedback Fiber Lasers

Distributed Feedback (DFB) fiber lasers comes both as single-frequency and dual-frequency lasers [89,90]. Both single- and double-frequency DFB lasers have drawn interest for application in 5G C-RAN due to their outstanding performance in term of low noise, narrow linewidth, and their inherent long coherence length emerging from the use of fibers as their cavity [89]**.** The unique geometry of the fiber gain medium allows for efficient heat dissipation due to the large surface-area-to-active volume ratio. This makes it easy to control thermal parameters of single-frequency fiber lasers and benefits the laser power scaling. This is an excellent property when using these lasers to design photonic RF transmitter within high temperature astronomical areas such as the Karoo in South Africa [91]. The confinement of laser radiation in the fiber waveguide structure ensures very good output beam quality. Thermally-induced mode distortion is normally encountered in traditional solid-state lasers. In DFB fiber lasers, this can significantly be avoided if accompanied by a specific physical design of the fiber. The use of a single structure to design the laser eliminates the need for complicated alignment of free-space optical components and thus simplifies the laser architecture. This contributes to the compactness and ruggedness of the photonic RF transmitter for RFI mitigation.

Low-noise, single-frequency fiber laser sources with linewidths close to several kilohertz or even sub kilohertz were developed in different configurations [89]. The small linewidth of fiber lasers allows them to be used with precise control for RFI mitigations because the resulting RF carriers generated from these lasers are coherent and does not contain extra radio frequencies which can occupy forbidden frequencies outside their assigned bandwidth.

As the research on single-frequency fiber lasers continued to develop, different configurations have been proposed to demonstrate single-longitudinal-mode operation. In general, single-frequency fiber laser can be summarized as distributed feedback (DFB) fiber lasers [92-94], distributed bragg reflector (DBR) fiber lasers [95,96], and ring cavity fiber lasers [97,98]. In a DFB single-frequency fiber laser configuration, the laser contains a piece of FBG written directly in the active fiber. This FBG introduces a phase change in the middle of the grating area. The resulting system functions as a very narrow optical filter that generates single mode oscillation.

When designing photonic RF transmitters to coexist within radio astronomy areas, there are still some limitations with respect to the applications of fiber lasers. Firstly, although achievable, the compatibility between the active specialty fiber and the passive silica present in other fiber components of the laser cavity could be costly to achieve. When this compatibility is not achieved, the mechanical strength of the splice joints becomes weaken, owing to the different physical properties of these two glasses. This implies that the laser needs to be maintained continuously to keep the 5G C-RAN stable and avoid unnecessary RFI due to photonic RF transmitter system failure. Secondly, although fusion splicing between the highly doped soft glass fiber and silica fiber with low loss can be achieved with specialized fusion splicers, it is still challenging and requires careful handling. This can make the entire 5G C-RAN sophisticated.

As far as the design of a photonic RF transmitter for 5G C-RAN is concerned, fiber lasers emitting multiple wavelengths simultaneously is attractive. This is because they can provide useful features such as the generation of narrow linewidth and low noise RF signals. To realize dual-frequency operation in fiber lasers, two 180-degree phase shifts are introduced in an FBG [99]. Dual-frequency fiber lasers can also be achieved by using two independent single-frequency Er-doped fiber lasers [100]. The Brillouin fiber cavity introduces common mode noise cancellation between the two laser modes sharing a common cavity. This allows to achieve high frequency stability of the optical modes without using a supercavities.

Others have proposed and demonstrated simple schemes to generate highly stable dual-wavelengths fiber lasers. Their setup is pumped by a single-frequency distributed feedback semiconductor laser, and two different kinds of fibers are inserted in the cavity. The generated wavelengths are equivalent to the difference between the Brillouin Stokes shifts in the two fibers [101]. Without using any frequency-stabilized mechanism on the light source, the generated dual frequencies exhibit high stability both for the injected pump wavelength variation and the environmental temperature fluctuation.

Despite such exciting discoveries concerning the development of dual frequency fiber laser, their configurations are quite complex. An example is given in figure 4.2. It will therefore take time before adopting dual frequency fiber lasers in real and practical systems.

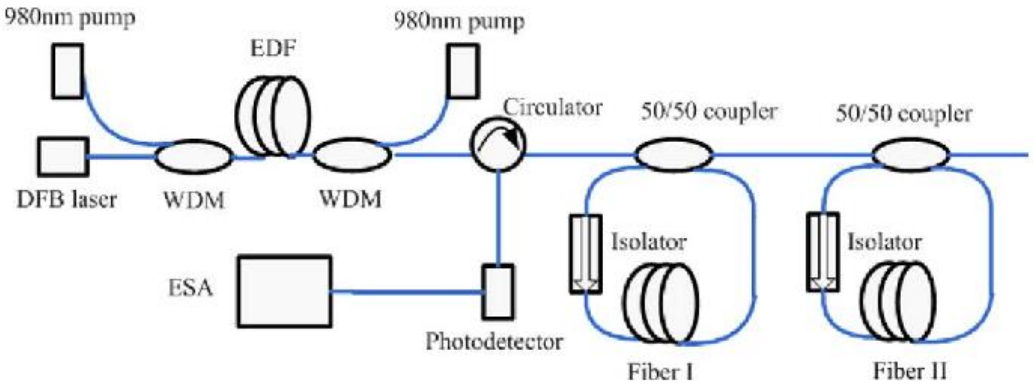

Figure 4.2 Typical schematic of a dual-frequency DFB fiber laser [101].

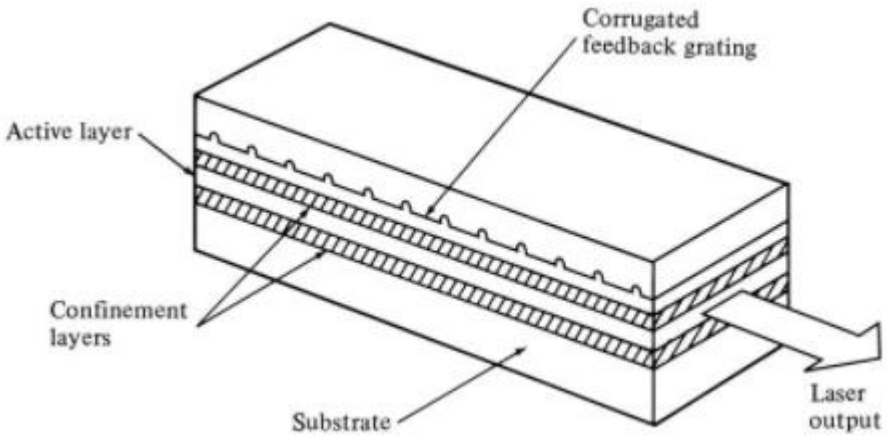

Figure 4.3 Structure of DFB semiconductor laser [102]

4.1.3 Distributed Feedback Semiconductor Lasers

One key requirement for a photonic RF transmitter for 5G C-RAN is that it should be compact in order to reduce OPEX and CAPEX. With an integral frequency selective element, DFB semiconductor lasers are promising candidates to fulfil this requirement [102]. This is because of their capability for stable single-mode operation under direct modulation at high frequencies. A typical DFB semiconductor laser structure is shown in figure 4.3. A semiconductor DFB laser is a laser where the whole resonator has a periodic structure in the laser gain medium [102]. This structure acts as a distributed Bragg reflector in the wavelength range of laser action. Typically, the periodic structure is made with a phase shift in its middle. The device has multiple axial resonator modes, but there is typically one mode which is favored in terms of cavity losses [103]. This is true in single-frequency semiconductor DFB lasers [103]. Therefore, single-frequency operation is often easily achieved despite spatial hole burning due to the standing-wave pattern in the gain medium. With the single frequency operation, together with its compactness, the DFB semiconductor laser is promising for designing RF transmitters that can coexist within radio astronomy areas.

Semiconductor DFB lasers are designed to operate in different wavelengths between 0.8 μm and 2.8 μm [104]. The wavelength of interest in our study is that around 1.5 μm. Typical output powers are some tens of milliwatts [105]. The linewidth is typically a few hundred of MHz [106], larger than the DFB fiber lasers discussed in the preceding section. Tuning within the free spectral range of the laser resonator can be achieved with a separate phase section, which can for example be electrically-heated. Tuning can also be simply by varying the temperature of the gain region with the drive bias current [107]. During this process, the injected current produces a recombination of electrons and holes. The recombination process produces heat which in the cavity which then affect the wavelength at which the laser is operating. Using the drive bias current is the common mechanism for tuning the wavelength of DFB semiconductor lasers. We have adopted this tuning mechanism to realize a flexible photonic RF transmitter in chapter 9. The wavelength tuning in DFB semiconductor laser is significantly bigger than for an ordinary single-mode laser diode. This is an excellent requirement when narrow spectra bands are needed to be occupied by the 5G C-RAN in order to avoid RFI. The typical bias current for a DFB semiconductor laser can be as high as 130 mA [108]. The threshold can be as high as 10-50 mA [108]. Temperature stabilization systems are normally used to achieve a high wavelength stability in semiconductor DFB lasers at the chosen bias current. This wavelength stabilization system was used in our study of chapter 9. The used temperature

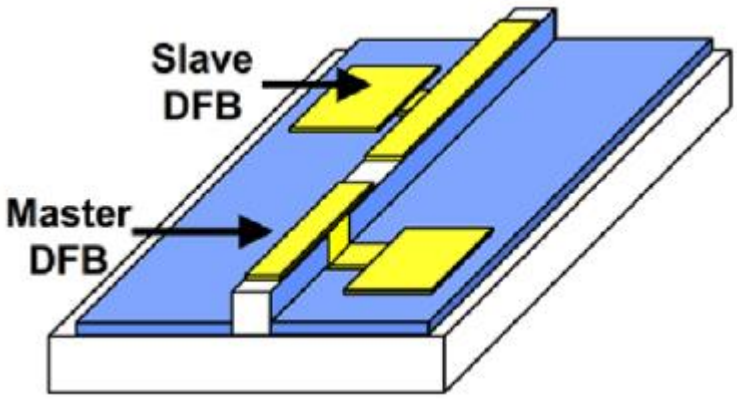

Figure 4.4 Dual-wavelength semiconductor DFB laser [109]

control system improved the overall stability of the designed photonic 5G C-RAN, leading to a stable RFI mitigation system.

When designing a photonic 5G C-RAN, a photonic RF transmitter based on a two-mode DFB semiconductor laser will be desirable. During the last 20 years, a great number of monolithically integrated multi-section semiconductor laser (MI-MSSLs) have been proposed to realize dual-frequency DFB semiconductor lasers. This is done for a better performance in comparison with the conventional single-section semiconductor lasers. The first structure of an MI-MISLs contained only two DFBs laid back-to-back as shown in figure 4.4 [109,110]. In figure 4.4, due to the rather short distance between the two DFB lasers, their polarizations are automatically matched, making the polarization controller not necessary. Due to the shortage of the polarization matching enabled by the short distance between the lasers, the light emitted from the two individual DFB laser sections will optimally interact with each other at the photodiode. This thus make it able to generate coherent radio frequency and mmW signals. This also results into a more simplified photonic RF transmitter for used in 5G C-RANs. In the conventional single-section semiconductor DFB lasers, the working wavelength is controlled by adjusting the corresponding control current or working temperature of the semiconductor laser through the effect of heat and carrier density variation. Unfortunately, using temperature parameter to control the wavelength does not work for laser configuration of figure 4.4. This is because the two DFB laser sections are fabricated together on the same Peltier refrigerating tablet and are packaged in one chip. Therefore, both temperatures of two DFB laser sections share the same value. Thus, the laser wavelength in this device can only be tuned independently by the respective injection currents.

Recently, a novel development of a three-section dual-frequency semiconductor DFB laser was presented in [111,112]. Its structure is depicted in the figure 4.5. Compared to the previous structure of figure 4.4 which consisted only of two DFB laser sections, one more 400-um-long grating-less phase-tuning section is added. This is used to tune the coupling strength and the coupling time delay between the two 400-um-long DFB lasers. This was found to have significant influences on determining the locking or unlocking behavior of the dual-frequency semiconductor DFB laser. By tuning the current of the phase-tuning section, the selectivity of the dynamic lasing modes can be enhanced. This is as a result of the constructive and destructive interferences of the optical fields in the two coupled laser cavities. The designs in figures 10 and 11 give the photonic 5G C-RAN designer a degree of freedom as to the type of lasers to be used in their photonic RF transmitters. Each design has its own advantages and disadvantages.

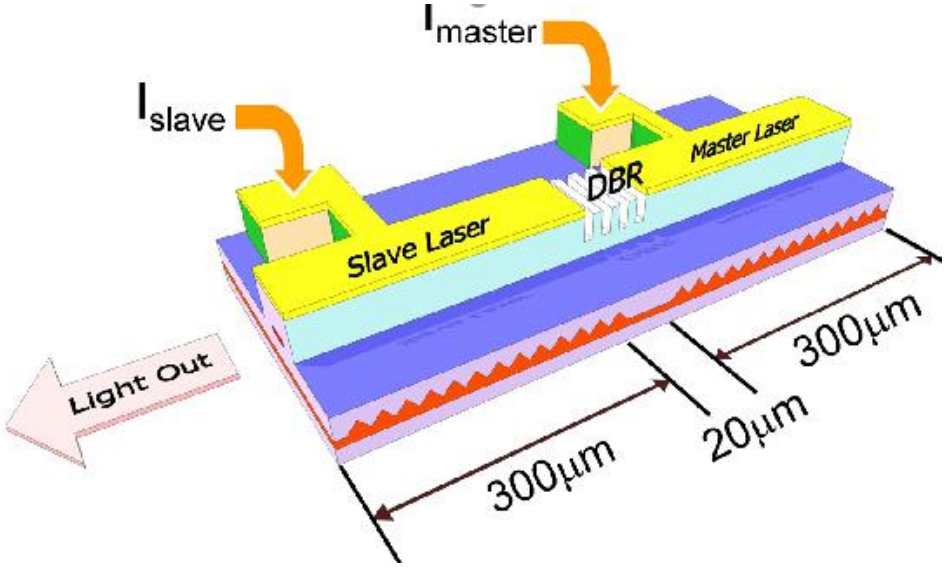

Figure 4.5 Three-section dual-wavelength semiconductor DFB laser [111]

4.1.4 Vertical Cavity Surface Emitting Lasers

The VCSEL is a class of semiconductor lasers that can monolithically be fabricated. A typical structure shown in figure 4.6. Initial designs operated in the wavelength regions of 1300 nm and they were demonstrated in the year 1979 [113,114]. They were fabricated on GaAs and InP materials for active region. VCSELs based on GaAs have been extensively studied. The first room temperature continuous wave (CW) operation devices using GaAs material were demonstrated and commercialized into lightwave systems by 1988 [115-117]. Aiming at exploring applications in the 1300–1550-nm-long wavelength region, considerable effort made these devices being developed and are now readily available. Long-wavelength VCSELs in the 1550nm region have been used for long-distance metropolitan area networks. It should be noted that continuous and wide range wavelength tunability is a distinct characteristic for VCSELs operating at 1550 nm wavelengths. This makes them the best choice for designing photonic RF transmitter for 5G C-RANs. Chapters 5, 6, 7, and 8 of this thesis used VCSELs in the 1550-nm wavelength region to demonstrate novel 5G C-RANs for adaptation in radio astronomy areas.

The structure of a VCSELs (figure 4.6) consists of two parallel reflectors which sandwiches a thin active layer. The VCSEL structure may provide a number of advantages. These advantages include the ultralow threshold operation due to its small cavity volume V. When these devices are applied for photonic RF transmitters to be used within radio astronomy areas, the overall 5G C-RAN systems becomes power-efficient. The threshold current of surface-emitting lasers and common to most semiconductor lasers is the volume-dependent [117]. This means it is important to reduce the volume of the active region in order to decrease the threshold current of the VCSEL. When comparing the dimensions of VCSELs and conventional edge-emitting lasers, it is noticeable that the volume for VCSELs is smaller. This directly reflects the low threshold currents requirement for the VCSEL. A typical threshold current for an edge-emitting lasers is about tens of mA or higher. For the VCSEL, it can be less than a sub milliampere (sub-mA). It could be even as low as several tens of microamperes by implementing sophisticated carrier and optical confinement structures. In [118] for example, the authors demonstrated the importance of identifying and reducing cavity losses in high-Q cavities in order to obtain very low threshold currents with high slope efficiency in VCSELs.

The modulation response is very important for any laser device. The laser modulation

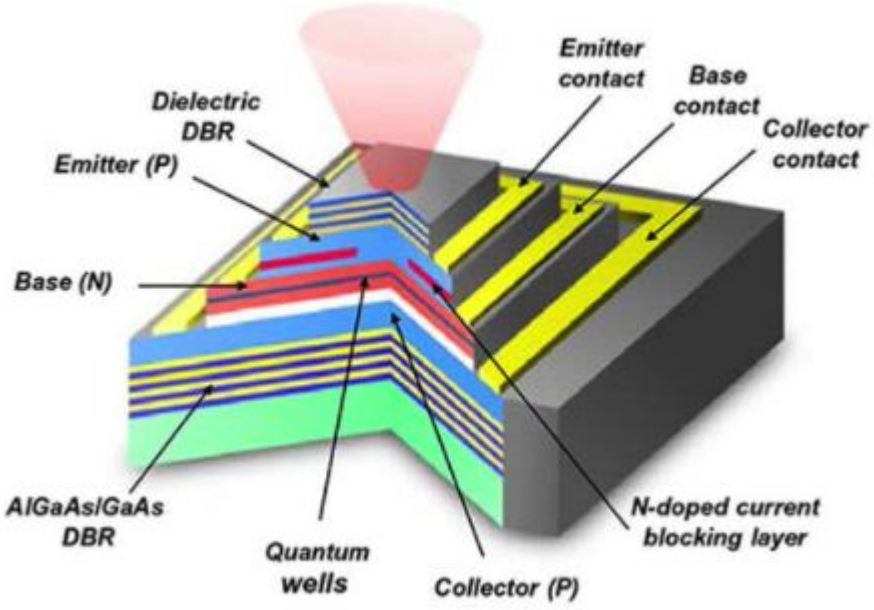

Figure 4.6 The 3-D structure of a VCSEL [119].

frequency is inversely proportional to the square root of the active volume [119]. It can be enhanced by reducing the volume as much as possible. VCSELs are inherently low-volume devices. They therefore possess good modulation frequencies. VCSELs having modulation speed of 10 GHz are available. In this thesis, we have used a 10-GHz VCSEL to demonstrate novel 5G C-RAN offering high data rates to the radio astronomer without any concern for RFI.

Compared with standard edge emitting lasers, the VCSEL may provide a number of advantages as follows: 1) ultralow threshold operation is expected from its small cavity volume; 2) dynamic single-mode operation; 3) wide and continuous wavelength tuning; 4) large relaxation frequency even at small driving current; 5) easy coupling to optical fibers; 6) monolithic fabrication and easy device separation without perfect cleaving requirement; 7) vertical stack integration by microelectromechanical system (MEMS) technology.

The VCSEL device has been contributing to the realization of green information, communication, and energy technologies in various aspects. It has also been already applied to different lightwave subsystems, including gigabit Ethernet and storage area networks. Optical interconnect of largescale integration, and circuit boards in supercomputers and personal computers, are the most interesting applications of VCSELs. VCSEL-based photonics also created other various fields such as laser printers, computer mice, optical sensors, and so on.

The VCSEL device technology will be very useful in 5G C-RANs systems for their great ability to be integrated into practical photonic systems. Despite the many advantages associated with VCSELs, their applications for designing 5G C-RANs is yet to be demonstrated. This thesis presents the first step toward the application of VCSELs in coherent 5G radio communication networks.

Different laser technology such as those discussed in section 4.1 have been applied in the design of photonic RF Transmitters for 5G C-RANs. Different design architectures have been proposed. We review few of these design techniques relevant to this thesis in the following section.

4.2 RF generation techniques using photonic RF transmitters

In section 4.1, we discussed the different types of laser that are commonly used in the design of photonic RF transmitters for 5G C-RANs. Using these lasers, many photonic RF transmitter configurations have been proposed. In this chapter, we will review some of these design techniques. The advantages and disadvantage for each transmitter configuration will be highlighted. As this thesis seek to adapt these photonic RF transmitter configurations for 5G radio communication services within astronomical areas, there is an important need to select the best technique to meet the overall system requirements, hence the review.

4.2.1 RF generation technique based on heterodyning of independent laser

The techniques of optical heterodyning of two independent lasers rely on the principle of coherent mixing in the photodiode to generate the RF signal. It is considered to be the simplest photonic transmitter configuration to generate high-frequency RF signals. The technique is generally referred to as Remote Heterodyne Detection (RHD). The system configuration is illustrated in figure 4.7. While performing optical to electrical conversion, the photodiode also acts as a mixer thereby making it a key component in RHD-based 5G radio communication systems. The principle of optical heterodyning is theoretically explained as follows [120]. If two optical fields with angular frequencies ω_1 and ω_1 can be represented as:

$$E_1 = E_{01}\cos(\omega_1 t) \tag{1}$$

$$E_2 = E_{02}\cos(\omega_1 t) \tag{2}$$

and when both fields are incident on a photodetector, the resulting photocurrent at the output of the photodiode will be proportional to the square of the sum of the optical fields. The normalized photocurrent will be:

$$i_{PD} = (E_1 + E_2)^2 \tag{3}$$

$$= E_{01}E_{02}cos[(\omega_1 - \omega_2)t] + E_{01}E_{02}cos[(\omega_1 + \omega_2)t] + high\ order\ terms$$

The term of interest is $E_{01}E_{02}cos[(\omega_1 - \omega_2)t]$, which shows that by carefully establishing the difference in wavelength ω_1 and ω_2 between the two optical fields, RF signals of any frequency can be generated. The bandwidth limitation of the used photodiode determines the maximum frequency that can be generated. In chapters 5 and 9, we used the technique of optical heterodyning with a 10-GHZ photodiode. Therefore, our demonstrated 5G C-RAN could only operate up to 10 GHz RF frequencies. The technique has high spectral flexibility; thus, it can be used to maximize the spectrum efficiency of the 5G C-RAN. However, this requires lasers with excellent wavelength tunability. In this thesis, it will be demonstrated, for the first time, that VCSELs are excellent optical sources to achieve this requirement.

When consider optical power signals instead of optical fields, the generated photocurrent is given as follows:

$$i_{PD}(t) = 2R\sqrt{P_1(t)P_2(t)}.\cos[\{\omega_1(t) - \omega_2(t)\}t + \theta_1(t) - \theta_2(t)] \tag{4}$$

where R is the responsivity of the photodetector, t is the time, $P_1(t)$ and $P_2(t)$ are the two instantaneous optical power signals having instantaneous frequencies, $\omega_1(t)$ and $\omega_1(t)$, respectively.

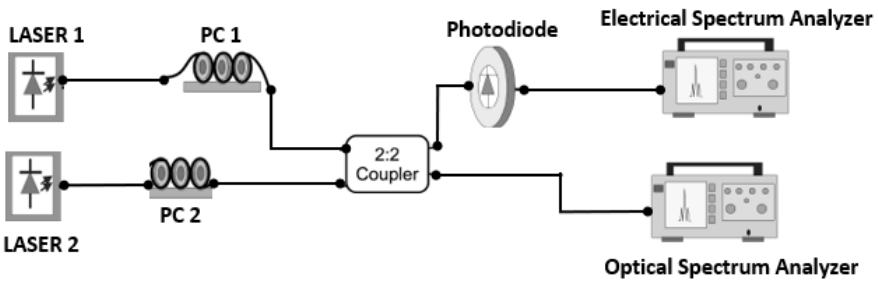

Figure 4.7 Configuration of a heterodyning technique using two free-running lasers.

The instantaneous phases of the signals are given by $\theta_1(t)$ and $\theta_1(t)$, respectively. Equation 1 shows that the stability of the instantaneous frequency of the generated signal depends on the instantaneous frequency difference between the two independent lasers being mixed. Therefore, in this technique, it is necessary to control the instantaneous frequency difference accurately in order to keep the frequency of the generated RF signal stable. When the RF frequency is not stable, this technique will be unsuitable to use for RFI -free 5G communication services in radio astronomy areas. Equation 1 shows that the phase noise of the generated RF signal is influenced by the optical linewidth of the two lasers. Given that the laser emission frequency is highly sensitive to temperature variations, temperature stabilization techniques are used to maintain the required frequency offset and RF phase noise performance. In our demonstration, we used laser diode controllers to keep the lasing wavelength stable in order to achieve stable RF carrier frequency.

Heterodyning produces high link gain and higher carrier-to-noise ratio. The high link gain is due to the fact that the optical powers of both lasers contribute to the total power of the generated RF signal. Using optical heterodyning it is possible to achieve a 100% intensity modulation depth [121]. Many benefits are associated with optical heterodyning technique for RF generation. These includes photonic signal processing such as phase control, filtering, and frequency conversion [122].

The most noteworthy drawback for optical heterodyning is its strong dependance on the phase noise and the optical frequency variation of the used laser sources. The generated RF carrier signal is negatively affected if the used lasers have significant phase and frequency variations. Since semiconductor lasers have non-zero spectral widths, care needs to be exercised to reduce the linewidth of the generated RF signals. One way is by using temperature and wavelength stabilizing systems as highlighted above. This is done as follows.

Techniques used to reduce phase noise sensitivity include Optical Phase Locked Loops (OPLL) and Optical Injection Locking (OIL). However, this is often to an expenses of more complex systems. To keep the system as simple and natural as possible, recent studies have investigate the use optical heterodyning without having to establish the complex techniques for RF phase noise and linewidth enhancement techniques. For example, in chapter 5 of this thesis, we demonstrate the use of optical heterodyning of two independent DFBs without any complex control mechanism. The technique of envelop detection was used to cancel the associated RF noise from the system.

DFB fiber laser, DFB semiconductor lasers, and VCSELs have been applied in the technique of optical heterodyning of two independent light sources. A recent study presented a high-resolution temperature sensor using the beat frequency between the longitudinal modes of twin single-mode distributed feedback fiber lasers [123]. Combining the light from the two

single frequency fiber lasers on a photodetector produced a RF beat frequency signal which is dependent on temperature. Experimental results showed a sensitivity of 1900 MHz/°C, leading to a precision of 0.0007 °C. The stability of the generated RF signal motivates the application of these lasers for high frequency RF generation for application in 5G mobile communication networks.

Semiconductor DFB lasers with non-narrow linewidth were heterodyned where one of the lasers was directly modulated for the experimental generation of up to 2-Gb/s orthogonal frequency division multiplexing (OFDM) signals and their transmission over a 25-km long fiber span [124]. The DFB lasers had a combined linewidth of 2.1 MHz, and the resulting BER from the transmission and modulation of the generated RF signal was below 10^{-3}.

The beating of two VCSELs for photonic RF signal generation is attractive to realize compact and power-efficient photonic RF transmitters for 5G C-RANs. Generation of microwave signals by optical heterodyning using a VCSEL array was demonstrated in 1991 [125], where no optical locking was used, and the linewidth was quite high at about 109 MHz. It has been shown in [126] that optical heterodyning of two VCSELs can generate narrow linewidth microwave signals below 100 MHz. In a recent study [127], we presented the first-reported vertical VCSEL-based heterodyne technique in context of four-level pulse amplitude modulation (PAM-4) over 15 km single mode fiber (SMF) and 12 m RF wireless link. Two low-cost temperature stabilized VCSELs with an extinction ratio (ER) of 4.6 dB and aggregated bit rate of 7 Gbps on-off keying (OOK) data to meet the high data demands in wireless connectivity are heterodyned to dynamically generate low phase noise 37.9 GHz RF for 30 m wireless transmission link. Despite such interesting demonstration, VCSEL-based photonic RF transmitter based on both coherent and no-coherent techniques are yet to be demonstrated for their data transmission capabilities. Chapters 5 through 8 will demonstrate these novel VCSEL-based coherent and no-coherent 5G systems.

4.2.2 RF Generation technique using dual mode lasers

As discussed in section 4.2.1, the main disadvantage for optical heterodyning using two independent lasers is the sensitivity to phase noise of the two heterodyning optical signals. The dependence of the RF beat signal on the polarization state difference of the two heterodyning carriers is also a drawback. Techniques have been developed to improve the phase noise associated with heterodyning of independent lasers. Example of such techniques are frequency-locked loops [128] and phase-locked loops [129]. These techniques, even though effective, are complex and sensitive to temperature fluctuations.

To reduce the beat signal phase noise, the heterodyning optical modes are made to be correlated. One way to achieve this is by using dual mode lasers. The design and operation dual mode lasers is discussed in section 4.1. A study in [130] demonstrated the use of widely tunable dual wavelength distributed feedback (DFB) laser for THz communication application. The wavelength separation between the two modes could be thermally tuned between 96 GHz and 1510 GHz. The device could be directly modulated by high-speed data at up to 25 Gb/s, which facilitated high speed data modulation in a THz communication system.

A recent study developed a dual wavelength DFB laser for the generation of a widely tunable microwave signal [131]. Utilizing the reconstruction-equivalent chirp (REC) technique, dual-wavelength lasing was obtained by introducing two symmetric equivalent phase shifts in a chirped sampled Bragg grating. The laser operated at 1650 nm and the wavelength spacing was about 0.8 nm at room temperature. The frequency of the beat signal between the two wavelengths was 88.47 GHz, and the linewidth of the beat signal was 5.1 MHz.

A dual-wavelength fiber laser was demonstrated experimentally for the generation of RF signals in the millimeter band (up to -110 GHz) [132]. The fiber laser was based on a nonlinear polarization rotation ring-cavity consisting of erbium-doped fiber and a high birefringence fiber of 1 m and 10 m length, respectively. By properly adjusting the laser cavity birefringence via the polarization controllers, the laser output spectrum could be tuned to attain a dual-wavelength spacing in the range of 0.1 nm–0.89 nm to generate flexible and stable millimeter waves with an adjustable span of 12.3 GHz to 110 GHz.

Both VCSELs and Fabry Perot lasers are inherently dual mode lasers. Naturally however, the secondary mode has less power compared to the dominant mode. This makes it difficult to generated RF signals without injection locking technique. Using injection locking schemes, both these lasers have been applied for high frequency RF signals generation. In [133] for example, they propose and demonstrate a new technique of generating microwave frequency combs using a single mode Fabry Perot laser. The laser was obtained by modifying the commercially available Fabry Perot laser diode (FP-LD) by adding an external cavity. This provided only single longitudinal mode at the output and had a tunability range of about 10 nm. The basic principle involved injecting the modulating beam to any of the side modes of the laser. In this way, one of the sidebands is locked with the corresponding injected mode. The injected beam had a negative wavelength detuning to the corresponding mode. It did not matter whether it was the dominant mode or the side mode of the laser that was injected. By heterodyning the injected modulated beam with the dominant mode, an RF frequency comb was generated.

In [134], an optically-heterodyned 28-GHz RF carrier generated for 5G communication was reported by using an orthogonally-polarized dual-mode VCSEL as the frontend transmitter. The power envelope detection was employed for self-heterodyne down-conversion of the generalized frequency division multiplexing data stream. The demonstrated radio over fiber link exhibited superior immunity to the residual frequency and phase noises as well as the inter-carrier interference induced by the free-running dual-mode carrier. In comparison with the mutual heterodyned from two incoherent optical carriers, the self-heterodyned frequency fluctuation can be suppressed between 500 and 330 MHz with significantly suppressed phase noise.

The main advantage for using the dual mode approach is that it does not require complex feedback circuitry as does the different optical injection locking methods. The application of dual mode laser for RFI mitigation in 5G C-RANs will be attractive because of their demonstrated wide wavelength tunability. However, it will be at an expenses of complex transmitter architectures.

4.2.3 Multicarrier generation for RF signal generation

The multicarrier technique for photonic RF generation can be divided into two categories. The first technique is called the optical frequency comb method and the second is known as the Harmonic Generation method. Both these schemes generate a number of optical carries from a single-mode laser source. The resultant optical modes are normally coherent with each other since they come from the same laser cavity. This technique is different from the above-discussed technique of RF generation from a dual mode laser in two ways. First, the technique of multicarrier generation does not produce the extra optical carriers by physically modifying the optical cavity of the laser. Instead, external optical or electrical devices are used to achieve the multicarrier optical spectrum. Secondly, the generated spectrum is not limited to two optical modes but can range from three up to more than 50 modes, depending on the system

configuration. In chapter 5 of this thesis for example, we demonstrated the generation of an optical frequency comb having more than 20 coherent optical lines. The resultant optical carriers were used to design novel 5G C-RANs reported in chapters 6, 7, and 8. We will discuss the two techniques of optical frequency comb and harmonic generation in the following subsections, starting with the optical frequency comb method.

4.2.3.1 Optical Frequency Comb Generation Technique

The optical frequency comb generation technique involves directly modulating the laser by applying an electrical signal to the RF terminal of the laser [135]. This generates a number of optical spectral lines (optical comb) which are separated by the value of the electrical frequency of the switching electrical signal as shown in figure 4.8. Any two sidebands from the generated optical comb source, separated by the required mmWave are then filtered out for radio-over-fiber transmission [136]. The selected sidebands are allowed to beat at the photodiode and mix coherently to generate the desired RF signal as explained earlier in the content of optical heterodyning of two independent lasers. Different techniques such optical filtering using filters or through optical injection locking can be used to select the required sidebands [137]. Using any of the two techniques, the required sidebands can be selected while the rest are rejected. During our demonstration in chapters 7 and 8, we used wavelength selective switches to select the desired wavelengths. The approach of optical filtering was used to remotely deliver mm-wave signals at 54 GHz, 90 GHz and 126 GHz to a RRH fed by a 9-km SMF link [138]. The filtered optical signal was transmitted over the length of the fibre link, amplified, and detected with a waveguide based photomixer. In our studies, we used a 10-GHz photodiode to realize optical to electrical conversion. In [138], the power of the detected mm-wave signal at 90 GHz was -8 dBm. The measured phase noise of the 90 GHz signal at 100 kHz offset was -95 dBc/Hz, which was about 13-dB higher than that of the 22.5 GHz reference signal.

The article in [134] identified two problems associated with the optical frequency comb generation scheme for RF generation. They particularly highlighted polarisation sensitivity attributed to the photomixer and the severely limited tuning range as the main draw back for the technique. However, there are some noteworthy disadvantages associated with the technique. For example, the sideband selection system must accurately track any shifts in the position of the sidebands. Therefore, adopting this technique for 5G C-RANs in radio astronomy areas with RFI mitigation capabilities will require novel stabilization techniques for keeping the sidebands fixed. Additionally, optical filters having high quality factor will need to be used, which maybe expensive. These issues will tend to increase the complexity of the 5G C-RAN architecture.

The advantages of the optical frequency comb technique are normally attributed to the fact that the mixing sidebands are generated by the same laser source, and they are well correlated [139]. Therefore, this technique is capable of generating high frequency RF signals with small linewidth. For example, a linewidth of just 10 Hz at 35 GHz was reported in [140]. Depending on the overall system requirements, the network designer can choose to compromise on system cost when for example, the network is required to transmit coherent data signals. We have demonstrated the application of this technique for coherent data transmission in chapters 8, showing the benefits of adopting this technique when the network cost and complexity is not a serious concern to the service provider.

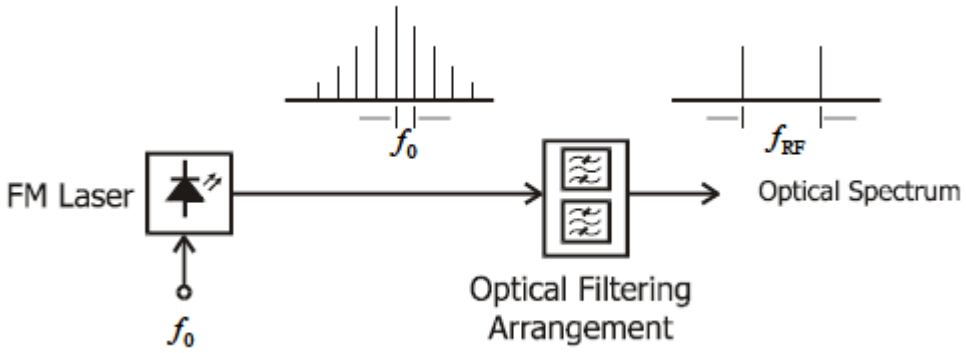

Figure 4.8 The technique of Optical Coherent Mixing based on the FM Laser [142]

The technique of optical frequency comb generation has been investigated using both semiconductor and fiber lasers. In [141], a Fabry Perot laser was used to generate an optical frequency comb by using the gain-switching technique. The work investigated the performance of an externally injected Fabry Perot laser under gain switching for optical frequency comb generation. Due to the inherent multimode characteristic of a Fabry Perot cavity, a single mode was selected by externally injection-locking it with a master laser. At the same time, it was being gain-switched by an electrical signal. They demonstrated the generation of an optical frequency comb with a free spectral range of 6.25 GHz to 25 GHz and wavelength tunability of 31 nm. The phase noise of the tones generated from the optical comb was measured to be similar to that of the externally injected light. The measured optical linewidth was ~ 40 kHz.

DFB semiconductor lasers are naturally single mode, and therefore do not require optical injection to produce optical combs via gain-switching. A study in [143] demonstrated, through experimental and numerical results, the optimum conditions to generate an optical frequency comb via gain-switching of a single-mode DFB semiconductor laser. The DFB laser was biased appropriately and gain-switched with a large amplitude electrical signal. This resulted in the generation of a train of short optical pulses. The study established that the conditions for creating an optical frequency comb exist when the modulation frequency is greater than or equal to the relaxation oscillation frequency of the laser. In our demonstration of chapter 5, the 10-GHz VCSEL was gain-switched with a 14-GHz RF signal which was indeed close to the relaxation oscillation frequency of the laser. In [143], corresponding optical pulses were shown to exhibit lower levels of temporal jitter at these optimum points of operation.

In the experimental and numerical chapters 6 to 9, we will demonstrate, for the first time, the application of VCSELs-based optical frequency comb in a 5G C-RAN. However, the characteristics of a VCSELs-based optical frequency comb have been analyzed and reported. A study in [144] analyzed the performance of an optical frequency comb source from a VCSEL diode. The direct gain switching technique was used together with other techniques such as electro-optic modulation. They observed that the combination of gain-switching and electro-optic modulation technique gave birth to an enhanced optical frequency comb. The combined optical frequency comb offered an improvement in terms of frequency span, flatness, and coherence with respect to the case when single technique was used independently. Very recently [145], a broadband optical frequency comb generation by a gain-switching a VCSEL subjected to optical injection was investigated experimentally. In their experimental setup, a 1550 nm VCSEL under a large signal current modulation was driven into the gain-switching state with a broad noisy spectrum. By further introducing an optical injection, a high-

performance optical frequency comb was produced. The experimental results demonstrated that under proper optical injection parameters, two sub-combs originate from the two orthogonally-polarization components of the VCSEL and splice into a broadband total comb with stable comb lines having high coherence, wide bandwidth, and low phase noise at the fundamental frequency.

4.2.3.2 Modulation Sideband Techniques

Using a Mach Zehnder modulator (MZM), optical sidebands can be generated. Two or four sidebands can be generated, centre at the optical lasing wavelength. Depending on whether two or four sidebands are generated, the technique of sideband modulations can be categorized into two methods known as the 2*f* and 4*f* methods, respectively. The modulation sideband method is different from the technique of optical frequency comb generation discussed above. Firstly, the optical frequency comb method relies on the nonlinearity of the gain-switched laser to generate the needed modes. However, the technique of modulation sidebands generates high-order harmonics by exploring the inherent non-linear transfer characteristic of the MZM itself.

When the MZM is biased at the maximum transmission point, the optical carrier is suppressed together with the even modulation harmonics [142]. The remaining are the two strong components separated by twice the modulating frequency of the signal. The higher-order odd terms have lower amplitudes and can be reduced to 15-dB below the two major components by careful control of the bias point [146]. It is important to note that when this system is applied in radio astronomy to realize 5G mobile services while avoiding RFI, these higher order terms need to be optimally suppressed. Otherwise, they will generate additional unwanted RF carriers which can interfere with astronomical observations. Adding data modulation to the generated mm-waves is achieved by filtering one of the optical sideband components and then modulating it with the data before combining and transmitting both sidebands.

The *2f* method is capable of generating high-frequency mm-waves. However, their performance depends on very careful control mechanisms to avoid Stimulated Brillouin Scattering (SBS) that can significantly affect the phase noise performance of the RF system. In some designs, a phase modulator modulated with an RF modulation frequency of 300 MHz is used to avoid this effect after the MZM [147]. However, when this stabilization method is adopted, the overall system becomes bulky. Additionally, the bias voltage of the MZM needs be carefully controlled. If the bias voltage is not maintained, different RF signal are generated with different power, depending on the bias drift. Using such an unstable photonic RF technique for radio astronomy 5G system could bring more RFI to the astronomer unless sophisticate control systems are designed. The *2f* method has some strong advantages. Since the same MZM generates both optical fields, the phase noise is highly correlated resulting in very narrow linewidth RF signal. It is believed that the performance of this method in terms of phase noise is comparable to the OPLL system. The modulation depth achievable with this technique in practice is larger than in FM-filter techniques. For example, the maximum modulation depth for the 3rd harmonic is about 0.7. A comparison between the theoretically and practically achievable modulation depths is reported in [121]. The *2f* method for RF signal generation has been investigated using laser discussed in section 4.1 of this thesis. A very recent numerical study in [148] demonstrated a radio-over-fiber architecture transmitting 60-GHz wireless signals. The sideband modulation technique was used for

delivering in-building wireless personal area network data. With the proposed system, an acceptable bit error rate of less than 10^{-9} with a reasonably good carrier suppression of 40-dB was achieved after modulation. This facilitated lower power consumption architecture for future 5G networks. In [149], the authors demonstrated a technique to produce eightfold mmW frequency by using the same setup as that of the *2f* method. They propose a novel and simple scheme to achieve eightfold increase in RF frequency with optical carrier suppression based on only one single-drive MZM. According to their theoretical analysis and experimental demonstration, by adopting the bias voltage of the MZM and the amplitude of the radio frequency drive signal, two fourth-order optical subcarriers are generated via a single-drive MZM. Furthermore, the corresponding optical central carrier and undesired sidebands are suppressed simultaneously. Based on their proposed scheme, the generation of 72-GHz optical mm-wave by an RF signal of 9 GHz without any optical filtering was experimentally demonstrated. The radio-over-fiber system with 3.5-Gb/s binary data downstream link based on the generated 72-GHz signal was also experimentally demonstrated. To their knowledge, it was the first time to realize eightfold increase in mm-wave signal generation with simultaneous carrier suppression by using only one single-drive MZM in an experiment.

The review on the sideband modulation technique presented here is necessary to give the reader an idea on the number of matured photonic techniques to generate flexible RF carrier signals. Any of these technique can be adopted to design a 5G C-RAN that can coexist within radio astronomy areas without introducing any RFI effects. In this thesis, the modulation sideband technique was not demonstrated. As the research area expands and gain interest, this technique can also be used to achieve similar results.

4.3 Proposed RFI mitigation solutions in 5G networks

To achieve network convergence, two options are proposed to realize integrated 5G radio communication networks without the consequences of RFI. The first proposed solution is to slice the network into small chunk of spectrums [150]. Depending on the network capacity and requirements, these slices can either be shared among different applications or be dedicated to a unique service [151]. Sharing of network slices brought about a great research interest to mitigate the co-channel interferences within the shared spectrums. Co-channel interference (CCI) is a crosstalk from two different radio transmitters using the same channel [152]. It is one of the RFIs that radio astronomers experience. Co-channel interference can be caused by many factors ranging from weather conditions to administrative and design issues. The type of co-channel interference experienced by radio astronomer normally come from radio network design and administrative issues. In radio astronomy, co-channel interference occurs when external radio devices are not properly managed or designed such that they occupy the spectrum at which the telescope is observing. Thus, besides the intended signal from the space, signals at the same frequencies (co-channel signals) arrive at the telescope from the undesired transmitters located far away or closer to the observatory areas, leading to a deterioration in telescope receiver performance. In this thesis, we seek a solution to co-channel interference caused by radio network design imperfections. If the 5G radio communication systems proposed here do not contain good RFI mitigation techniques, they will introduce additional co-channel interferences to the radio astronomer. In our proposed 5G networks to be demonstrated in the coming chapters, carefully-designed RFI control algorithms were

demonstrated to avoid such effects. In sections 4.3.1 and 4.3.2, we will review recent techniques developed to avoid co-channel interference in 5G shared networks.

4.3.1 Radio resource management for CCI mitigation

Radio communication systems of the 5G era are facing challenges of supporting a huge number of users, better quality of service, and higher energy consumption. All these challenges result in an increasing demand for spectrum resource. Evidently, the traditional spectrum allocation policies are no longer appropriate for 5G communication systems [153]. Cognitive radio is proposed as one of the most promising approaches that can improve the spectrum efficiency and alleviate the spectrum scarcity problem. Cognitive radio is a novel radio spectrum resource management approach where secondary users can access vacant spectrum resource without causing unacceptable interference to primary users in the licensed and shared system [154,155]. This thesis takes up this challenge by introducing novel 5G systems which are able to occupy vacant radio astronomy spectrum without causing RFIs.

At present, there are three access paradigms for cognitive radio networks. They are underlay, overlay, and hybrid [156]. In the overlay paradigm, secondary users are only allowed to access the spectrum if these channels are not used by primary users. In the underlay paradigm, secondary users are allowed to transmit simultaneously and coexist with primary users if the interference caused by secondary user at primary user receivers is under a tolerable threshold called interference temperature [156]. The hybrid paradigm is a mixed approach of overlay and underlay. It is more complex to implement than the other two paradigms. The underlay sharing mode is known to be more efficient in terms of spectrum utilization than the overlay sharing mode. The overlay technology can easily be implemented than the hybrid sharing mode.

The cognitive radio technology enables the network to perform self-organization roles such as spectrum sensing, spectrum sharing and adaptive transmission [157-159] It is also used to determine the level of transmit power in order to minimize interference and maximize the throughput of primary user in a statistical way [160].

Most of the existing cognitive radio-based radio resource management algorithms reported in literature do not effectively address the problems of co-channel interference because they assume accurate spectrum sensing. However, this is not always the case in real-life implementation of radio communication networks. Moreover, most of the algorithms are not scalable and do not consider the design factors such spectral efficiency.

Studies in [161-163] have all proposed cognitive-based radio resource management algorithms. These algorithms were mainly software-based. Implementation of such radio resource management schemes for radio frequency interference mitigation and management could be costly and power-hungry. Inherently, they will require digital signal processing systems which are naturally the sources for ambient RFI to the astronomer.

In this thesis, we present a self-organizing radio resource allocation scheme for radio frequency interference management based on flexible photonic RF transmitter technology. The radio resource allocation problem is formulated as a two-objects optimization problem and the performance of the proposed algorithm is evaluated in a laboratory setting. Our proposed method is simple to implement. This is due to the fact that the flexibility required for radio resource management is implement at the photonic RF transmitter hardware. These transmitters are inherently flexible and can easily be designed to scan a given spectrum. In our demonstration, we adopted an overlay approach were our 5G C-RAN occupy vacant radio astronomy spectrum without causing RFIs. In the next section, we will conduct a review on the currently proposed flexible photonic RF transmitter designs.

4.3.2 Flexible photonic RF transmitter for CCI mitigation

Dynamic spectrum allocation enabled by a flexible photonic radio transmitter is currently a subject of great research interest.

A very recent study [164] presented an innovative tunable software-defined RF transmitter based on integrated photonics. The RF transmitter was able to work in 1-50 GHz with very fast tuning. The system has been characterized and verified in a communication scenario. They presented a novel implementation using hybrid integration technology with silicon nitride with high-Q resonators for extremely low linewidth and polymer with low permittivity material for highly efficient radiation. Even the innovative, the used materials and technique is not yet matured and it will take time before such solution can be realized in practical applications.

Another study [165] proposed and demonstrated a novel approach for flexible and simultaneous generation of millimeter waves at microwave and millimeter wave. They demonstrated that by injecting multiple external beams in a spatial-mode laser diode, they could generate simultaneously, multiband signals with negative wavelength detuning. The generated signal ranged from microwave to terahertz. In their study, they injected four external beams in a spatial-mode laser diode to generate RF frequencies that lied in the Ku-, K-, Ka-, V-bands, and higher millimeter waves. The frequency of generated signals could be tuned from a few gigahertz to several terahertz. The maximum linewidth of the generated RF signals with multiple input beams (up to 42.5 GHz) was found to be about 300 kHz.

The possibility of having two single-frequency wavelength-tunable lasers on a single chip is a promising approach to address the issues of optical heterodyning of independent laser sources (discussed in detail in section 4.2.1). It was motivated that when the two laser sources are on the same chip, both would experience the same environment fluctuations reducing the drift. Using monolithic integration on Indium Phosphide, a fully-integrated millimeter-wave photonic RF transmitter including two distributed feedback (DFB) lasers was achieved [166]. The results showed 1.5 nm (~ 188 GHz) wavelength tuning range for each DFB laser and optical linewidth greater than 1 MHz, a figure that is common for this type of devices.

Even those these latest design are attractive; they are still very costly to realize. They require sophisticated algorithms to maintain the wavelength differences and thus make the entire system prone to unplanned failures. In this thesis, we will demonstrate the use of simple optical devices to realize high-performance flexible photonic RF transmitters. Their application and performance for in practical flexible 5G C-RANs will be presented in the experimental chapters, starting with chapter 5.

Chapter 5: Application of VCSEL in flexible 5G C-RAN systems

In section 3.4.1, we established that a 5G centralized radio access network (5G C-RAN) is the best radio access network (RAN) architecture to be used within astronomical areas to realize radio communication services without introducing radio frequency interferences (RFIs). Section 4.1 discussed the different types of fiber and semiconductor lasers used in the design of photonic RF transmitters. We have also established that VCSELs are power- and cost-effective semiconductor lasers which possess excellent wavelength tunability for designing flexible photonic RF transmitters to be used in 5G C-RANs. Additionally, Section 4.3 reviewed the commonly adopted techniques to design photonic RF transmitters. We also noted that despite the attractive characteristics of VCSELs, they still do not find application in designing photonic RF transmitters for 5G C-RANs. It was mentioned in the preceding chapters that photonic RF transmitter based on optical heterodyning of two independent lasers is attractive as it is simple to implement and wavelength tuning is relatively easy to achieve. In this chapter, we will demonstrate, for the first time to our knowledge, the application of VCSEL-based photonic RF transmitter in 5G C-RANs. The optical heterodyning of two independent lasers scheme will be used to realize this.

5.1 Electrical and optical characteristics of VCSELs

The optical and electrical characteristics for the used VCSELs were first experimentally analyzed. Two 10-GHz Raycan VCSELs were optically heterodyned to generate flexible RF carrier signals photonically. The electrical characteristics for the two VCSELs in terms of their bias current is shown in figure 5.1. As can be seen in that figure, each of the two VCSELs has a threshold current of about 1.2 mA and a saturation current below 10 mA. Such low-current characteristics make VCSELs attractive for designing photonics 5G CD-RAN requiring low-power optical RF transmitters.

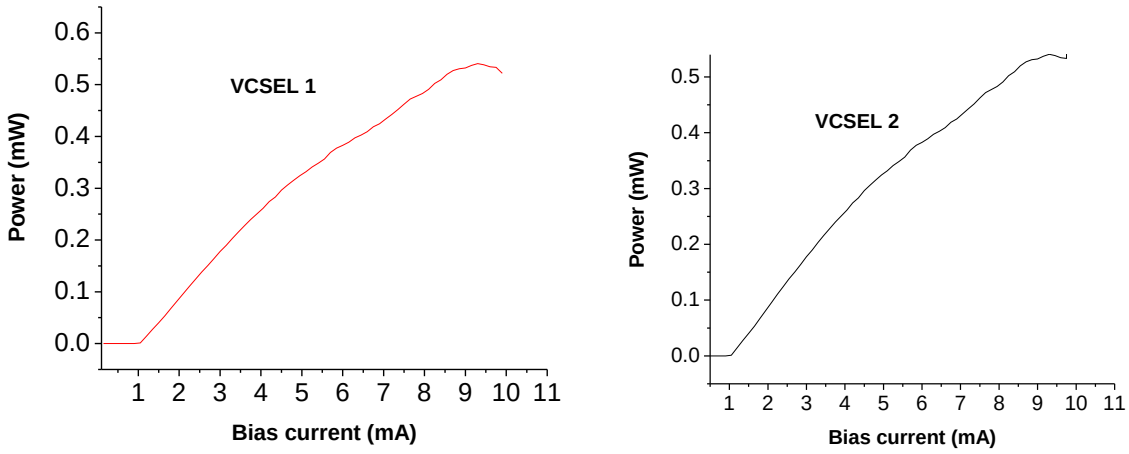

Figure 5.1 Bias current characteristics for VCSEL 1 and VCSEL 2

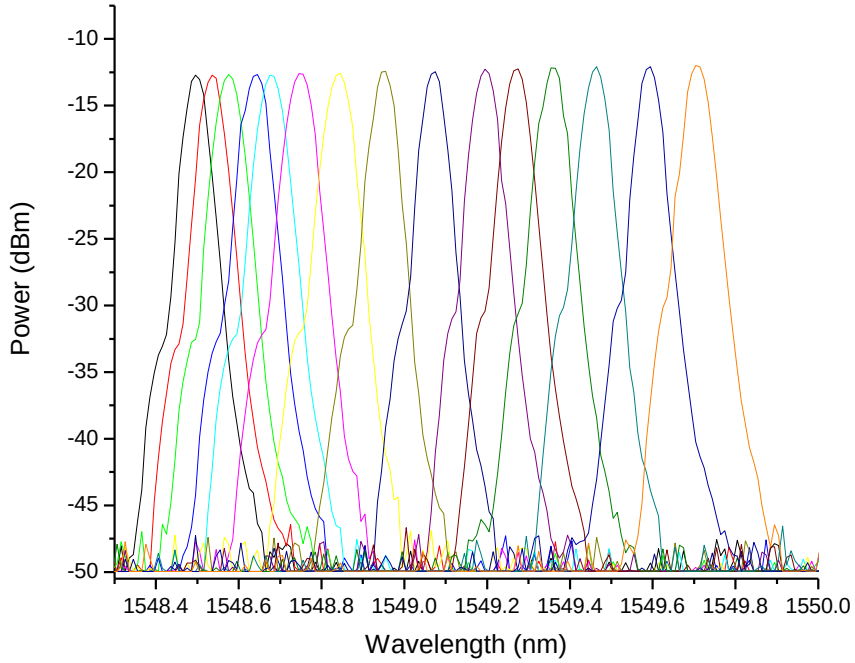

Figure 5.2 The wavelength flexibility of the VCSEL as function of bias current

To design a flexible photonic RF transmitter base on optical heterodyning of two independent VCSELs, it is necessary that one or both lasers have a varying wavelength. The two VCSELs used in our experiment have a bias current-dependent wavelength. When the bias current is varied, the corresponding wavelength also changes. In our study, the bias current for one of the VCSELs was varied to demonstrate their wavelength tunability. The bias current was varied from 1.2 mA to about 10 mA. The corresponding wavelength spectrums were measured and are shown in figure 5.2. We can see on that figure that the VCSEL could produce different wavelengths from 1548 nm to 1549 nm. This feature was exploited for cost-effective and flexible RF carrier generation for spectral resources optimization.

5.2 VCSEL-based optical heterodyning as RF transmitter for 5G C-RAN

Co-channel interference in radio astronomy areas where telescopes are subjected to 5G radio communication transmitters can be eliminated by designing flexible photonic RF transmitters for dynamic radio resource management. Choosing among the photonic techniques discussed in the preceding chapters could depend on a number of factors. These may include factors like the required maximum capacity that the 5G radio communication network is expected to support, the phase-noise tolerance of the 5G radio communication system, the flexibility needed for the 5G radio communication network, and the cost needed to implement the 5G radio communication network. Coherent photonic RF transmitter schemes can generate high-quality RF signals for 5G radio communication networks [167]. However, this is achieved at a cost of complex photonic RF transmitter architectures. Non-coherent photonic RF transmitter techniques are however simple and cost-effective to implement. The simplest non-coherent photonic RF transmitter system is based on optical heterodyning of two independent lasers [120]. However, this scheme generates RF carriers with high phase and amplitude noise. Additionally, this photonic RF transmitter have low spectral efficiency since information is

preferably encoded only in the amplitude of the RF carrier. Furthermore, the use of amplitude modulation with non-coherent photonic RF transmitter systems requires good signal-to-noise ratio in order to realize error-free data transmission [168]. When a solution is presented that can mitigate the above limitations of non-coherent photonic RF transmitter systems, they can be adopted to realize cost-effective flexible 5G C-RANs within radio astronomy areas without RFI effects.

In [124], it was shown that the envelop detection scheme is insensitive to RF phase noise associated with non-coherent photonic RF transmitters such as the optical heterodyning of two free-running lasers scheme. This eliminates the phase-noise limitation of non-coherent photonic RF transmitters. The spectrum efficiency of non-coherent RF transmitters can be enhanced if advanced amplitude modulation techniques are used [169]. Additionally, the high RF power requirement associated with advanced amplitude modulation techniques can be supported using novel RF power enhancement techniques. The scheme in [170] demonstrated RF power enhancement using optical pulse compression without the need for an electrical amplifier. Finally, 5G network implementation cost can be reduced considerably if cost- and power-efficient optical sources such as VCSELs are used [169, 171, 172].

A network that is designed using the combination of solutions in [124], [169], [170], and [171-172] will be cost-efficient, flexible, and attractive for 5G C-RANs that can coexist within radio astronomy areas services without the effects of RFI. However, to the best of our knowledge, such a 5G C-RAN is yet to be demonstrated experimentally.

Previous reports demonstrated the use of energy-efficient VCSELs as optical sources in designing cost-effective microwave photonic transmitters [144]. However, the reported design architectures are relatively complex. In [173], a seemingly less-complex photonic RF transmitter system based on VCSELs was demonstrated. However, attempts were not made to improve the spectral efficiency of the system. Recently, we demonstrated the use of VCSELs and PAM-4 modulation format to realize a simple and spectrally-efficient wireless network [174]. However, most of the reported work in [174] was done numerically. In the following section, we will present and discuss novel results based on our simple and yet spectrally-efficient 5G C-RAN. We have used a VCSEL-based optical heterodyning scheme and PAM-4 modulation format to realize this.

5.2.1 Demonstration of the VCSEL-based heterodyning transmitter for 5G C-RAN

The experimental procedure was divided into three subsections. The first subsection demonstrates a VCSEL-based flexible RF signals generator. PAM-4 modulation format was used in the experiment to double the spectral efficiency of the network. The second subsection describes our laboratory-based PAM-4 signal generator. The last subsection discusses the full experimental setup for the proposed 5G C-RAN to be used within radio astronomy areas.

5.2.1.1 VCSEL-based optical heterodyning for flexible high-frequency RF generation

High-frequency RF carrier generation based on the proposed transmitter was demonstrated using the setup in figure 5.3. The frequency instability of the used VCSELs due to thermal variation requires careful temperature control of the laser cavities before application. This is especially important in radio astronomy areas where such photonic transmitters are proposed to be used to realize 5G radio communication without RFIs. If the VCSEL frequency instabilities are not taken into consideration, the photonically-generated RF spectrum will drift rapidly across the assigned frequency.

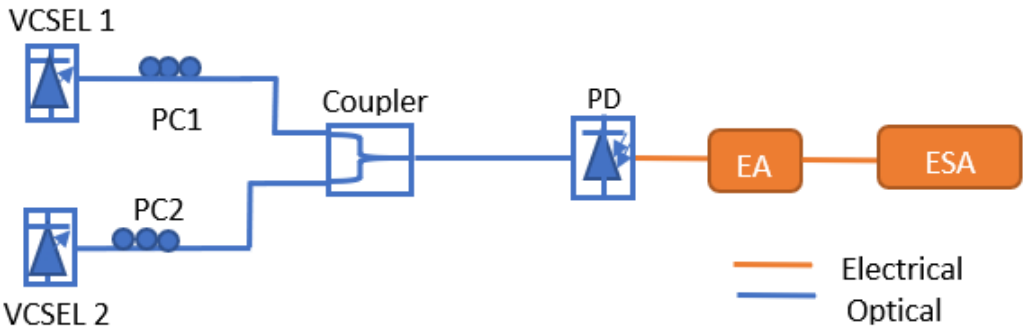

Figure 5.3 VCSEL-based Optical Heterodyning scheme

This will cause serious system failure as the control mechanism try to track this RF shift and correct for RFIs. In our work, this was avoided by using temperature controller boards to stabilize the emission wavelength of the two VCSELs. To generate the 10-GHz RF carrier, VCSEL 1 was biased at 7.69 mA while VCSEL 2 was biased at 8.83 mA. Their outputs were combined at the optical coupler and allowed to heterodyne at the photodiode (PD). The polarization controllers (PC1 and PC2) were used to ensure that the coupled light at the photodiode had the required coupling efficiency for maximum beating to occur. By keeping the bias current of one VCSEL constant while tuning that of the other, different RF carrier signals could be generated, limited by the bandwidth of the photodiode. The flexibility of the VCSELs in term of RF generation was reported in our work [174].

The generated 10-GHz RF spectrum is given in figure 5.4 (right). As discussed in the theory chapters above, the generated RF carrier frequency equals the wavelength difference between the two heterodyning VCSELs. The 3-dB bandwidth of the photodiode limited the maximum RF carrier signals that could be generated. In our demonstration, the generated RF carrier signals were limited to 10 GHz. The phase-noise performance of the photonically-generated 10-GHz RF signal using the two VCSELs was also reported in [174].

For many applications, sufficient RF power is necessary to provide error-free data transmission, especially when amplitude modulation is used, which is normally the case with non-coherent optical heterodyning technique. As can be seen in figure 5.4 (right), our VCSELs could generate an RF carrier signal with -20-dBm optical power. At this RF power, the use of RF power amplifiers with gain below 30-dB is possible to reach the RF power requirement for

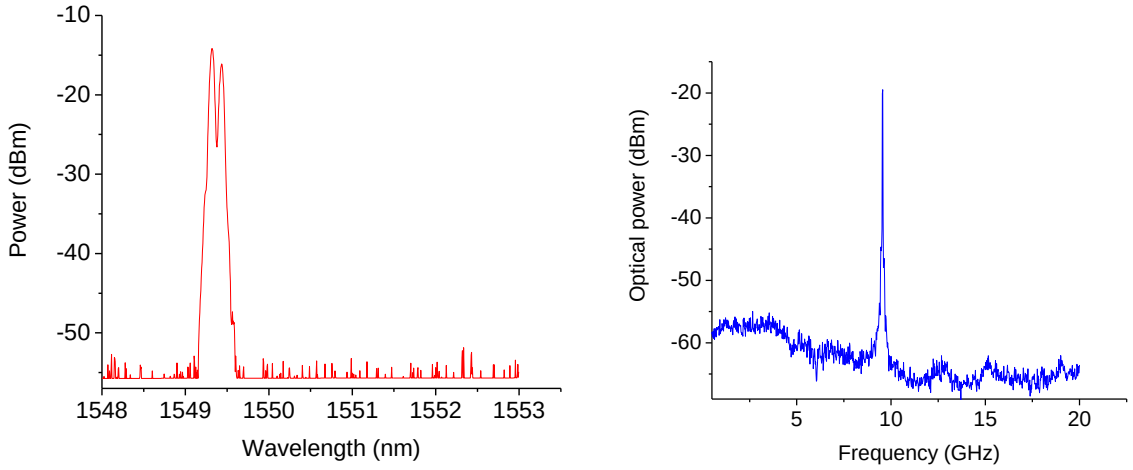

Figure 5.4 Optical spectrums of the VCSELs (left) and the resultant 10 GHz RF carrier (right)

future 5G C-RANs [175]. The beating optical spectrums of the two VCSELs is given in figure 5.4 (left). As can be noted in that figure, both VCSELs had output optical powers above -2 dBm. The optical coherency of the two VCSELs can also be seen where the two optical spectrums are clearly visible.

5.2.1.2 M-Level electrical pulse generator

PAM-4 modulation format offers a spectral efficiency of 2 bits/symbol. Real-time PAM-4 transmitters are commercially developed [176]. In a laboratory where a PAM-4 transmitter is not available, an electrical PAM-4 signal can be generated by using a two-port/channel pulse pattern generator (PPG). Figure 5.5 shows the configuration of our PAM-4 signal generator realized from a two-channel PPG in our laboratory. PAM-4 bit-error rate (BER) can be calculated in real-time or offline by developing software-based PAM-4 receivers using platforms such as MATLAB. Our laboratory-based PAM-4 generator was configured as follows: two channels, the pseudorandom binary sequence (PRBS) channel and the inverted logic PRBS channel (N and P channels) of our pulse pattern generator (PPG), were used. The first channel was attenuated by 9-dB while the second channel was attenuated by 3-dB. These two channels were then decorrelated using a longer RF cable in one of the two electrical arms. This was necessary to make the two channels be in-phase and also so that they can overlap effectively. These two channels were then combined using an electrical T-connector. The output produced an electrical PAM-4 signal. The PAM-4 electrical signal is shown in figure 5.6, both as an electrical pattern (left) and as an electrical eye (right). We can see the effectiveness of our laboratory-based PAM-4 signal generator. The four amplitude levels are clearly visible. The corresponding eye diagram is also showing three distinct eye which are clearly open. This makes this configuration practical for PAM-4 data transmission experiments.

5.2.1.3 Fiber transmission performance of the VCSEL-based 5G C-RAN

Data transmission performance of the VCSEL-based optical heterodyning transmitter scheme was investigated using the setup in figure 5.7. Figure 5.7 shows a fully centralized 5G radio access network (C-RAN) as described in section 3.4.1. The C-RAN architecture is attractive for application in radio astronomy areas to realize mobile services. Firstly, as the name implies, the C-RAN is a centralized network. This means that all the radio resource control algorithms can be shared with other base station from a central location. This central location is chosen to be at the radio astronomy observation office. As will be demonstrated in chapter 9, when this photonic RF transmitter is adopted, the 5G C-RAN can easily shifted its RF carrier to a different frequency by changing the bias current of one of the VCSELs. When this happens, a different wavelength is generated and the beating of the two VCSELs at the photodiode will generate a different RF signal. The 5G system is therefore able to mitigate any RFI effects.

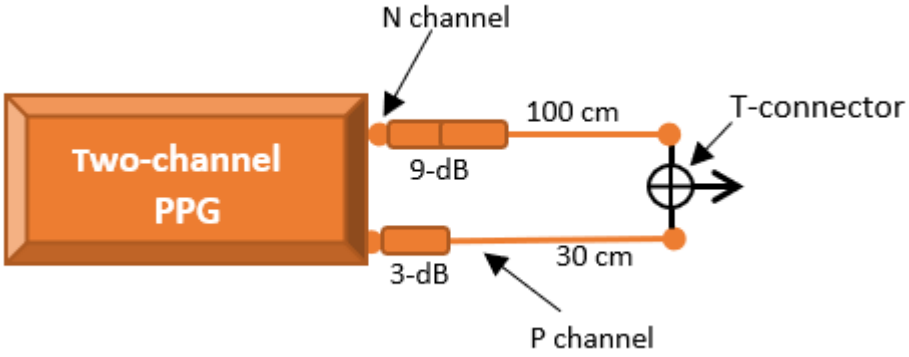

Figure 5.5 Configuration of a PAM-4 generator from a two-channel PPG

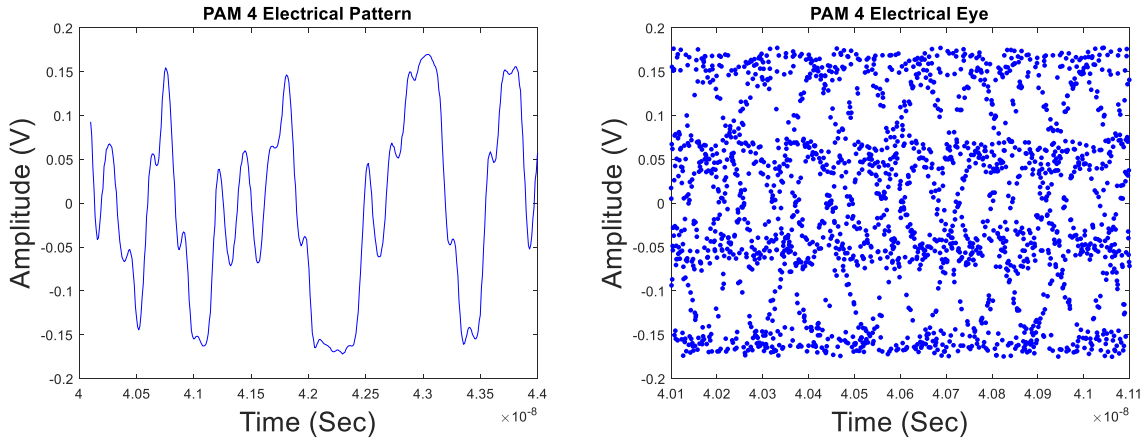

Figure 5.6 PAM-4 electrical signal pattern (left) and eye diagram (right)

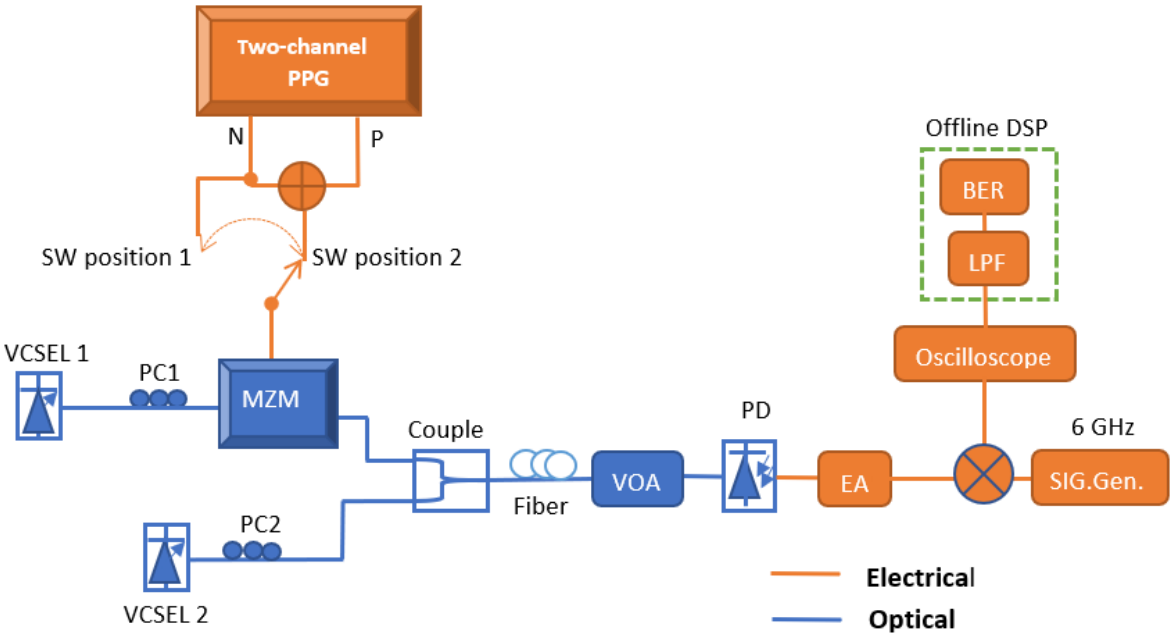

Figure 5.7 Full experimental setup of VCSEL-based RF generation and PAM-4 modulation

Since the RAN architecture in figure 5.7 is designed to offer 5G services to radio astronomy areas without any RFI effects, it is also expected to fulfil 5G data transmission requirements as discussed in section 3.4.2. In our demonstration, these requirements were achieved as follows. To act as the baseline for system performance evaluation, an 8.5-Gbps binary data modulation without optical heterodyning was performed. A Mach-Zehnder modulator (MZM) was used to modulate VCSEL 1 with 8.5-Gbps binary data. The 8.5-Gbps binary data was received from the N channel of the PPG when the switch in figure 5.7 was at position 1. The modulated single optical signal from VCSEL 1 was transmitted and received after 24-km of non-zero dispersion shifted fiber (NZ-DSF) before being detected by a 12.1-GHz photodiode as shown in figure 5.7. Since no RF carrier was generated in this case, the signal generator and the mixer were not used. The binary signal was received by the oscilloscope immediately after the photodiode. The BERs were then calculated numerically from the saved data to determine systems performance.

Figure 5.8 (left) is the BER results for 8.5 Gbps binary data when only a single VCSEL was used and no optical heterodyning was implemented. This was necessary to get results against which the performance of the optical heterodyning-based 5G C-RAN transmitter could be validated. The BER results shown in figure 5.8 (left) were calculated before and after 24-km

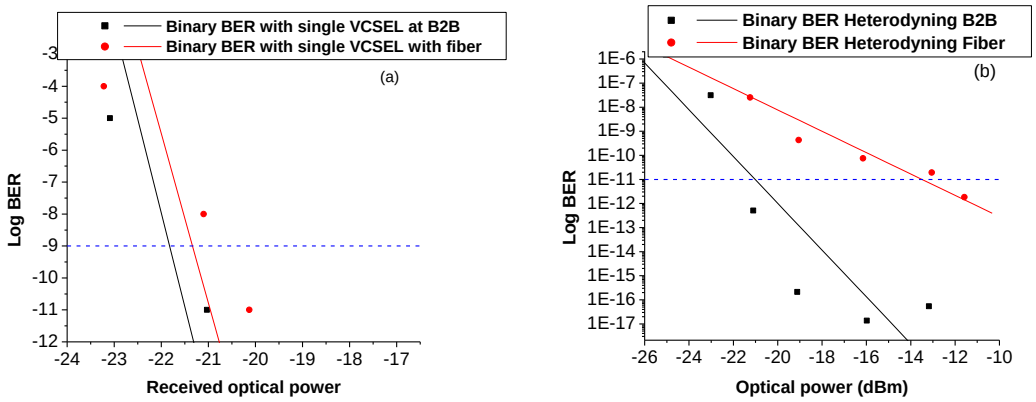

Figure 5.8 BER results for 8.5 Gbps binary (left) and 8.5 Gbps binary with optical heterodyning (right)

fiber transmission. We can see in figure 5.8 (left) that in this case when only a single VCSEL was used, error-free BER of 10^{-9} was achieved with an optical power of less than -22 dBm. This power is below the receiver sensitivity of the used photodiode which is -21 dBm [177]. A transmission penalty of 0.4-dB was achieved in this case when a single VCSEL was modulated at 8.5 Gbps.

In the second demonstration, to photonically generate a 10-GHz RF carrier signal with data, VCSEL 1 was modulated with the same 8.5 Gbps data before being coupled with VCSEL 2. The combined signal was also launched into the same 24-km fiber before being detected by the 12-GHz photodiode. A signal generator and a mixer were used to down-convert the 10-GHz RF signal to an intermediate frequency (IF) of 4 GHz. The 4-GHz signal was saved on the oscilloscope for offline BER calculations.

Using our designed digital receiver in MATLAB, the received IF carrier at 8.5 Gbps was demodulated offline first by using a digital low pass filter before BER calculations. It was important to design a digital filter that removes any IF signal. If part of the IF signal remained, it could distort the data pattern and will negatively affect the BER results. The designed filter was numerically optimized considering the current hardware mixers available in the market. The performance of our designed digital filter in MATLAB is given in figure 5.9 (right) for the 8.5 Gbps binary data. In figures 5.9 (right), we can see that our digital filter was able to remove the high-frequency IF signals, allowing only the baseband pattern to pass through from which BER could be calculated.

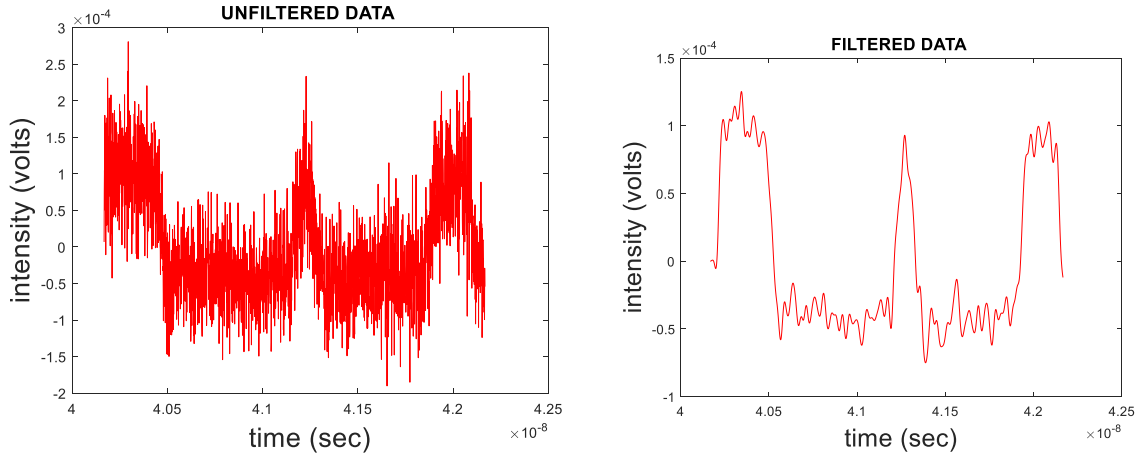

Figure 5.9 Unfiltered binary data (left) and filtered binary data (right)

Figure 5.8 (right) shows the BER results for the second case when VCSEL 2 was added to generate an optical heterodyning-based 10-GHz RF carrier signal that is modulated with 8.5 Gbps binary data. In this case, an error-free transmission BER of 10^{-9} was achieved at a receiver sensitivity of -19 dBm and a 4-dB transmission penalty. These results shows that when two VCSEL are used as RF transmitters in radio astronomy areas to realize 5G services, the designed 5G network is expected to offer a data rate of at least 8 Gbps without data error. The optical power needed to achieve this is also low, avoiding the necessity for optical amplifiers that can make the entire 5G C-RAN complex and costly. The remote radio head (RRH) can also be extended up to 24 km to support distant communities with 5G services.

In the third demonstration, VCSEL 1 was modulated with 17 Gbps PAM-4 data to improve the spectral efficiency of the 5G C-RAN. The photonically-generated and modulated 10 GHz RF signal was again transmitted over the same 24-km NZ-DSF to the photodiode. During this steps, due to the needed RF power for high-level amplitude modulation formats such as PAM-4, a low-noise linear electrical amplifier (EA) was used to amplify the received photonically-generated and modulated PAM-4 signal. An electrical mixer was also used to down-convert the 10-GHz RF carrier to an IF of 4 GHz. This was achieved using our 20-GHz signal generator to generate a 6-GHz local oscillator signal for the local oscillator port of the mixer. The output of the electrical mixer was an IF signal that was then recorded by an oscilloscope for offline signal processing.

On the figure 5.10 (right), we can see the PAM-4 signals after filtering. We can see that our digital filter was also able to remove the high frequency IF carrier signals, allowing only the baseband PAM-4 pattern to pass through from which BER could be calculated.

Improving network capacity without the need for additional spectrum is attractive, especially when low bandwidth optical sources such VCSELs are used in 5G C-RANs. The BER performance using PAM-4 signal is shown in figure 5.11 (left). When a minimum BER of 10^{-9} is considered, an extrapolation of figure 5.11 (left) shows that this BER could be achieved with an optical power of about +2 dBm. This translates to a transmission penalty of 16-dB as can be determined in figure 5.11 (left). This power can be achieved using either low-gain optical amplifiers or electrical amplifiers after the photodiode. Forward error correction techniques could also be adopted to improve the BER [178].

In figure 5.11 (right), the system performance at 8.5 Gbps binary data using a single VCSEL, at 8.5 Gbps binary when optical heterodyning two VCSELs, and at 17 Gbps PAM-4 when

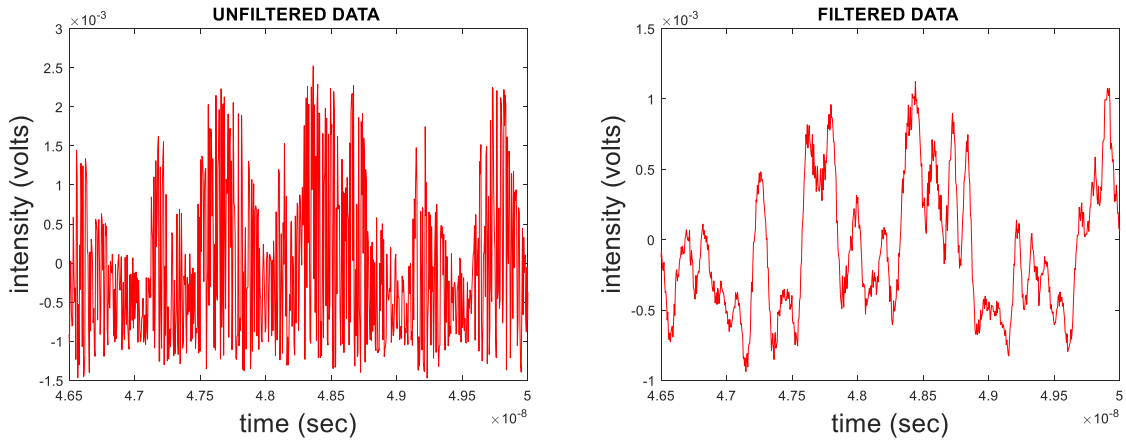

Figure 5.10 Unfiltered pam-4 data (left) and filtered PAM-4 data (right)

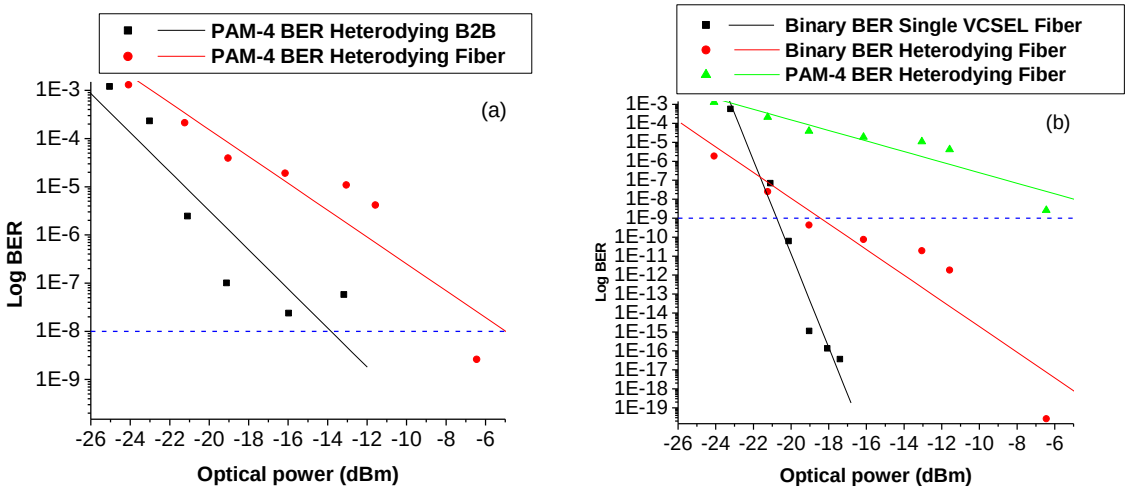

Figure 5.11 BER for 17 Gbps PAM-4 (right); 8.5 Gbps binary single VCSEL, 8.5 and 17 Gbps optical heterodyning (left)

optical heterodyning two VCSELs is shown in term of BERs. Both BERs were measured after 24 km fiber transmission. We can see in that figure that both systems were able to give error-free data with optical powers within +2 dBm. On figure 5.11 (right), when considering a minimum BER of 10^{-9}, binary data transmission using a single VCSEL performed better. Comparing the performance of a single VCSEL with optical heterodyning of two VCSELs at 8.5 Gbps, a transmission penalty of 3-dB was achieved. A transmission penalty of 15-dB was recorded when optical heterodyning of two VCSELs was modulated with 17-Gbps PAM-4 data. Figure 5.11 (right) shows that it is possible to use low-power VCSELs to enhance the system capacity using PAM-4 modulation format. This was possible within a practical optical power below 0 dBm. These results motivate the potential of adopting VCSELs and PAM-4 modulation formats in designing flexible, high bit rate, low-cost, and less complex 5G C-RANs within radio astronomy areas without the consequences of RFI to the astronomer.

5.3 VCSEL-based OFC as RF transmitter for 5G C-RAN

In section 5.2, we have demonstrated a simple and cost-effective 5G C-RAN system at 10-GHz RF frequency using VCSELs as light sources. The spectral efficiency was doubled by adopting a four-level pulse amplitude modulation (PAM-4) scheme. We realize however that, using two free-running VCSEL lasers for designing photonic RF transmitter is attractive if the 5G C-RAN is intendent to operate at low data rates. Radio astronomers will require enhanced data rates to have access to novel applications that 5G radio access network will support. Therefore VCSEL-based 5G C-RAN with enhanced data throughputs are necessary. However, this will require coherent VCSEL-based photonic RF transmitters.

Recent studies showed both numerically and experimentally that gain-switched VCSELs can generate coherent optical frequency combs (OFC) for potential application in 5G C-RANs [179-180]. Despite such promising findings, their application in designing future 5G C-RANs is yet to be demonstrated both numerically and experimentally.

In this section, for the first time to our knowledge, we will present numerical results showing the application of VCSEL-based optical frequency combs to realize coherent high-performance 5G C-RANs. Special emphasis is placed on the feasibility of these photonic RF transmitters in designing 5G radio communication network which can coexist within radio astronomy areas

without the effects of RFI. We have investigated the study in the frequency band around 60-GHz, frequency of interest for future 5G radio communication networks.

5.3.1 Demonstration of VCSEL-based OFC for 5G C-RAN

The section is divided into two subsections. The first subsection will discuss the configuration of a VCSEL-based optical frequency comb generator. The second subsection discusses the full schematic used to realize the reported VCSEL-based flexible 5G C-RAN for radio astronomy.

5.3.1.1 VCSEL-based optical frequency comb generation

Features of VCSELs discussed in section 4.1.4 make them attractive optical sources for use in cost- and power-sensitive 5G C-RANs for radio astronomy. One of the VCSELs used for the study in section 5.2 was first characterized to extract its intrinsic parameters which are necessary for numerical analysis. These parameters were calculated and are given in table 2. Using these parameters, we numerically generated and evaluated the characteristics of the optical frequency comb generated by the system. The numerical study was carried out using Optiwave software version 17.0. At the time of demonstration, this was the latest version from the producer.

For exclusively generating the optical frequency comb and the RF carrier signals, as well as for studying the dynamics of the resultant optical frequency comb, figure 5.12 was modified as follows. The polarization controller (PC), Mach Zehnder Modulator (MZM), the pulse pattern generator (PPG), the optical fiber, and the bit error rate tester (BERT) were initially not connected. As discussed in the preceding theoretical chapters, it is suggested that the electrical switching frequency from the sine generator should be close to the relaxation oscillation frequency of the VCSEL, and the modulation current should be determined empirically [180]. Increasing the modulation current from the sine generator will need to be compensated by reducing the bias current of the VCSEL below the saturation current and above the threshold current.

Table 2. Measured VCSEL Intrinsic Parameters

Parameter Name	Value
Wavelength	*1552.43 nm*
Bias Threshold Current	*8 mA*
Active layer volume	*2.5e-012 cm^3*
Group velocity	*8.5e+009 cm/s*
Quantum efficiency	*0.4*
Differential gain coefficient	*0.25e-015 cm^2*
Mode confinement factor	*1*
Carrier lifetime	*2.73e-009 s*
Photo lifetime	*60e-012 s*
Spontaneous emission factor	*1e-006*
Gain confinement coefficient	*10e-018 cm^3*
Linewidth enhancement factor	*2.8*

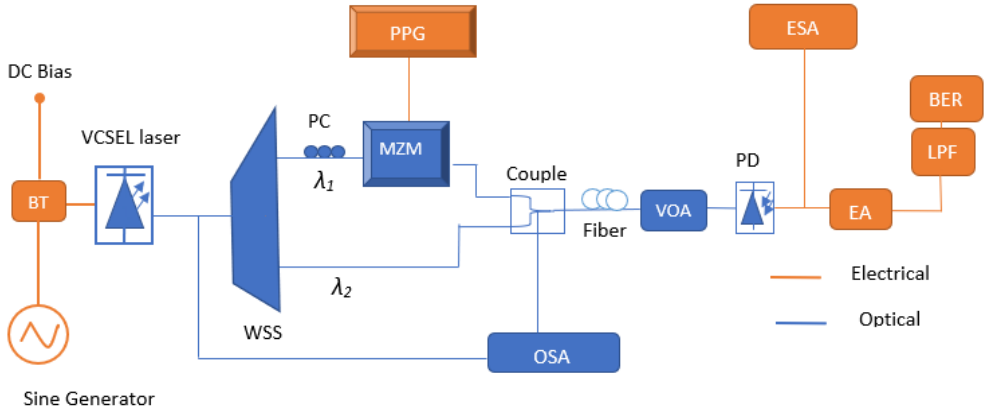

Figure 5.12 Experimental schematic of the proposed VCSEL-based fronthaul system; BT, Bias Tee.

Adhering to the above suggestions, the switching frequency of our sine generator was set at 14 GHz, slightly above the 10-GHz relaxation oscillation frequency of the VCSEL. The switching current of the sine generator was set at 10 mA, also just slightly above the saturation current of the VCSEL. It is worth mentioning that these operating points of the system were to be determined empirically by the system designer.

Figure 5.13 shows the generated optical frequency comb. The results show a well-spaced optical frequency comb with clearly resolved spectral lines. Remarkably, at such low bias current and low modulation current, the VCSEL-base system was able to give a 3-dB bandwidth with 11 comb lines.

In the same study, an investigation was carried out to determine the dependency of the frequency comb on both the electrical switching frequency and the modulation current above or below their optimum values. Figures 5.14 and 5.15 show how the comb behaved when the modulation current was reduced above and below the optimum modulation current, respectively. When the modulation current was above the optimum value, the comb kept its shape, but the extinction ratio for each comb line was reduced. The side modes of the comb were also consumed as can be seen in figure 5.14. This was because at high modulation currents from the sine generator, the VCSEL received power above its maximum saturation bias current. As a result, the VCSEL was driven into a highly-nonlinear regime. In this regime, the dynamics in the VCSEL cavity modifies its gain bandwidth, resulting into new optical lines being generated between each pair of the comb lines. Below the optimum modulation peak power, the combs lines remained clearly visible, but the number of comb lines were reduced as can be seen on figure 5.15. These behaviours were well-reported in a numerical study of a gain-switched VCSEL [179]. We have reported them here for completeness.

It is very important to note that when the 5G network designer choses to use this photonic RF transmitter scheme when designing a 5G C-RANs within radio astronomy, these comb dynamics needs to be taken into consideration, and they should be avoided. For example. When the 5G radio communication system designer does not optimize and maintain the optimal operation conditions of the photonic RF transmitter, a shift in parameters will deteriorate the generated optical frequency comb. The systems could therefore stop to work completely, affecting the 5G end-user or it can shift to unmonitored RF signals that will become an RFI to the radio astronomer.

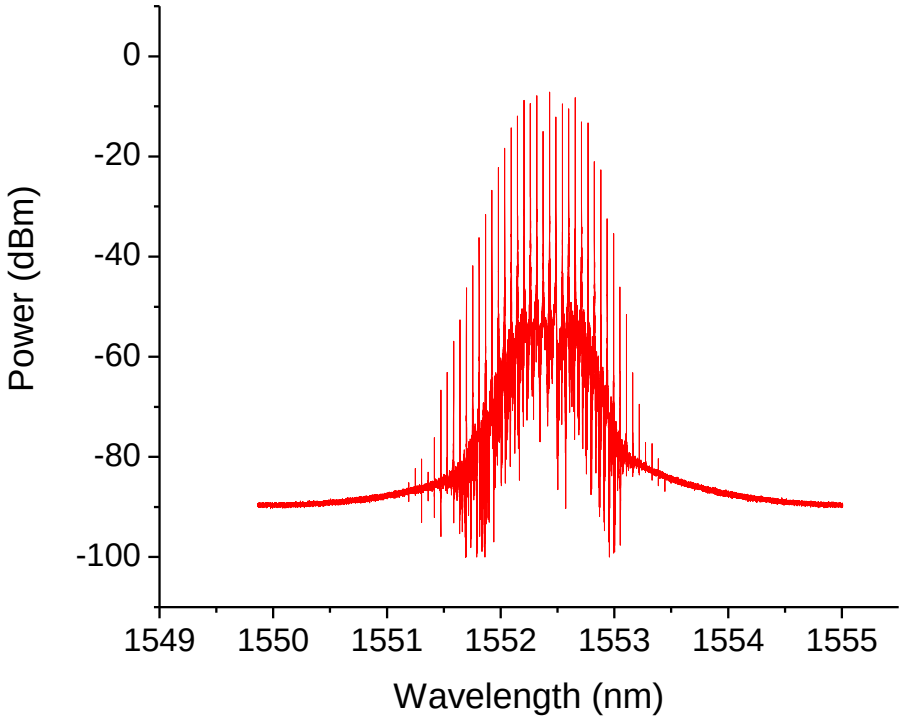

Figure 5.13 The generated optical comb of the gain-switched VCSEL laser at optimum switching current and frequency

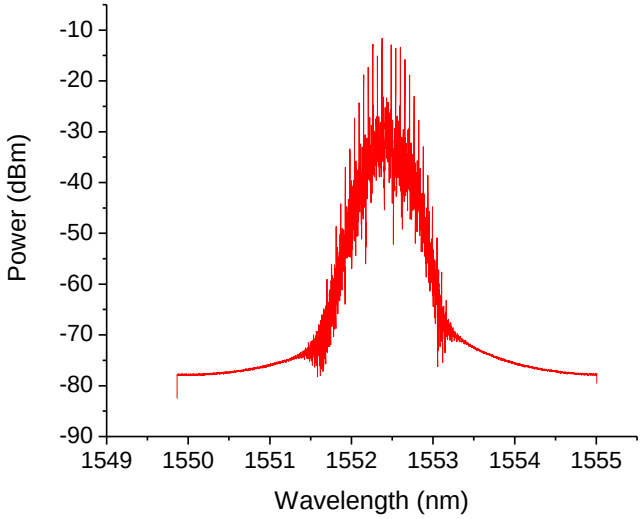

Figure 5.14 The generated optical comb when VCSEL laser is switched with current above optimal

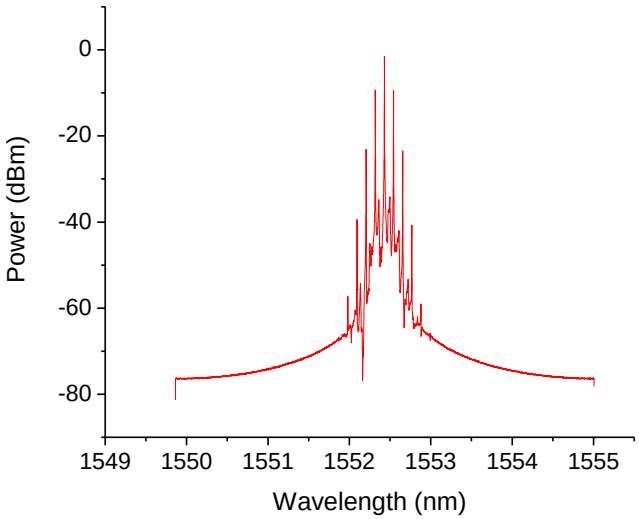

Figure 5.15 The generated optical comb when VCSEL laser is switched with current below optimal

When care is exercised to keep these operating parameters constant, the optical frequency comb of figure 5.13 generated through the proposed technique of figure 5.12 can be a good solution for designing photonic RF transmitters to coexist within radio astronomy areas. For example, the generated comb lines are coherent. Any two combs, spaced by the desired RF carrier frequency at which the 5G C-RAN should operate, can be filtered out and heterodyne them at the photodiode to generate the wireless signal. The resultant RF signal will be very coherent and will have very narrow linewidth because both optical lines are from the same optical cavity. This will be demonstrated in the following section. Higher frequency RF carriers can be generated, limited by the span of the achieved optical frequency comb. This feature allows the 5G C-RAN to operate at high bandwidth. Most importantly, the system is flexible. By changing the switching frequency of the electrical oscillator, the spacing between two consecutive comb lines can be varied resulting in a different RF carrier. It is important to note however that this will require some electrical or optical filters that can accurately tracks the shift in each comb line as discussed in section 4.2.3. Digital tunable optical filters can be used to select the desire comb line in case of RFI with the radio astronomer. This action will generate a different RF carrier which different from which the astronomer is observing. The most noteworthy advantage of this photonic RF transmitters is that only a single laser is used. In the next section, we will demonstrate the data transmission performance of this photonic RF transmitter when applied in a 5G C-RAN.

5.2.1.3 Fiber transmission performance of VCSEL-based OFC 5G C-RAN

We proposed a 5G C-RAN operating at 56-GHz carrier frequency for enhanced bandwidth to realize high data rates to the radio astronomer. The proposed network is based on the same configuration as figure 5.12. During this demonstration however, the PC, the MZM, the PPG, the optical fiber, and the BERT were now connected. Two optical channels at 1552.2048-nm and 1552.6549-nm, separated to give an RF carrier frequency of 56-GHz, were selected by a wavelength selective switch (WSS).

It is important to realize that it is possible to use this photonic system to realize radio communication services in radio astronomy without the effect of RFI. When RFI occurs, one of the selected channels can be changed to produce an RF carrier different from that at which the telescopes are observing. It is also worth noting that the WSS is needed for the experimental

characterization only. It is not needed for a real-world implementation, where instead a passive WDM splitter could be used to reduce network costs.

One of the filtered channel was modulated with data. The modulated channel was connected to a PC to match its polarization to that of the MZM biased at quadrature point [181]. To emulate a PPG, pseudo random bit sequence of 10- and 16.3-Gbps were generated and passed to the pulse generator. This resulted into 10- and 16.3-Gbps electrical data to the MZM. The modulated wavelength was combined at the optical coupler with the unmodulated wavelength acting as a local oscillator. The two combined wavelengths were then transmitted over a 20.5-km of standard single mode fiber (SSMF) to a 60-GHz PIN photodiode having a responsivity of 0.8 A/W. The optical spectrum analyzer (OSA) was used to monitor the two optical channels. The variable optical attenuator (VOA) was used to vary and keep the power to the photodiode constant. The modulated RF carrier signal at the output of the photodiode was monitored on an electrical spectrum analyzer (ESA) before amplification with an electrical amplifier of 26-dB gain. The low-pass filter (LPF) acted as an envelope detector and was then used to recover the transmitted baseband data. System performance analysis was performed based on bit error rate calculations using the BERT.

The two filtered wavelengths with one wavelength modulated with data is shown in figure 5.16. We notice in figure 5.16 that the WSS was able to accurately select the desired comb lines. The power of the two comb lines is also comparable, showing that the used WSS is not wavelength-dependent across its design bandwidth. The resultant 56-GHz RF carrier signal is shown in figure 5.17. The same data that was carried in one of the filtered wavelengths in figure 5.16 is also transferred to the generated 56-GHz RF carrier of figure 5.17.

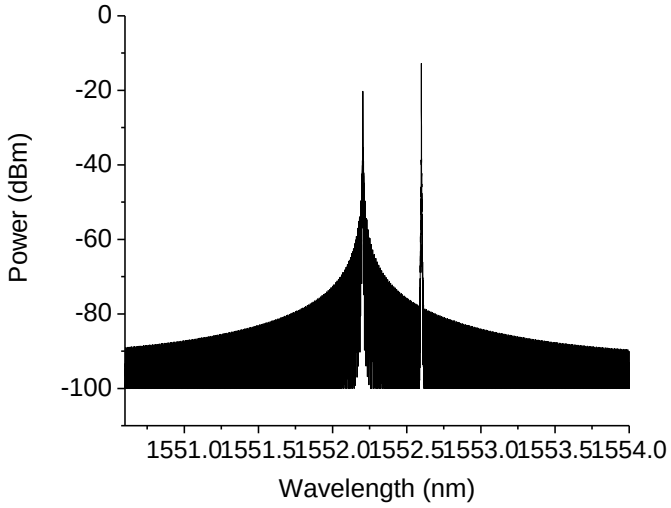

Figure 5.16 The two photonically-filtered comb lines with one comb carrying data

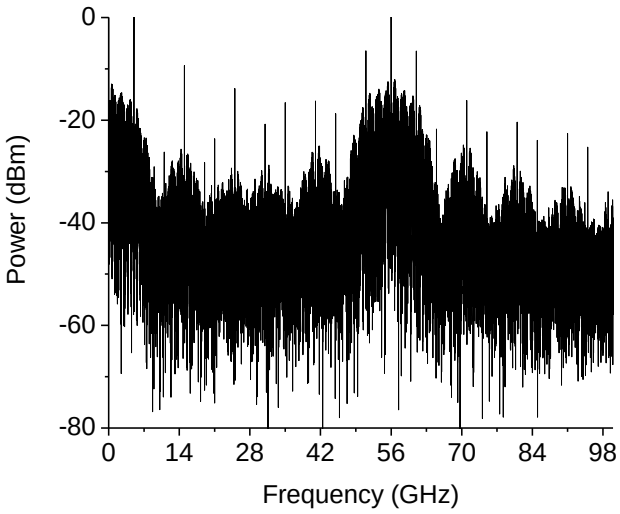

Figure 5.17 The resultant 56-GHz RF carrier signal amplitude-modulated with data

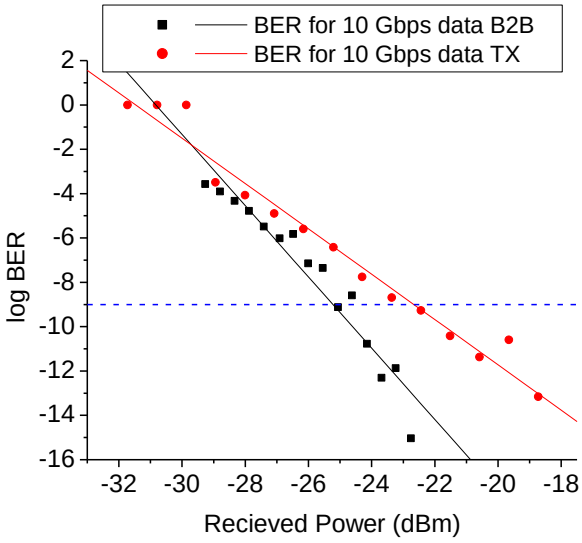

Figure 5.18 The BER curves for B2B and after 20.5-km fiber transmission at the 10-Gbps data rate

Data transmission performance of the VCSEL-based coherent 5G C-RAN was determined using BER calculations at both bit rates. The BER measurements were carried out for back-to-back (B2B) and over 20.5-km SSMF. The BER results at 10 Gbps data rate at B2B and over 20.5-km SSMF are shown in figure 5.18. As can be seen in figure 5.18, considering a BER of 10^{-9}, a fiber transmission penalty of 2-dB was obtained with a receiver sensitivity of -22.4 dBm. These results indicate that RF carrier signals generated from a gain-switched VCSEL comb are competitive for designing 5G C-RANs at 10-Gbps with fronthaul distance beyond 20 km. In section 3.4.1, we stated that the 5G C-RAN will have its central office located at the radio astronomy observing station. The 20-km distance over which the RF signal was transmitted in this demonstration shows that this photonic 5G C-RAN can be used to support remote areas around the astronomy areas at 20 km or less. By using optical fiber cables as fronthaul links from the radio astronomy station, neighboring farms and villages can be supplied with 5G

services. As the transmitter has the capability to mitigate RFI, both the astronomer and the 5G user in the community can enjoy advanced 5G applications supported by the photonic network.

The eye diagram at 10-Gbps after 20.5-km fiber transmission is given in figure 5.19. The eye is clearly open even after 20.5-km fiber transmission. The eye has an extinction ratio of 2.65-dB, qualitatively supporting the BER results.

Figure 5.20 shows the system performance at 16.3-Gbps data transmission for B2B and over 20.5-km SSMF. Considering the same BER of 10^{-9}, a slightly high transmission penalty of 7-dB was obtained with a receiver sensitivity of -18 dBm. Nevertheless, the system still demonstrated an attractive data transmission performance even at such a high bit rate. This further demonstrates the potential of VCSEL-based optical frequency combs for application in the proposed 5G C-RAN for high-speed data transmission. Corresponding eye diagram at 16.3-Gbps after 20.5-km fiber transmission is given in figure 5.21. The eye was still well open and had an extinction ratio of 2.49-dB.

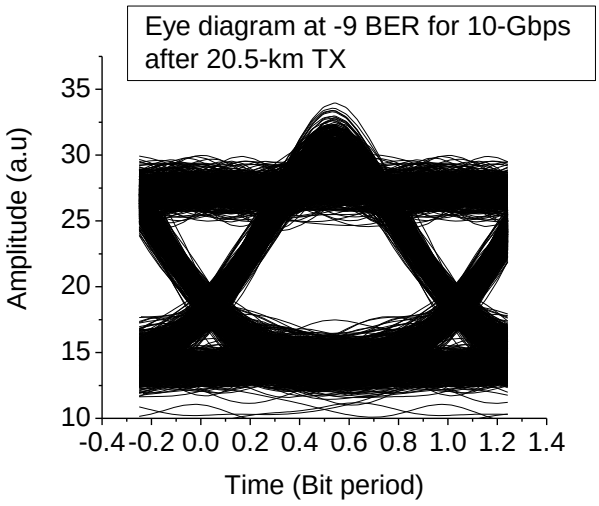

Figure 5.19 The Eye diagram after 20.5-km fiber transmission at the 10-Gbps data rate

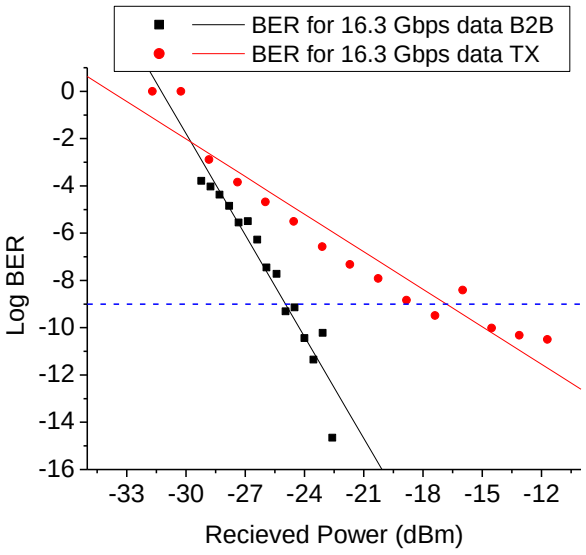

Figure 5.20 The BER curves for B2B and after 20.5-km fiber transmission at 16.3-Gbps data rate

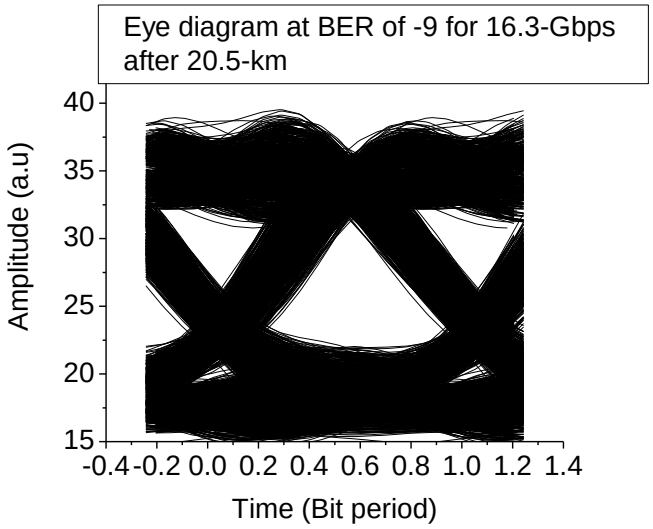

Figure 5.21 The Eye diagram after 20.5-km fiber transmission at 16.3-Gbps data rate

The results reported in this section have shown that VCSEL-based optical frequency combs can support error-free data transmission above 16-Gbps and could therefore be an attractive solution for designing the proposed 5G C-RAN in radio astronomy areas. Considering the broadband requirement for future 5G networks, our demonstration fulfilled this by delivering enhanced data rates beyond 10 Gbps.

Chapter Summary

In this chapter, we have demonstrated the application of VCSELs to realized intelligent 5G C-RANs which can be designed to coexist within radio astronomy areas. In the first demonstration, we developed a VCSEL-based photonic RF transmitter that is based on optical heterodyning of two independent VCSELs. The bias current-dependent wavelength for the VCSEL was interrogated to realize a flexible photonic 5G C-RAN that are capable of mitigating RFI due to spectrum collision with any radio system observing or operating at that same RF frequency. The limitations encountered by optical heterodyning as a photonic RF transmitter was mitigated by proposing novel techniques to overcome the resultant RF phase noise associated with this photonic RF generation scheme. The spectral efficiency was increased, for the first time, to an impressive data rate of 17 Gbps using advanced pulse amplitude modulation.

In the same chapter, we demonstrated an alternative technique to overcome the limitations of non-coherent photonic RF transmitters such as the optical heterodyning of independent lasers. We demonstrated a VCSEL-base coherent RF transmitter by gain-switching a single VCSEL. The advantages and adoptability of this novel photonic RF transmitter for use in radio astronomy areas without the effects of RFI was also unpacked. Improved data rates were demonstrated using this techniques. The results reported in this chapter are novel. They pave the way toward an exciting future. A future where low-cost VCSEL lasers are used to realize intelligent 5G systems that can be used in radio astronomy to realize radio communication services without the threat of radio interference to the astronomer.

Chapter 6: Optical Carrier Power Optimization in VCSEL-based OFC Generation

A well-known photonic technique for generating high-frequency RF carrier signals was discussed in section 4.2, and it was demonstrated for the first time, using low-cost VCSELs, in section 5.3. This photonic RF transmitter is based on optical frequency comb (OFC) generation. Section 5.3 demonstrated how this photonic RF transmitter can be used in 5G centralized radio access networks (5G C-RAN) to realize radio communication service within radio astronomy areas without the effects of radio frequency interference (RFI) to the astronomer. The results of section 5.3 showed the efficiency of the photonic RF transmitter for such applications.

In the optical frequency comb generation technique, the photonic generation of RF signals involves filtering out two optical signals and optically heterodyning them at a high-speed photodiode [182]. One of the filtered signals is modulated externally with an optical modulator and the other unmodulated signal acts as a local oscillator. High frequency RF signal generation based on optical frequency comb generation [182] is more attractive because it can generate coherent multi-mode optical sources. The generated multi-mode optical spectrum (see figure 5.13) consists of phase-correlated wavelengths. Any two optical lines from generated comb can be filtered and be heterodyned to generate RF carriers with good phase noise performance [183]. For radio astronomy areas to realize mobile communication services, the optical frequency comb generation technique is considered attractive both in its design and the phase-noise performance of the resultant RF signals. The advantages and disadvantages for optical frequency comb generation technique were discussed in section 4.2.3 of this thesis.

In optical comb generation techniques, the quality of the comb is measured by the number of combs lines generated by the system. The flatness of the resultant optical frequency comb is also a factor of merit [184]. Many techniques have been suggested to expand and improve the flatness of a single-stage optical comb generation generator [185]. Such techniques seek to ensure that any two filtered optical lines from the comb should have equal optical powers to be detected by the photodiode. The main reason for improving the optical span of the comb is to enable the generation of high-frequency RF carriers in the terahertz region [182]. However, achieving both flat and wide optical frequency combs is rather costly and complex. This can jeopardize the application of such photonic RF transmitters for novel 5G communication.

Researchers have suggested that for radio communication purpose, the flatness of the comb is more critical. They have also suggested that the useful comb lines are those having an optical power ratio of 3-dB or 10-dB relative to the most powerful comb line [144]. However, this requirement is yet to be validated. The effects of the optical power ratio between the two optical lines selected from an optical frequency comb on the generated RF carrier signal and on the baseband data signal is yet to be studied. It is not yet clear whether there is necessity that both optical comb lines should have equal powers. It is also not clear how the power ratio between the two selected optical lines affects the 5G C-RAN performance.

In this chapter, for the first time to our knowledge, we numerically investigated the effects of optical local oscillator signal power on a photonically-generated RF carrier signal power and on the baseband signal. We used a VCSEL-based optical frequency comb in our study. The study was considered in the frequency band around 60-GHz, frequency of interest for future 5G C-RANs.

6.1 Study on effects of optical power ratio between two selected comb lines

To investigate the effects of optical power ratio between the two selected comb lines on the generated RF carrier signals and the transmitted baseband signal, we adopted a 5G C-RAN architecture given in figure 5.12. The two channels chosen by the wavelength selective switch (WSS) are 1552.20-nm and 1552.65-nm. For the purpose of this study, and in order to replicate a flat comb that is being suggested by many researchers, both channels were chosen to have comparable optical powers of -7.19 dBm and -8.01 dBm, respectively. The channel spacing was selected to give a 56-GHz RF beat frequency. The wavelength with -7.19-dBm optical power was then connected to an MZM biased at quadrature point [181] and modulated with 16-Gbps baseband signal. The modulated optical carrier signal was connected to a polarization controller (PC) to align the light polarization to that of the MZM. A pseudo random bit sequence of 16-Gbps was generated and used to modulate the optical carrier. The modulated optical carrier signal was then combined with the optical local oscillator signal at the optical coupler. These two combined signals were then amplified by an optical amplifier with 20-dB gain and 6-dB noise figure. The signal was then transmitted over 21-km SSMF to a photodiode. The variable optical attenuator just after the fiber was used to vary and keep the power to the photodiode constant. For baseband signal analysis, the RF carrier signal at the output of the photodiode was then amplified with a transimpedance amplifier (TIA) having a noise figure of 3-dB and a 700-ohm feedback resistor. A low-pass filter (LPF) with 16-GHz cut-off frequency was then used to recover the transmitted baseband data signal for its analysis. The RF carrier signal was received immediately after the photodiode so that the effect of the electrical amplifier is not included in its analysis.

6.2 Results and analysis on the effects of optical power ratio

We present and discuss the effects of optical power ratio between the two selected wavelengths on both the generated RF carrier signal and the transmitted baseband signal. The investigation was to study how the BER results are affected when the power of the optical local oscillator signal is above that of the modulated optical carrier signal. Figure 6.1 shows the two filtered optical lines before modulating one. At this point, we notice that both optical signals had equal powers. The optical carrier signal at lower wavelength was then amplitude-modulated with 16-Gbps binary data using an MZM. Due to the MZM's insertion losses, the power of the modulated optical carrier signal was reduced below the power of the optical local oscillator signal. This is visible in figure 6.2. It is important to realize that figures 6.1 and 6.2 is how a typical two-tone spectrum, filtered from a flat optical frequency comb will appear, before and after modulation of the optical carrier signal, respectively. The two signal of figure 6.2 were then transmitted to the photodiode to generate a photonically-modulated RF carrier signal. The photonically-modulated RF signal now have both the baseband and the RF carrier signal.

Figure 6.3 is the RF spectrum when the optical signals of figure 6.2 were beating at the photodiode. The RF power of the carrier signal is -15.3 dBm. Figure 6.4 is the time waveform of the spectrum of figure 6.3. We notice in figure 6.4 that when the optical spectrum of figure 6.2 was beating at the photodiode, the generated RF carrier signal fully filled up the baseband pattern. Figure 6.5 shows the eye diagram for the time waveform of figure 6.4 after envelop detection using a low-pass filter. We observed on figure 6.5 that the 0-bit value of the data signal is shifted above zero. It will be shown in this section that the eye diagram of figure 6.5 was strongly influence by the optical power ratio between the optical carrier signal and the optical local oscillator signal.

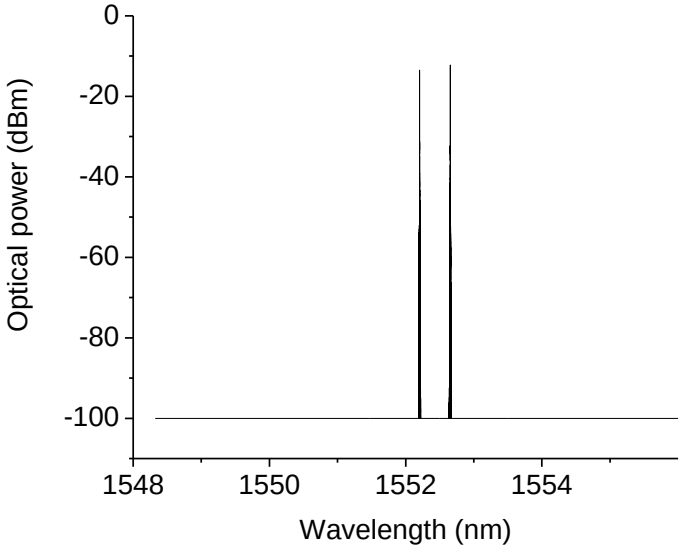

Figure 6.1 Two comb lines separated by 56 GHz before one comb line being modulated. The -100-dBm noise floor is due to the WSS used to filter the two signals.

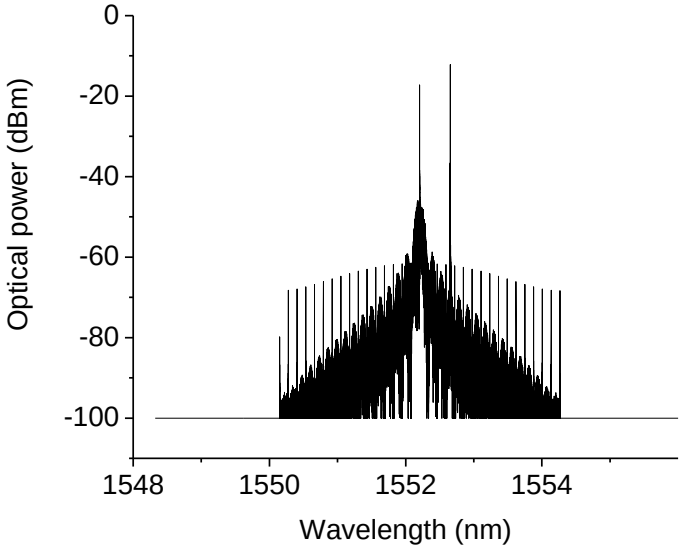

Figure 6.2 Two comb lines separated by 56 GHz after one comb line is being modulated. MZM insertion losses introduced a power reduction in the modulated line.

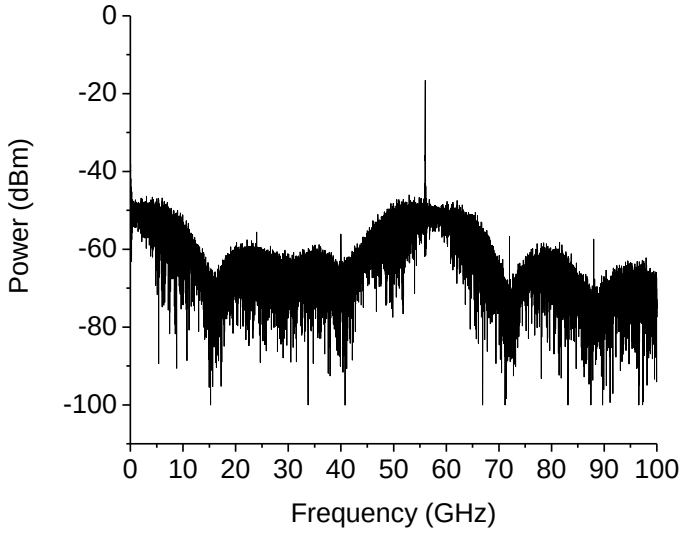

Figure 6.3 The 56-GHz RF carrier with 16-Gbps data before attenuation of the optical local oscillator signal power.

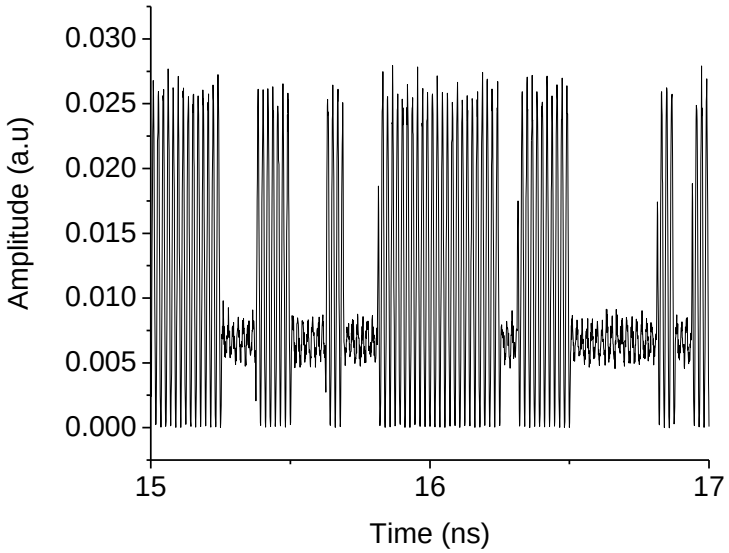

Figure 6.4 RF and baseband signals time waveforms when optical local oscillator signal power is above the optical carrier signal power, corresponding to an attenuation value of 0-dB on figure 6.7.

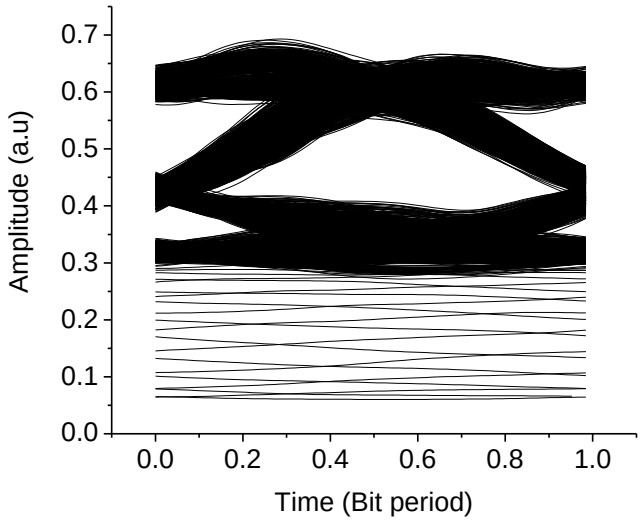

Figure 6.5 Eye diagram at BER of 10^{-9} before attenuation of the optical local oscillator signal power

The next step was to determine the bit error rate (BER) results under the condition of figure 6.2. This was necessary to determine how the 5G C-RAN will perform under the condition when the optical carrier power is below the optical local oscillator power, a situation inherently experienced with flat optical frequency combs due MZM losses. The BER calculations were determined for back-to-back (B2B) and over 21-km SSMF. For baseband signal analysis, the RF carrier signal was filtered out for BER calculations. It is very important to explain the reason for filtering out the RF carrier in this case.

It is worth mentioning that the 5G C-RAN proposed in this thesis can find application not only in wireless communication networks, but also in next-generation hybrid systems where both mobile and fixed user are supported. This case was demonstrated in chapter 8 of this thesis. In such hybrid 5G networks, wavelength division multiplexing (WDM) will be used. It will involve the multiplexing of two or more optical lines to support both fixed and wireless users [186]. It is therefore necessary to investigate how the power ratio between the selected optical lines affects both the fixed and wireless astronomical user. Therefore, the filtering out of the RF carrier signal applies to a case when the 5G C-RAN is connecting a fixed astronomer who does not need the photonically-generated high-frequency RF signal.

The effects on the fixed user were determined by calculating the BER values. The results are shown in figure 6.6. As can be seen in that figure, when considering a BER of 10^{-9}, a power penalty of 14-dB was obtained. The receiver sensitivity at this BER value was 7.5 dBm. In figure 6.6, we can notice how the BER values improved after fiber transmission when considering optical powers of -15 dBm and above. It was demonstrated in [170] that RF carrier signal power can be enhanced in photonic-based RF generation when the optical pulse is compressed through fiber transmission. This effect could have ultimately contributed to the improved BER results after fiber transmission and after envelop detection when filtering out of the RF carrier signal to receive the baseband pattern.

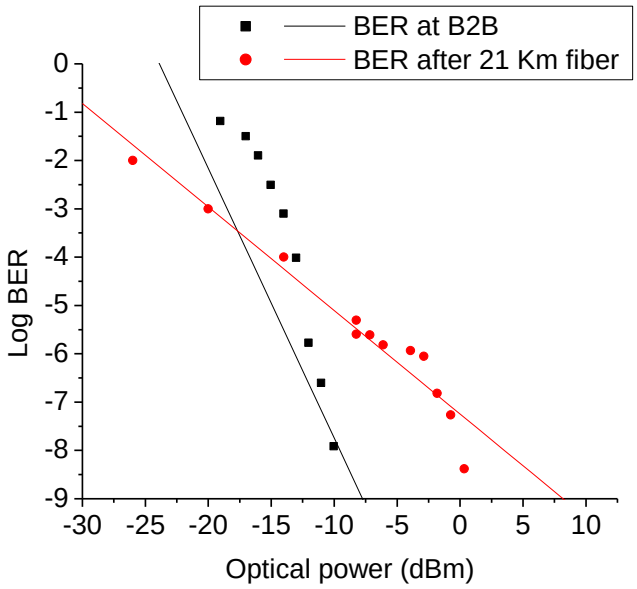

Figure 6.6 BER for B2B and after fiber transmission before attenuation of the optical local oscillator signal power.

In the next study, we investigated how reducing the optical local oscillator signal power below the power of the modulated carrier will affect both the RF power and the baseband signal. Naturally, as seen in figure 6.2, due to the intrinsic insertion losses of the MZM, especially in a system employing a flat optical frequency comb [187], the optical local oscillator signal power will always be high relative to the power of the modulated optical carrier signal. We were interested on how reducing the optical local oscillator signal power below the power of the modulated optical carrier signal affects both the baseband signal and the RF carrier power.

It is worth mentioning that the case when the optical local oscillator power is below the modulated optical carrier signal can only be obtained if the generated optical frequency comb is not flat and an MZM with some insertion loses is used. As highlighted in the preceding paragraphs, the generation of flat optical frequency comb is complex and requires additional systems to achieve them. Additionally, low-insertion-loss MZMs can be expensive to realize. In our proposed 5G C-RAN, we needed to make the photonic RF transmitter as simple as possible. This can only be realized if the necessity for a flat optical combs is avoided, and when cheap MZMs with some reasonable insertion losses are used. However, before these recommendations, we needed to validate our arguments that flat optical combs and low-insertion-loss MZMs are not strict requirements in designing 5G C-RAN based on optical frequency comb photonic RF transmitters.

To study the effects of reducing the optical local oscillator signal power below the power of the modulated optical carrier signal, the optical local oscillator signal power was attenuated using a variable optical attenuator before being combined with the modulated optical carrier signal at the optical coupler. These results are shown in figure 6.7. We can see that when increasing the attenuation for the optical local oscillator signal power, the BER results are improved. However, attenuating the optical local oscillator signal power results into a loss of power in the generated RF carrier signal. These effects can be explained intuitively as follow.

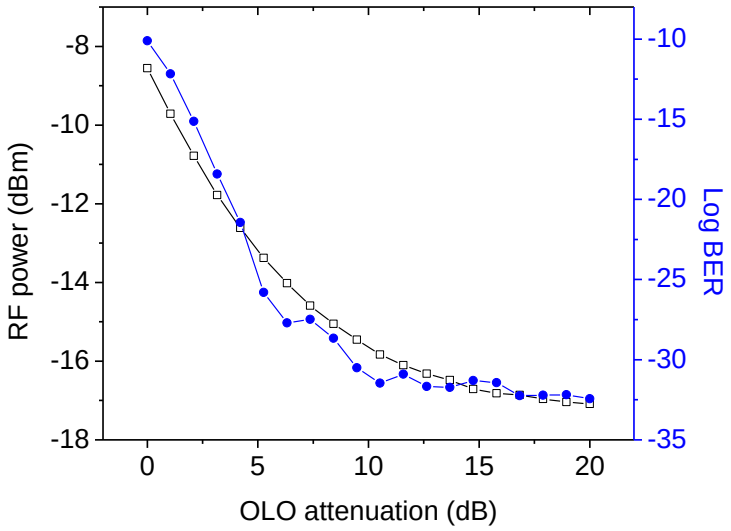

Figure 6.7 Effects of optical local oscillator signal power attenuation on both the BER (baseband signal) and the RF carrier signal.

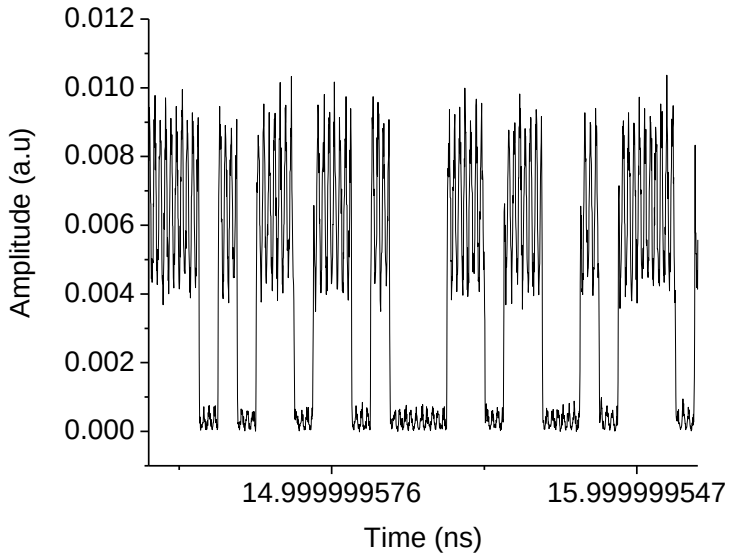

Figure 6.8 RF and baseband signals time waveforms when optical local oscillator signal power is below the optical carrier signal power

When the optical local oscillator signal has more power than the modulated optical carrier signal, the cross talk between the two optical signals is increased. Therefore, the beating frequency at the two heterodyning optical signals at the photodiode is increased. This can be seen in figure 6.4 where the signal at the beat frequency is flooding the baseband signal. Without effective filtering at the receiver, the received baseband signal will be erroneous, as supported by figure 6.6 and can be noted in figure 6.7.

However, when the optical local oscillator signal power is below the power of the modulated optical carrier signal, the beat frequency power is reduced. This is evident on figure 6.8. This favors the baseband signal and hence a better BER is expected, supported by figure 6.7.

To validate this, we calculated the BER values when the optical local oscillator signal power is below the power of the modulated optical carrier signal. From figure 6.7, we can see that minimum BER was obtained with a 15-dB attenuation of the optical local oscillator signal power. We therefore evaluated the transmission penalty and the receiver sensitivity at this attenuation value. The two filtered comb lines with the optical local oscillator signal power being attenuated are given in figure 6.9. The BER curves and the eye diagram as a result of figure 6.9 are given in figure 6.10 and figure 6.11, respectively. We can see that the same BER value of 10^{-9} was now achieved with a lower receiver sensitivity of -13dBm compared to the power at the same BER when the optical local oscillator signal had more power.

A careful analysis of figure 6.7 shows that, by keeping the optical local oscillator signal power fixed and attenuating the optical carrier signal power, there can exist a power ratio between the two optical signals where the power of the RF carrier signal could be enhanced.

From the above findings, we can conclude that when this technique is used for hybrid 5G C-RAN to the astronomer, the RF designer can optimize the power of the RF carrier such that both the fixed user and the wireless user does not suffer any consequences due to the presence of the other. For example, when a 5-dB attenuation is applied to the local oscillator signal, the wireless carrier signal will have about -14 dBm of RF power. This power can be radiated to support 5G mobile devices. In case this power is not enough, low-gain electrical amplifiers can be used to achieve the needed link gain. At the same attenuation of 5-dB, the fixed user will receive error-free data with an excellent BER of 10^{-25}, way below the recommended minimum BER of 10^{-9}.

Figure 6.12 shows BER performance of the 5G C-RAN before and after attenuation of the local oscillator signal power. We can notice on that figure that, for the baseband signal, a power penalty of more than 18-dB is introduced when care is not taken to attenuate the optical local

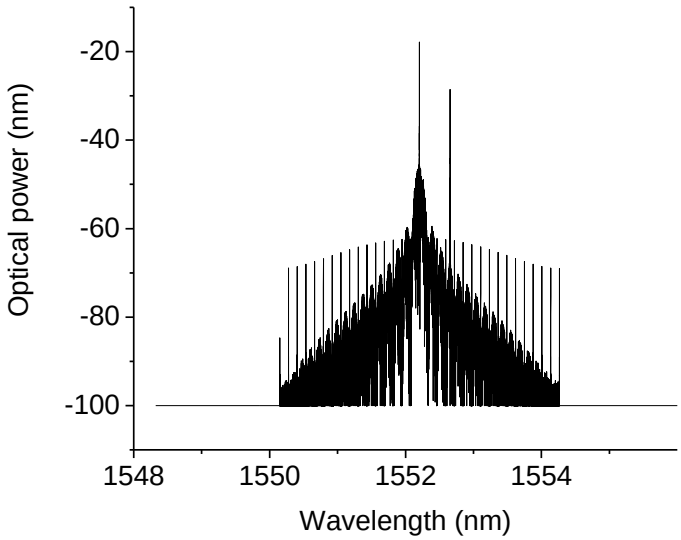

Figure 6.9 Two comb lines separated by 56 GHz after optical local oscillator signal power attenuation.

oscillator signal power optimally to reach an error-free BER. This power penalty can get worse in amplitude-modulated and high-bit-rate networks. The attenuation of the optical local oscillator power below the optical carrier power produced more than 18-dB improvement in term of receiver sensitivity. This is also supported by figure 6.11 where the 0-bit value was lowered toward the minimum value, consequently improving the extinction ratio and the BER of the system.

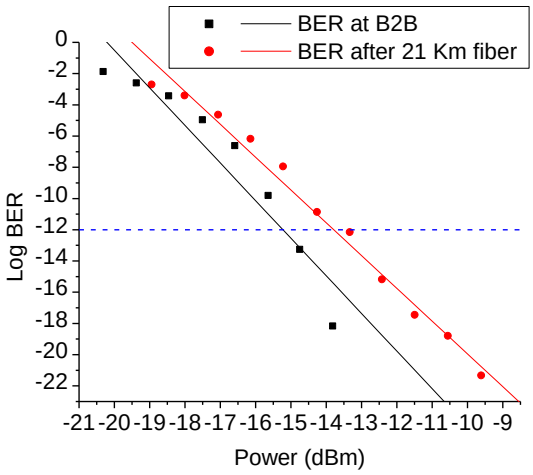

Figure 6.10 BER after attenuation of optical local oscillator signal power.

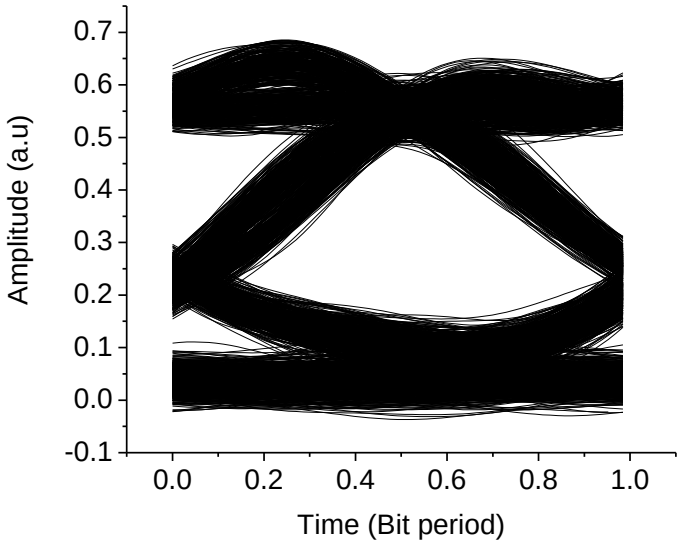

Figure 6.11 Eye diagram after attenuation of the optical local oscillator signal power.

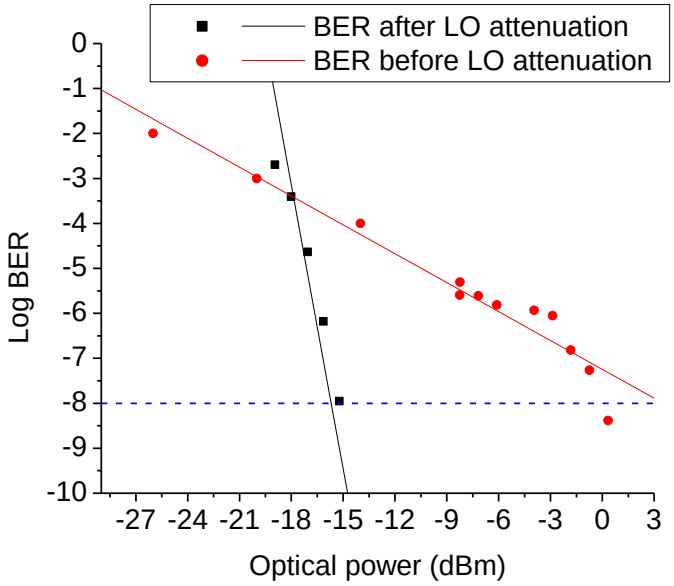

Figure 6.12 BER after and before 15-dB attenuation of the optical local oscillator signal power

Chapter Summary

In summary, this chapter has demonstrated that complex photonic RF transmitter configurations to achieve flat optical frequency combs in photonic 5G C-RANs is not a strict requirement. Also, the study demonstrated that optical frequency comb-based RF transmitters can be used with MZMs having reasonable insertion losses to the advantage of the network user. By appropriately selecting the heterodyning comb line powers, guided by figure 6.7, the 5G network designer can use non-flat optical frequency combs and low cost MZMs to achieve excellent network performance for both the fixed and wireless user. This ultimately reduces the over photonic RF transmitter cost.

The results reported in this chapter will also help 5G C-RAN designers to determine the degree to which the neighboring combs lines can be attenuated to achieve a certain BER value. This will in turn assist with the selection of appropriate WSS to meet the required system performance. Figure 6.7 also predicted that by reducing the power of the modulated optical carrier signal below the power of the optical local oscillator signal, the RF carrier power could be increased. Interestingly, results reported in this chapter suggest that indeed MZM with some degree of insertion loses can improve the RF power in system where flat optical frequency combs are used as flexible photonic RF transmitters.

At this point of the study, the dependence of the effect optical local oscillator power on the modulation format, system bit rate, transmission distance, and the driving and bias voltages of the MZM cannot be generalized. However, we can conclude from the findings that amplitude-modulated systems are likely to be affected positively when care is exercised to reduce either the optical local oscillator signal power (for baseband signals) or the optical carrier signal power (for the wireless RF carrier signal).

Chapter 7: VCSEL-based OFC for Application in WDM-based 5G C-RAN

The fifth generation (5G) of radio communication networks target unprecedented performance, not only in terms of higher data rates per user and lower latency, but also in terms of network intelligence and capillarity. Hybrid 5G centralized radio access networks (5G C-RANs) based on wavelength division multiplexing (WDM) are considered as outstanding candidates for realizing such performances. The WDM network can be used to transport different services across the 5G network. Each wavelength can be used to transport a unique data signal to the intendent user. In chapter 5, we demonstrated two 5G C-RANs based on vertical cavity surface emitting lasers (VCSELs). Section 5.3 of that chapter specifically used a VCSEL-based optical frequency comb to transmit coherent wireless data signals at high bit rates to the astronomer. In that demonstration, the 5G C-RAN was used to support only a single application where only the wireless 5G user was served by the network. The optical comb in figure 5.13 has more than 50 comb lines, each with good optical power. These optical carrier can be harnessed to support multiple applications.

In this chapter, we will demonstrate for the first, a novel VCSEL-based 5G C-RAN where an optical frequency comb (OFC) is used as the photonic RF transmitter to support more than one application scenario. Recall that the photonic 5G C-RANs proposed in this thesis are to be used in radio astronomy areas to realize radio communication services. In addition to that purpose, chapter 7 will demonstrate an additional application of a VCSEL-based optical frequency comb. The new application to be demonstrated is very relevant to radio astronomy. It involves the coherent dissemination of clock signals over optical fibers to the telescope arrays. Telescope arrays are synchronized with precise RF clock signals for accurate time-stamping of the observed data [188]. The clock signals are transported to the telescope through optical fiber. In legacy network, different lasers are used for the transmission of data and clock signals [188]. This becomes costly to implement and manage. In this chapter, we demonstrate a novel technique where a single VCSEL is used to transport both 5G data signals and clock signals for telescope synchronization. The VCSEL laser is gain-switched to obtain an optical frequency comb such as that in figure 5.13. The resultant comb lines were used for the transmission of 5G data and reference clock signals to the telescopes.

It is important to keep in mind that the clock performance results reported here were discussed in the content of 5G network latency monitoring. However, the same clock can also be used for synchronization of radio telescope arrays. This means that by using a single VCSEL carrier, the radio astronomer realizes a photonic systems that is able support three distinct services simultaneously. Firstly, a single VCSEL carrier is used to realize 5G radio communication services to the astronomer without the effects of RFI. Secondly, the same VCSEL is used to disseminate reference clock signals to the radio telescopes. Finally, same clock can be used to monitor the network latency of the implemented 5G C-RAN. To our knowledge, this is the first time such a 5G network scheme is reported.

7.1 Demonstration of VCSEL-based clock and data signals transmission

We have proposed a 30-Gbps VCSEL-based WDM 5G C-RAN with three amplitude-modulated optical channels at 10-Gbps and one carrier with amplitude-modulated 50 MHz reference clock signal which can be used either for telescope synchronization or for 5G network latency monitoring purpose. Our proposed network architecture is given in figure 7.1.

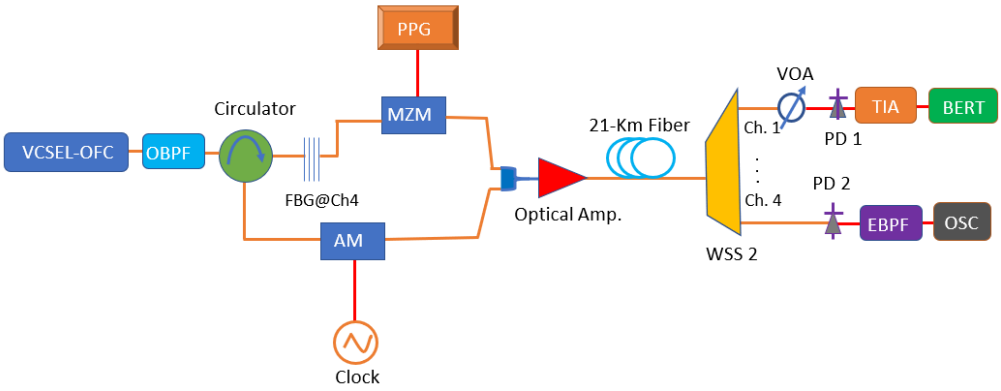

Figure 7.1 Experimental schematic of the proposed WDM VCSEL-based 5G C-RAN

In figure 7.1, the "VCSEL-OFC" box represents the setup in figure 5.12 where the VCSEL is gain-switched by an electrical signal from the sine generator to generate the optical frequency comb.

In order to mitigate the cross-talk effects, the switching frequency of the signal from the sine generator was increased to 20 GHz. The effect of increasing the switching frequency reduces the number of comb lines, but the spacing between two consecutive comb lines is increased. Increasing the frequency spacing between comb lines is necessary for high-speed data transmission. In our network, the number of comb lines within the 10-dB envelop were reduced to 5 comb lines from the 11 comb lines generated at 14 GHz switching frequency.

Four wavelength channels at 1552.27-nm, 1552.42-nm, 1552.59-nm, and 1552.75-nm were selected by an optical bandpass filter (OBPF) having a 100-GHz bandwidth. Using the circulator and a fiber Bragg grating (FBG), the fourth wavelength at 1552.75-nm was selected and amplitude-modulated (AM) with a 50-MHz clock signal meant either for latency monitoring at each optical network unit or for synchronization of telescope arrays. The three optical channels modulated with data were connected to a polarization controller to supply the MZM with the required polarized light. The MZM was biased at quadrature point [181]. To emulate a PPG generator, pseudo random bit sequences of 5- and 10-Gbps were generated and passed to an electrical pulse generator. The three modulated wavelengths were combined at the optical coupler with the fourth wavelength carrying the clock signal. The four channels were then amplified with a 20-dB gain and 6-dB noise figure optical amplifier before being transmitted over the 21-km standard single mode fiber to the receiving end.

For BER testing, the variable optical attenuator (VOA) was used to vary and keep the power to the photodiode (PD) constant. The baseband data signals at the output of the 10-GHz-bandwidth photodiodes (PD 1 to PD 3) ware amplified with a transimpedance amplifier having a noise figure of 3-dB and a 700-ohm feedback resistor. The BER tester (BERT) was used to calculate the bit error rate for each channel.

For clock signal recovery, a second photodiode (PD 2) with 10-GHz bandwidth was used to recover the 50-MHz electrical frequency. Due to the high bandwidth of the photodiode, the crosstalk effect on the clock signal was minimized by using a 50-MHz electrical bandpass filter (EBPF) having a 1-MHz bandwidth [189]. The recovered clock signal was then visualized on an oscilloscope (OSC).

7.2 Clock and data signals transmission performance

In this section, we will present and discuss the results from the procedures of section 7.1. The data transmission performance for the three optical carrier signals selected from the VCSEL-based optical frequency comb will be given and discussed in section 7.2.1, and the clock performance will be discussed in section 7.2.2.

7.2.1 Data transmission performance of optical carriers from the VCSEL OFC

The three optical carriers were simultaneously amplitude modulated with 5- and 10-Gbps binary data to model a broadcasting network where each end-user receive the same information [190]. Figures 7.2 and 7.3 show the four optical carriers before and after modulation, respectively. Both optical carriers had optical powers above -7 dBm, excellent optical powers to enable them to be transported over fiber distances beyond 20 km. Data transmission performance for the three optical carriers was determined based on bit error rate (BER) calculations. The BER calculation were based on the Q-factor method. The performance for each channel was determined independently. BER were calculated for back-to-back (B2B) and over 21-km standard single mode fiber (SSMF).

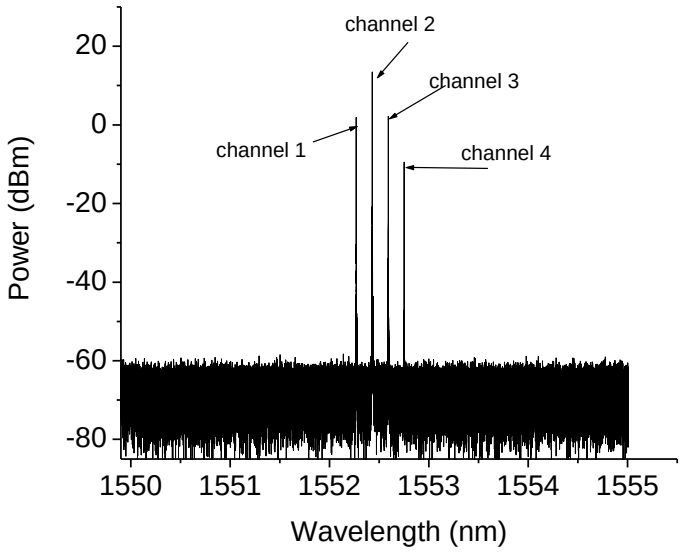

Figure 7.2 The four selected optical carrier channels before being modulated with data and clock signal. Channels 1 to 3 were used to carry data while channel 4 was used to carry the clock signal

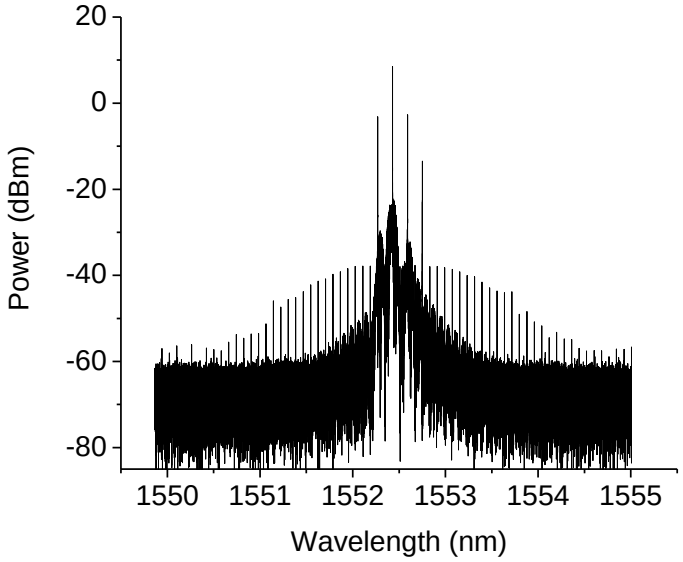

Figure 7.3 The four selected optical carrier channels after being modulated with data and clock signal. Channel numbers are as marked in figure 7.2 above.

The results for the three optical carrier at 5-Gbps binary modulation is shown in figure 7.4. As can be seen in figure 7.4, when considering a BER of 10^{-9}, a negligible fiber transmission penalty was obtained after 21 km fiber transmission. This was the case for channels 1 and 2. Channel 3 had a slightly high transmission penalty compared to the other two channels since this carrier was sandwiched between a data- and a clock-carrying carrier. It performed less effectively compared to channel 2 which was also sandwiched between two data-carrying carrier because channel 2 had much power relative to channel 3. Nevertheless, both carriers were able to deliver error-free data at receiver sensitivities less than -18 dBm. These results indicated that a gain-switched VCSEL optical frequency comb can be used to in 5G C-RANs to support error-free data transmission at 5-Gbps over optical fiber lengths exceeding 20 km. The 20-km fronthaul distance reported here is attractive. This is because in cases where a 5G network designer choses to locate the central office some 20 km away from the radio astronomy area, the 5G C-RAN can still support the astronomer with high-speed data without the consequences of RFI.

The results for the three optical carrier at 10-Gbps binary modulation is shown in figure 7.5. As can be seen in figure 7.5, when considering a BER of 10^{-9}, fiber transmission penalties of 0.7-dB, 2.5-dB, and 4.8-dB were obtained after 21 km fiber transmission for channel 1, channel 2, and channel 3, respectively. Channel 3 had a high transmission penalty compared to the other two channels since this carrier channel was sandwiched between data- and clock-carrying carriers and therefore experienced more cross talk. It also performed less effectively compared to channel 2 which was also sandwiched between two data-carrying carrier because channel 2 had much power relative to channel 3. Nevertheless, both carriers were able to deliver error-free data at a receiver sensitivity of less than -10 dBm. Channels 3 and 2 had an error floor at 10^{-9} and 10^{-14}, respectively. These results indicated that a gain-switched VCSEL optical frequency comb can also support error-free data transmission at 10-Gbps over optical fiber lengths exceeding 20 km. The high data rates reported here are also useful because the radio

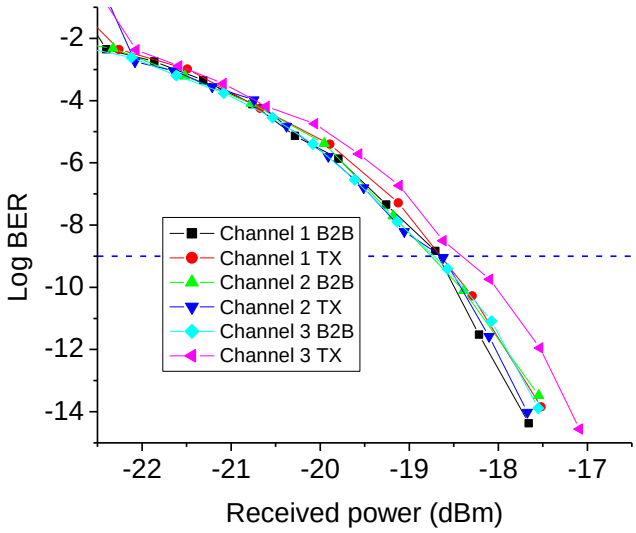

Figure 7.4 BER at 5-Gbps for the three data-carrying optical carriers

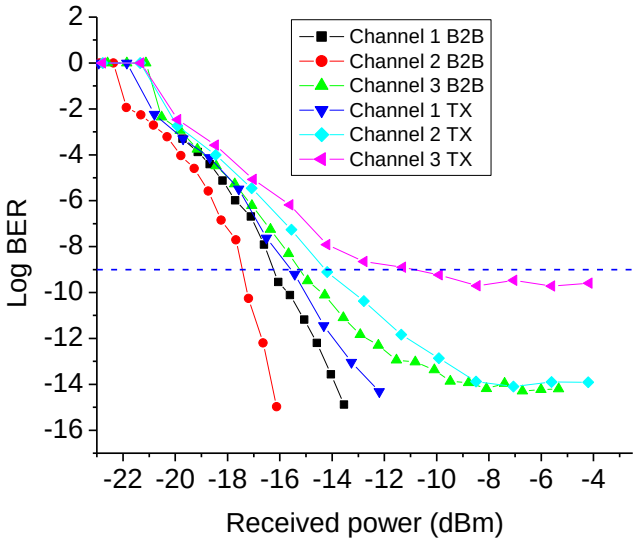

Figure 7.5 BER at 10-Gbps for the three data-carrying optical carriers

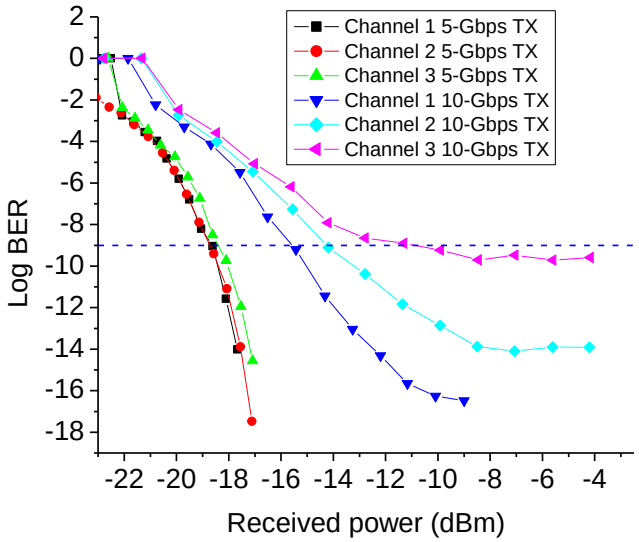

Figure 7.6 BER performance at 5- and 10-Gbps for the three optical carriers

astronomer will be provided with novel mobile and fixed applications requiring such bandwidths. For example, most of the applications for 5G will require broadband communication systems. Our 5G C-RAN proposed here is therefore promising to fulfil the network requirements for modern and future application scenarios.

Figure 7.6 shows a summary of the transmission performance for the three optical carrier signals at 5- and 10-Gbps. From figure 7.6, we can notice that the three optical carriers had a comparable performance at 5-Gbps. Both carriers had a receiver sensitivity of around -17.9-dBm after 21-km fiber transmission. Increasing the system capacity from 5 Gbps to 10 Gbps resulted in a transmission penalty of 2-, 4-, and 6-dB for channel 1, 2, and 3, respectively. The receiver sensitivity for channels 1, 2, and 3 were -16 dBm, -14 dBm, and -12 dBm, respectively. These optical powers for the three channels at this BER are all practical and they can be attained in physical systems without the need for expensive optical amplifiers.

7.2.2 Clock transmission performance of optical carriers from the VCSEL OFC

We proposed a VCSEL-based WDM 5G C-RAN where a clock signal is transmitted together with the data signals. The clock signal can be used for monitoring of network latency or for time-stamping of astronomical data. For latency monitoring in future 5G C-RANs, the clock integrity in term of phase-noise should be good enough for strict system optimization. Since the clock was amplitude-modulated on the optical carrier, its spectrum can affect the data of its immediate adjacent carrier. This is especially true when the bandwidth between the clock-carrying carrier and the data-carrying carrier is not big enough to avoid cross-talk effects. We have shown in section 7.2.1 that, at 20-GHz frequency spacing between a data-carrying carrier and a clock-carrying carrier, the clock signal does not affect the data integrity of the network. Error-free data transmission was achieved at both bit rates when the clock was transmitted together with the data carrying carriers. In this section, we will show the effect of the data-carrying carriers on the performance of the transmitted clock signal. These results are shown in figures 7.8 and 7.9 for 5- and 10-Gbps data rates, respectively.

Figure 7.7 is the spectrums for the clock signal at the network bit rates for B2B and after fiber transmission. The power of the electrical clock signal was -0.83 dBm. The power was

slightly reduced to -0.96 dBm at B2B (before transmission over fiber). Fiber attenuation reduced the clock power to -16.2 dBm. This gave a transmission power penalty of about 15.37 dB. From figure 7.8, it can be seen that the amplitude-modulated 50-MHz clock signal was recovered without any phase-shift penalties when transmitted with optical carriers which are amplitude-modulated at 5-Gbps data rate. Apart from a reduction in the amplitude of the clock signal, the time-domain phase of the received clock signal is similar to that of the electrical clock signal. On the same figure 7.8, the peak-to-peak amplitude of the electrical clock signal was 0.05 a.u. This clock amplitude was reduced to 0.032 a. u and 0.014 a. u at B2B and after 21-km fiber transmission, respectively.

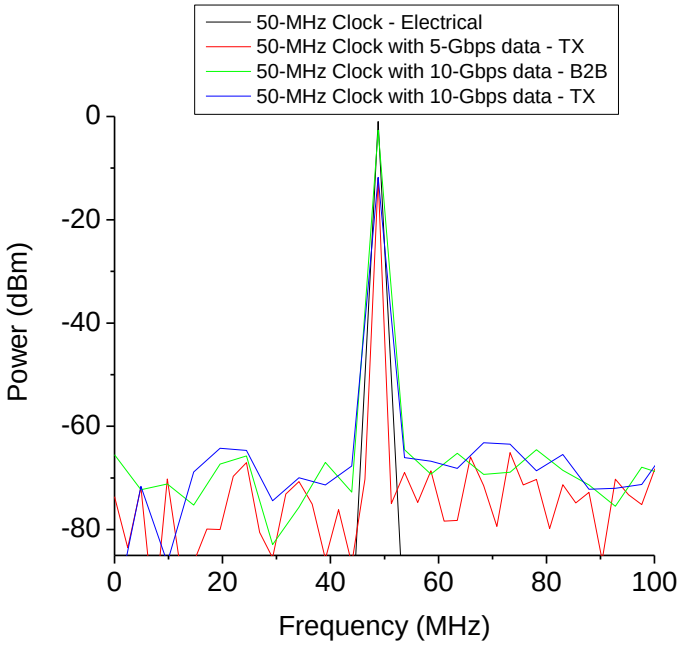

Figure 7.7 50-MHz clock spectrum transmitted at 5- and 10-Gbps data rate

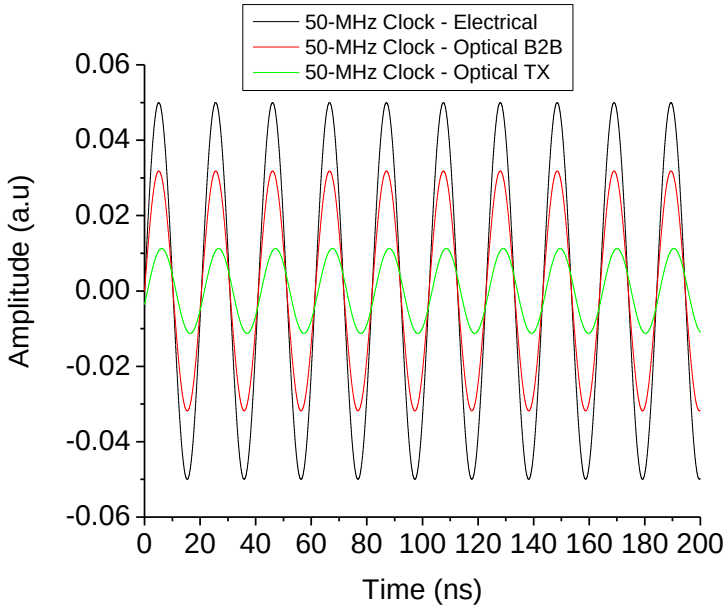

Figure 7.8 50-MHz clock signal transmitted with data at 5-Gbps bit rate

To investigate the effect of increasing the data rate on the clock performance, the clock was transmitted with optical carriers which were amplitude-modulated at 10-Gbps. The results are shown in figure 7.9. Comparing figures 7.8 and 7.9, we can notice that there are no penalties introduced as the results of increasing the data rate. In both cases, a noticeable amplitude reduction was observed. Due to fiber attenuation, the clock suffered an amplitude reduction of about 0.036 a.u.

The numerical software used in this study did not have a system to quantify the phase-noise performance of the clock. However, it was observed that the numerical results reported here are very comparable to the experimental results reported in [191] which used phase modulation and a 20-MHz clock signal. This gives us a platform to estimate the phase-noise performance of this numerical system. With that in mind, we can estimate a single sideband phase-noise values of plus/minus -70 dBc/Hz for this system. The applicability and superiority of a clock signal with such performance characteristic over other commercially available clock systems is well explained in [191].

The time domain results on figures 7.8 and 7.9 demonstrates the superiority of our 5G C-RAN in disseminating clock signals through fiber to be used either for network latency monitoring or for telescope synchronization. It is impressive how a single VCSEL carrier was able to generate a multi-wavelength system to facilitates these sophisticated applications.

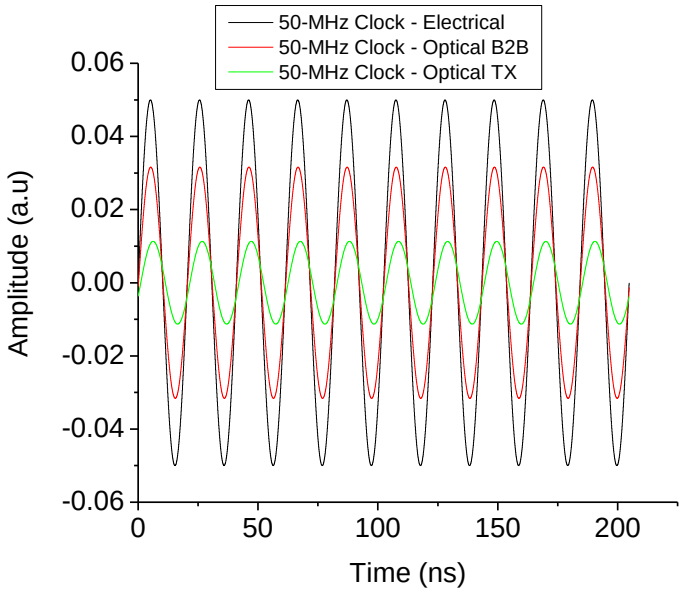

Figure 7.9 50-MHz clock signal transmitted with data at 10-Gbps bit rate

Chapter Summary

Chapter 7 demonstrated a novel application of VCSEL-base optical frequency combs to realize advance 5G radio communication services at high data rates within radio astronomy. The flexibility of the adopted photonic RF transmitter allows it to be used within radio astronomy areas to realize mobile communication service without the effects of radio frequency interference. The coherence of the generate optical modes enabled them to deliver high data rates up to 30 Gbps without errors. The multiwavelength nature of the photonic RF transmitter was harnessed for simultaneous transmission of different application services. In our demonstration, the multi-wavelength optical frequency comb was used for simultaneous transmission of clock signals and the data signals. Both the transmitted clock and data signals were received with integrity. This chapter also demonstrated that a single VCSEL laser can be used for transmission of reference clock signals to telescope arrays for time-stamping of astronomical data signals. Currently, this application is being realize through the use of independent laser sources. Our novel results are a steppingstone toward a great future where low-cost photonic devices such as VCSELs are used to design integrated photonic systems for real applications. The spectral efficiency of the 5G network was also enhanced through the application of advanced techniques such as wavelength division multiplexing to optimally utilizing the enormous bandwidth of optical fibers currently deployed across the majority of telescope facilities.

Chapter 8: VCSEL-based Fixed-Wireless Coherent 5G C-RAN

In the preceding chapters, we successfully demonstrated the design of 5G centralized radio access network (5G C-RANs) based on cost- and power-efficient vertical cavity surface emitting lasers (VCSELs). Chapter 5 proposed the design of two novel VCSEL-based flexible 5G C-RAN. In both cases, the studies demonstrated the use of photonic RF transmitters to generated high-frequency RF carriers for application in high-bandwidth 5G C-RANs. In chapter 7, we demonstrated a novel 5G C-RAN based on wavelength division multiplexing (WDM) where both clock and data signals are transmitted using a single VCSEL carrier. The WDM technique was used in chapter 7 to realize an effective use of the enormous bandwidth of optical fibers currently connecting radio telescopes.

Contrary to chapter 5 where the designed C-RAN connected an astronomer to a 5G radio communication network while mitigating RFI effects, chapter 7 demonstrated the application of a VCSEL-based photonic RF transmitter to support the astronomer with fixed optical network. However, a superior 5G C-RAN should simultaneously support the radio astronomer with both fixed and wireless 5G services, while avoiding RFI effects. The network will be more attractive if it can use spectrally-efficient modulation formats with a single laser sources to realize fixed-wireless transmission. Spectral efficiency is a key factor to improve and optimize fixed-wireless communication networks evolving from generation to generation. 5G C-RANs promise to deliver the gigabit experience to mobile users. At the physical layer, high-level modulation format such as QAM are being pursued [192]. Fixed-wireless implementation is necessary to realize an effective use of network infrastructure to support both the fixed and the wireless user.

There are several reported fixed-wireless 5G C-RANs. However, they suffer from common limitations. Firstly, in these networks, the used wavelengths carry similar data to both the wireless user and the fixed user. This results into broadcasting networks, which are spectrally-inefficient [193]. A unicast coherent fixed-wireless 5G C-RAN will provide an excellent use of the optical spectrum. Wavelength reuse could be used to realize unicast coherent fixed-wireless 5G C-RANs as will be demonstrated for the first time in this chapter. Wavelength reuse techniques includes driving an optical amplifier in the saturation region [194,195] and the phase modulation of the downstream signal with amplitude-modulating the upstream signal [196]. Some authors reported fixed-wireless networks where wavelength reuse techniques are adopted. However, the optical spectrum was not efficiency utilized. For example, the optical power contained in the optical local oscillator signal was not harness for downstream transmission, upstream transmission, and for photonic up conversion to high frequency RF signals for the wireless user. Additionally, they used power-hungry centralized laser sources such as DFBs in an uplink direction to realize these networks [197].

In this chapter, for the first time to our knowledge, we proposed a simple and cost-effective coherent fixed-wireless 5G C-RAN with optimal use of the optical local oscillator signal. In this proposed architecture, a VCSEL-based optical frequency comb of figure 5.13 was used. In our demonstration, the optical local oscillator signal was optimally used for three different network scenarios. Firstly, the optical local oscillator signal was used to carry downstream data for the fixed user. Secondly, it was reused for photonic up-conversion to high-frequency RF signal for the downstream transmission of coherent data to the wireless user. Lastly, it was reused for upstream transmission of data signal from the fixed user to the central office. Additionally, high order modulation formats were used to increase the spectral efficiency of the 5C-RAN.

8.1 Demonstration of a coherent VCSEL-based fixed-wireless 5G C-RAN

We numerically designed and demonstrated a 28-Gbps 16-QAM wireless and 8.5-Gbps downstream/upstream fixed coherent 5G C-RAN assisted with wavelength reuse technique. The numerical network configuration is given in figure 8.1. It is worth mentioning that the VCSEL-based optical frequency comb (OFC) of chapters 5 and 7 was also used in this chapter as the photonic RF transmitter for the fixed-wireless 5G C-RAN. To mitigate the cross-talk effects, the switching frequency of the electrical local oscillator was increased to 20 GHz. Increasing the switching frequency reduces the number of comb lines, but the spacing between two consecutive comb lines is increased. Increasing the frequency spacing between two comb lines is necessary for high-speed coherent data transmission both in the fixed and wireless domain. In our network, the number of comb lines within 10-dB spectral envelop were reduced to 5 from 11 obtained at 14-GHz electrical local oscillator switching frequency.

From the numerically-generated optical frequency comb, two wavelength channels at 1552.204-nm and 1552.655-nm were selected by a practical wavelength selective switch (WSS) with a 5-GHz (0.04 nm) center-frequency bandwidth for each channel [198]. The WSS was used to select each transmitting channel in order to measure its performance independently. The WSS is needed for experimental characterization only. It is not needed for a real-world implementation. Instead, a passive wavelength division multiplexing (WDM) splitter could be used to reduce the network cost.

One channel was modulated with 28-Gbps 16-QAM downstream data meant for the wireless user. The other channel was modulated with 8.5-Gbps downstream binary data meant for the fixed user. The two channels were combined at a 3-dB optical coupler, amplified with an erbium-doped fiber amplifier (EDFA) with 20-dB gain. The combined signal was launched into a 24-km standard single mode fiber (SSMF) having a loss of 0.2 dB/km. To achieve full-duplex transmission, the optical circulators before and after the fiber were used for switching the downstream and upstream signals between the three ports.

After fiber transmission, we used a circulator and a fiber Bragg grating (FBG) centered at the second wavelength (1552.665 nm) to select the wavelength carrying downstream data for the fixed user from the combined channels. The selected channel by the FBG was split into two paths using a 3-dB optical coupler. One path of the coupler was demodulated to recover the transmitted 8.5-Gbps downstream data. This was done by using a 10-GHz photodiode and a variable optical attenuator for BER measurements. The second path of the coupler was amplified by a second EDFA to a high-power signal to saturate the second semiconductor optical amplifier, consequently removing the data. This wavelength channel was thus recovered.

The recovered channel was recombined with the optical carrier having the downstream data for the wireless user at another 3-dB optical coupler. The combined signal was filter by an optical bandpass filter (OBPF) to remove the out-of-band frequencies. The filtered optical signal was fed to a high-frequency photodiode having a 60-GHz frequency response. The output of the photodiode produced a 56-GHz RF carrier for wireless transmission.

In case of RFI with radio astronomy at this generated RF frequency, the system can be shifted to a new RF carrier signal by tuning either the switching electrical oscillator or by tuning the optical filter to select a different optical carrier. This will avoid radio frequency interference to the astronomer while supporting radio communication services to users.

The generated 56-GHz RF carrier was amplified with an electrical RF amplifier having a gain of 25-dB and a bandwidth of 52-63 GHz. The amplified signal was fed to a horn antenna

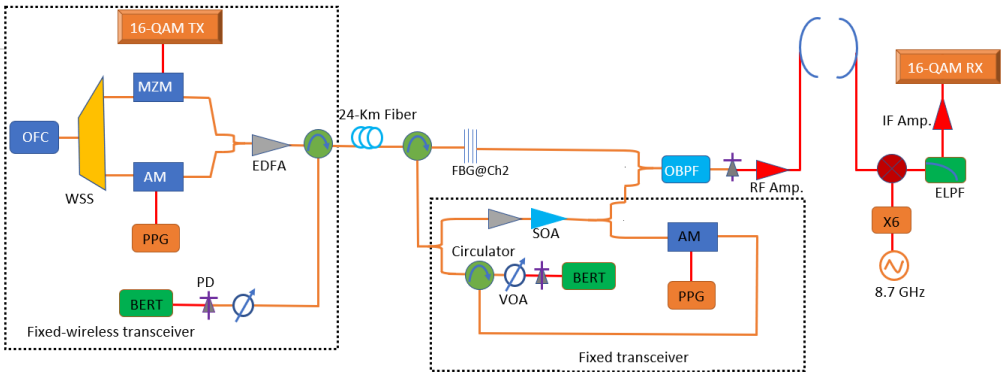

Figure 8.1 Experimental schematic of the proposed fixed-wireless WDM-PON using VCSEL-based

and then launched into a modelled wireless channel. A second horn antenna was placed 4-m away from the transmitting antenna. This receiving antenna was connected to an electrical mixer to mix the received RF signal with a locally-generated RF signal at 52 GHz. This generated a 4-GHz intermediate frequency (IF) signal which was amplified using an IF amplifier and analyzed with digital sampling scope.

The same recovered wavelength was remodulated with 8.5-Gbps upstream data. This data was transmitted and recovered at the central office using a second low-frequency (10-GHz) photodiode. It should be noted that an electrical low-pass filter with 10-GHz cut-off frequency was used after each low-frequency photodiode.

At this point, the designed VCSEL-based 5G C-RAN has supported both the fixed and mobile radio astronomer with information and communication technologies. The flexibility of the used photonic RF transmitter ensures that no radio frequency interferences are experienced by the radio astronomer while being supplied with these ICT services.

8.2 Performance of the VCSEL-based fixed-wireless 5G C-RAN

Figure 8.2 shows the two filtered optical comb lines at the output of the optical coupler after each was modulated with data. Due to different optical modulator loses, the optical carrier signal carrying the coherent data had power lower than the optical local oscillator carrier signal.

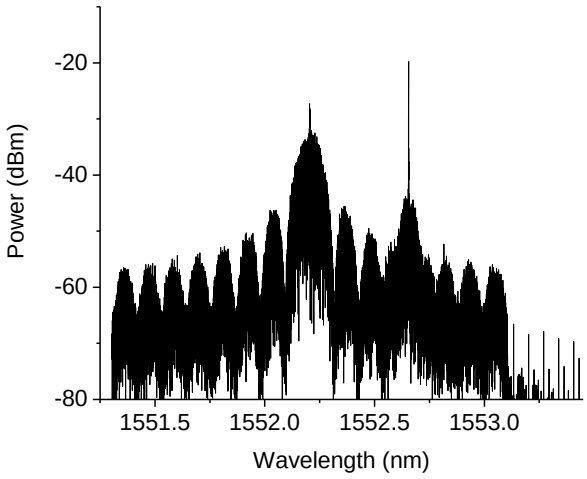

Figure 8.2 The two filtered optical carriers each carrying downstream data

The separation between these optical carriers gave an RF signal of 56 GHz. The two optical signals were transmitted over the fiber to a remote site.

Since the 5G C-RAN presented here is to be located at the radio astronomy office, the radio access point can be some few meters within the radio astronomy area where the remote radio head (RRH) is located. In case when the 5G C-RAN is expanded to support new remote radio astronomy stations, the fiber distance can be extended to reach these new astronomy sites. In case of RFI at these newly established radio astronomy areas, the interferences can be control by using the already-available mitigation techniques at the old site where the 5G C-RAN is located. Very important to note that the 5G C-RAN can also be used to supply 5G services to communities around the radio astronomy areas. This can be realized by pulling optical fiber cables to these surrounding areas. This makes the network scalable. It also results in excellent use of the network resources, greatly reducing the capital expenditure.

At remote site, the optical local oscillator signal was filtered from the two transmitted signals. The filtered signal is given in figure 8.3. The FBG that was used is able to attenuate the optical carrier signal wavelength by more than 30-dB. The reflected wavelength of figure 8.3 was split into two parts using a 3-dB optical coupler. One part was used to recover the downstream data of the fixed user. The second part was erased of the downstream data and reused. The recovered wavelength after data removal is given in figure 8.4. The recovered wavelength was again split into two parts using another 3-dB optical couple. The first part was recombined with the signal at the output of the FBG having the downstream data for the wireless user. This was done to photonically-generate an RF carrier of high frequency. The optical spectrum is given in figure 8.5. It is worth noting that due to insertion losses at the first coupler after FBG reflection, the power spectrum of figure 8.4 is lower than that of figure 8.3.

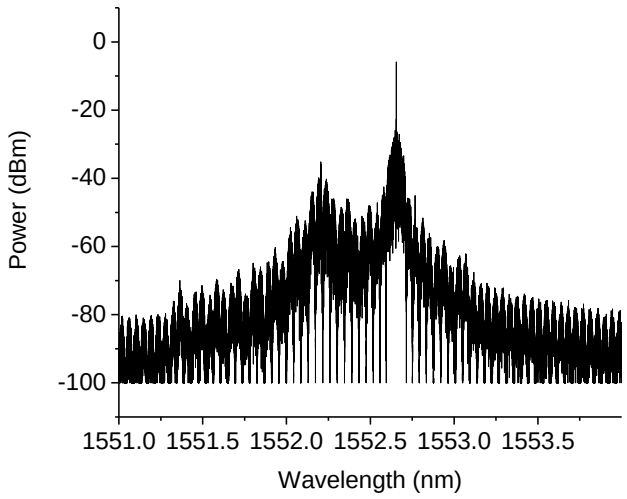

Figure 8.3 The reflected optical carriers at the FBG having the downstream data for the fixed user

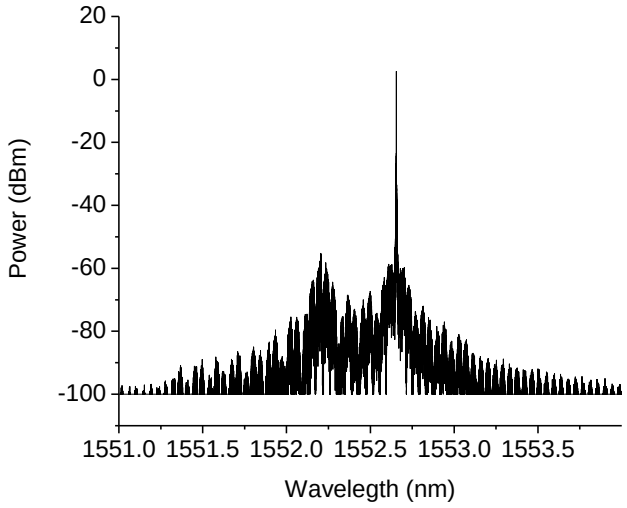

Figure 8.4 The reflected optical carriers at the FBG without the downstream data of the fixed user

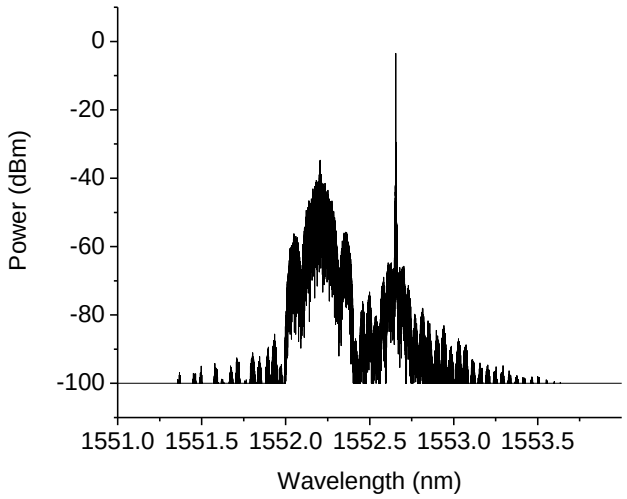

Figure 8.5 The reflected optical carriers with erased downstream data recombined with the wireless data optical carrier

8.2.1 Upstream and downstream data transmission performance for the fixed user

For the downstream data transmission to the fixed user, the optical carrier was amplitude-modulated with 10 Gbps binary data. Figure 8.6 shows the bit error rate (BER) for the downstream data to the fixed user. As can be seen in figure 8.6, when considering a BER of 10^{-9}, a negligible penalty was obtained after 24-km fiber transmission. We can see in figure 8.6 that BER values were not dependent on the optical signal power for powers of -17 dBm and above. This is evident on figure 8.6 where at optical powers of around -17 dBm and above, the performance for both back-to-back and after fiber transmission was the same. Nevertheless, an error-free data transmission was obtained at a receiver sensitivity of less than -18 dBm.

The BER results for the upstream data by the fixed user at 10 Gbps binary modulation using the recovered wavelength is shown in figure 8.7. In figure 8.7, when considering a similar BER

of 10^{-9} as in the case of the downstream data, a fiber transmission penalty of 0.6 dB was recorded. The recovered and remodulated carriers was able to deliver error-free data at a receiver sensitivity of less than -18.6 dBm. Results in figures 8.6 and 8.7 indicated that a gain-switched VCSEL-based optical frequency comb can be used as a photonic RF transmitter to support error-free data transmission for both upstream and downstream links. The excellent performance in the upstream data transmission is due to the effective carrier recovery of the adopted wavelength reuse technique.

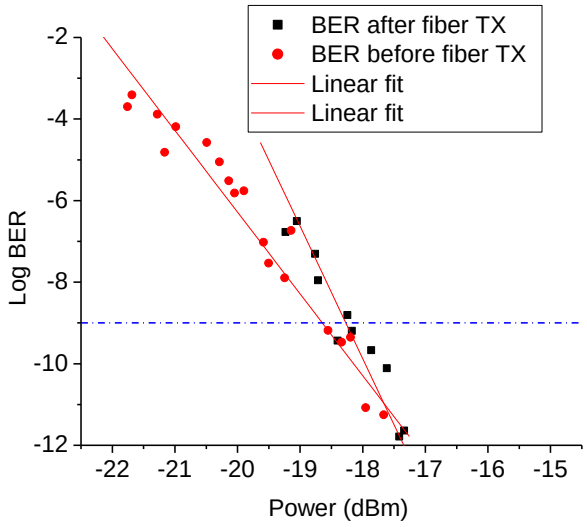

Figure 8.6 BER for the downstream data to the fixed user

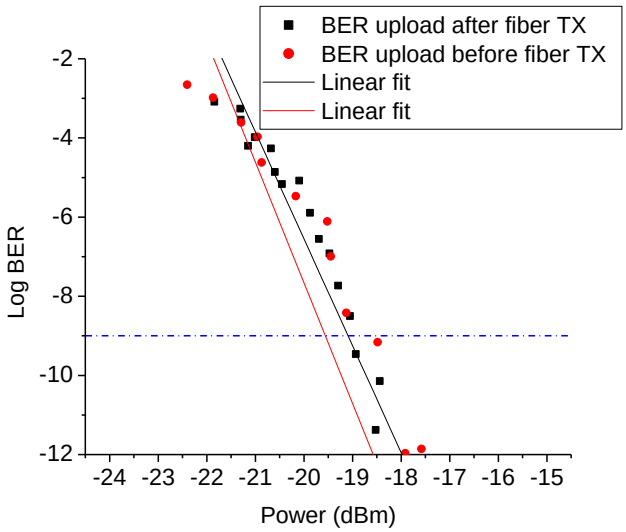

Figure 8.7 BER for the upstream data of the fixed user

8.2.2 Downstream data transmission performance for the wireless user

Our proposed 5G C-RAN is designed innovatively where the recovered optical wavelength is optimally used for simultaneous transmission of downstream data to the fixed user, upstream transmission by the fixed user, and for photonic up-conversion to 5G signal. Figure 8.8 is the electrical spectrums of the 56-GHz wireless signal at the output of the 60-GHz photodiode. It should be noted that this was the signal before RF amplification. We investigated the error vector magnitude (EVM) values against the wireless distance. The results are given in figure 8.9. This was done by varying the separation between the transmitting antenna and the receiving antenna from 1 m to 11 m. At the minimum distance of 1 m, the EVM value was 7%. Increasing the distance by tenfold gave an EVM of 13%. It should be noted that this was done at a fixed fiber distance of 24 km. We evaluated our proposed coherent fixed-wireless 5G C-RAN at fixed distances of 24 km and 4 m for fiber and for wireless, respectively. The wireless performance evaluation was carried out quantitatively in term of EVM calcuation against optical power delivered at the 60-GHz photodiode. This was done at back-to-back and after 4-m wireless distance. The term "back-to-back" here refers to the case when the wireless signal is evalauted at the output of the photodiode without any wireless transmission. The results are given in figure 8.10. We observe in figure 8.10 that EVM values decreased from 13% to 7% with optical power increase from -10 dBm to 2.5 dBm. A flooor is evident where power increase from 2.5 dBm to 7 dBm did not have any positive effect on the signal performance. This effect can be attributed to the intrinsic phase-noise of the used photonic RF generation technique and the choice of the laser used.

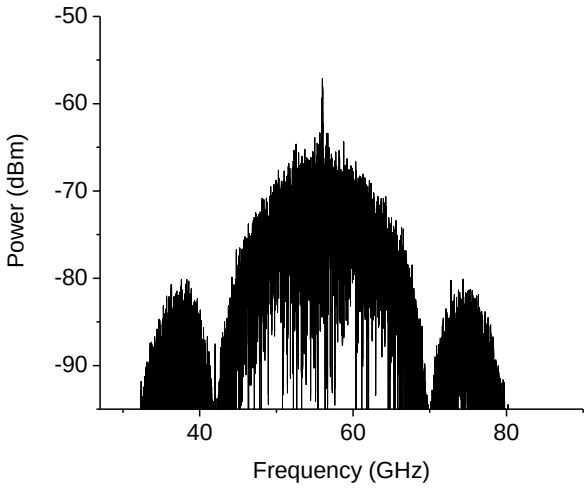

Figure 8.8 The 56-GHz wireless carrier at the output of the 60-GHz photodiode

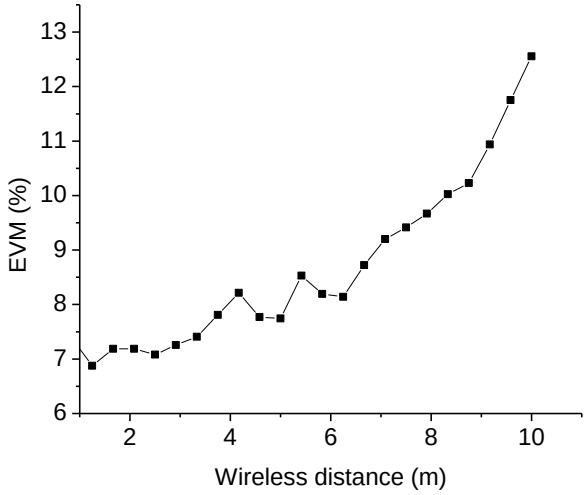

Figure 8.9 EVM performance against the wireless distance

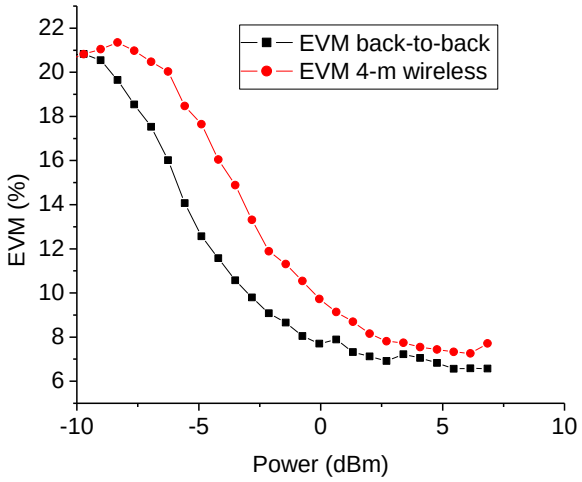

Figure 8.10 EVM performance against the optical power for back-to-back and after 4-wireless

We plotted the constellation diagrams for the 16-QAM 28-Gbps data in order to qualitatively analyze the wireless carrier's performance. This was done at EVMs of 7% and 21%, a 33% degradation in signal quality. The wireless distance was 4 m. The results are given in figure 8.11 left and right for EVM of 7% and 21%, respectively. At a fixed fiber length of 24 km and fixed wireless distance of 4 m, the constellation at the right of figure 8.11 can be improved to that on the left of the same figure with a 12.5-dB increase in optical power, as supported by figure 8.10. Where powerful DSP tools are readily available, such optical power requirements can be relaxed. Predistortion techniques can also be used to improve the 14% EVM of figure 8.11, relaxing the need for sophisticated DSP kits [199].

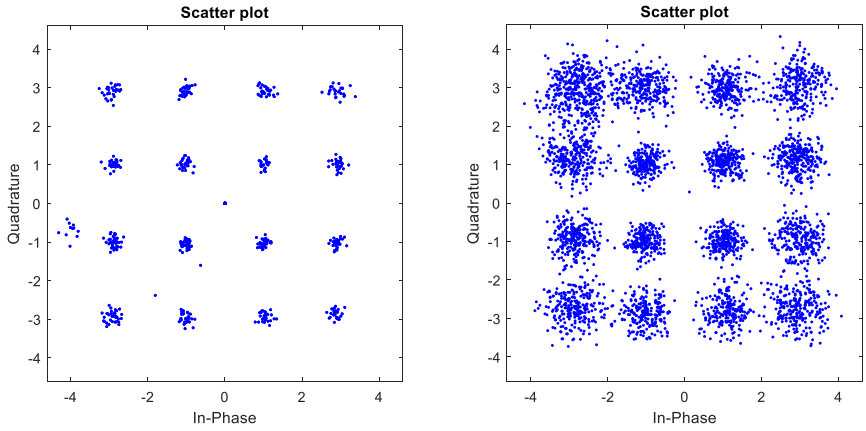

Figure 8.11 EVM performance qualitatively in term of constellation mapping

Chapter Summary

In this chapter, we have demonstrated a novel 5G C-RAN using a low-cost VCSEL. We adopted a gain-switched optical frequency comb generation technique as our flexible photonic RF transmitter. The photonic RF transmitter demonstrated its ability to generate coherent optical carriers to be used within radio astronomy for both fixed and wireless data transmission without the effects of RFI. The technique of wavelength reuse was demonstrated for the first time to support both downstream transmission, upstream transmission, and photonic up conversion to high-frequency RF carrier signals. The network through put was increased by using advanced coherent modulation formats. We achieved a network bit rate of 10 Gbps for the fixed user and 28 Gbps for the wireless user, using a single low-cost and low-power VCSEL. We propose that through innovative control of the generated RF carrier signals for the wireless user, this 5G C-RAN can be adopted in radio astronomy areas to realize advanced ICT service to both the fixed and mobile network user without any negative consequences such as RFIs.

Chapter 9: Application of photonic 5G C-RAN in radio astronomy without RFI effects

To date, the issue of radio frequency interference (RFI) due to mobile communication systems remain a challenge to a radio astronomer. As discussed in section 2.2, there are several proposed techniques to avoid RFI due to mobile communication systems in radio astronomy areas. Most of these techniques are proactive techniques based on government regulations.

Figure 9.1 depicts future converged communication networks where both mobile and fixed networks are shown. Future converged networks will promote coexistence by integrating different network access technologies such as optical access network (OAN), wireless radio access networks (RAN), together with other big-data science projects such as radio astronomy. These networks are expected to compete for spectrum resources. Evidently, the reported techniques of section 2.2 will soon become unproductive and inefficient as future converged networks compete for spectrum resource. New RFI mitigation techniques for 5G networks will require solutions that promote coexistence and spectrum sharing. Future 5G networks will need to be flexible at their transmitter subsystems to coexist with other telco services and big-data science projects.

In additional to the flexibility requirement for 5G networks to realize spectrum sharing and coexistence, future converged 5G access networks are also expected to meet the enhanced mobile broadband (eMBB) requirement [200]. The eMBB requirement is expected to be achieved through the use of high-frequency RF carrier signals. These high-frequency carrier signals are difficult to generate using electronic techniques. Therefore, we propose that a flex-spectrum photonic solution is necessary to support both spectrum sharing and easy generation of the needed high-frequency RF carrier signals.

The preceding chapters 5, 7, and 8 demonstrated the data transmission performance of photonic RF transmitter based on optical heterodyning and optical frequency comb generation. The results highlighted the capabilities of these photonic RF transmitter systems to support the radio astronomer with advanced high-bandwidth fixed and wireless 5G services. In both chapters 5, 7, and 8, the issue of RFI due to these 5G photonic RF transmitter was discussed briefly, pointing out features that makes these transmitters capable of controlling and mitigating the RFI effects. However, the actual performance in term of their intelligence to mitigate RFI to the astronomer was not demonstrated.

In this chapter, we will demonstrate for the first time, the flexibility of a photonic RF transmitter for automatic mitigation of radio frequency interference. The solution is intendent to promote spectrum sharing and coexistence. We intuitively suggest the following criteria for a feasible photonic RF transmitter to achieve spectrum sharing and coexistence. These criteria are necessary to integrate these photonic RF transmitters within astronomical areas to achieve 5G radio services without RFI effects. Firstly, the flex-spectrum photonic RF transmitter system should have a fine-tuning spectral resolution, i.e., the transmitter system should have small spacing between two consecutive spectral lines. Secondly, the ability for dense spectral signal generation, i.e., the ability to pack as many RF carriers as possible within a given spectral band. Additionally, the generated RF quality is also important, especial for coherence data transmission. However, in this study, the main focus is to demonstrate how a simple optical heterodyning scheme, without phase-locking mechanisms, can be used to realize 5G mobile services within a radio astronomy area without the effects RFI.

The optical heterodyning technique is considered to be the simplest photonic RF transmitter architecture [120]. This technique is depicted in figure 5.3 and is discussed in detail in section 4.2.1 of this thesis. Therefore, in our experimental demonstration, the optical heterodyning of two free-running lasers will be used as the flexible photonic RF transmitter to show its capability for automatic mitigation of RFI to the radio astronomer.

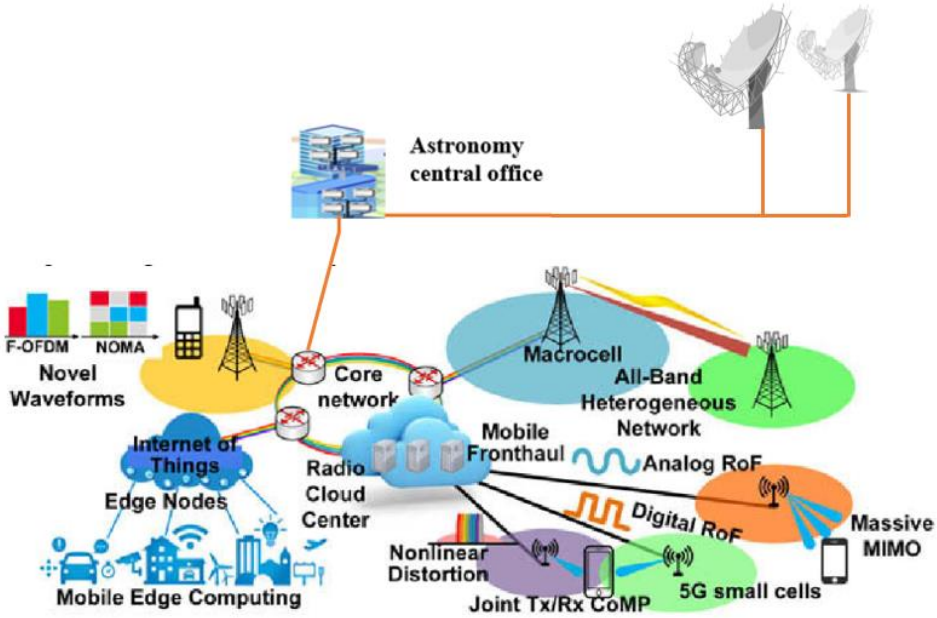

Figure 9.1 Future converged optical and wireless networks

It is worth noting that the capabilities for these transmitters to automatically mitigate RFI does not lie in their physical configuration. It is the separation between the two heterodyning modes that needs to be flexible. Therefore, any other photonic RF transmitter such as the optical frequency comb generation technique of chapters 5, 7, and 8 can also be adopted to achieve the same performance without any change to their physical configuration.

Therefore, the non-coherent optical heterodyning RF transmitter scheme is adopted in this thesis for the following reasons. Firstly, it has been shown that phase-noise of RF signals generated from optical heterodyning is insensitive when using envelop detection scheme [124]. This was demonstrated in chapter 5. Secondly, the phase noise associated with optical heterodyning can be mitigated through phase-locking mechanism [120].

9.1 Demonstration of a flexible 5G C-RAN with RFI mitigation capability

This section will experimentally demonstrate the application of optical heterodyning of two independent lasers to realize 5G mobile communication services within radio astronomy facilities without introducing RFIs. Chapter 3 discussed in detail, the different radio access networks (RAN) architectures starting from 3G until 5G.

As the amount of user-data has been increasing with respect to different quality-of-service requirements, network operators are forced to fulfill these requirements through centralization and cloudification of baseband units (BBUs) and their corresponding remote radio heads (RRHs). This new centralized and cloudified RAN, where network resources are pooled in a centralized BBU pool, is known as the centralized RAN (C-RAN) [71,72]. The main idea behind C-RAN is to bring all BBUs and their corresponding RRHs together and locate them into a centralized, cloudified, shared, and virtualized BBU pool. Every RRH is then connected through a fronthaul link to the BBU pool. Every BBU pool can support nearly tens of RRHs. The BBU pool is connected to the core network through backhaul links such as optical fibres. A detailed discussion on 5G C-RAN is given in section 3.4 of this thesis.

To our knowledge, as far as this thesis is concerned, the 5G C-RAN architecture is the best solution to realize mobile communication services within radio astronomy areas. When radio functions are fully centralized, it will be easier to manage the radio spectrum resources at the central office, consequently reducing and avoiding RFI to the astronomer. The flexibility of photonic RF transmitters will make it possible to manage RF resources from a central station where these systems are pooled. This also facilitate the design of a heterogeneous radio network that support different service scenarios using the same infrastructure. In this manner, the C-RAN architecture will decrease the CAPEX and OPEX of mobile service provider. It will also reduce the energy consumption and increases the network scalability. Additionally, C-RAN architecture simplifies network management and maintenance. It will improve the spectral efficiency and the network throughput. All these are attractive qualities which can facilitate mobile communication services within radio astronomy areas. Therefore, we have considered a fully-centralized 5G C-RAN as our radio access solution to demonstrate the integration of 5G communication systems within radio astronomy areas without the consequences of radio frequency interference.

9.1.1 Characterization of the used photodiodes in our experiment

The bandwidth of the photodiode needed to be characterized carefully to ensure that the wireless RF signals to be used are within this bandwidth. In our demonstration, we used a 10-GHz PIN photodiode. High bandwidth photodiodes are readily available and can be used to extend the wireless RF frequency of the 5G C-RAN. Figure 9.2 shows the electrical bandwidth of the used photodiode. The photodiode device was characterised in two steps. During the first step, the heterodyning RF frequency was tuned from low frequencies (brining the wavelengths of the two DFB lasers together) to higher frequencies (slowly tuning the wavelength of one DFB laser away from the other) while allowing them to beat at the photodiode. The results are given as black curve in figure 9.2. During the second step, the heterodyning RF frequency was tuned from high frequencies (tuning the wavelength of the two DFB lasers apart) to low frequencies (slowly tuning the wavelength of one DFB laser toward the other) while allowing them to beat at the photodiode. The results are given as the red curve in figure 9.2. In both cases, the spectrum is similar as can be supported by figure 9.2. Therefore, this photodiode can be used in the design of 5G C-RAN operating within 10 GHz RF frequencies.

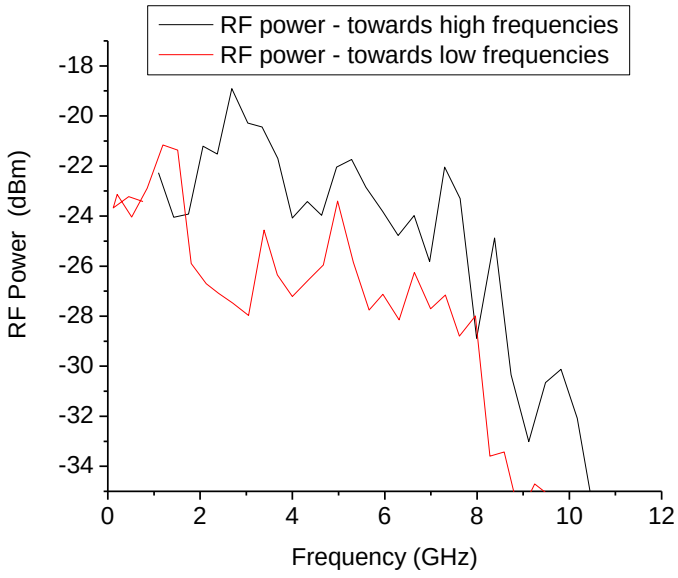

Figure 9.2 Electrical bandwidth of the used photodiode

It is rather necessary to mention that the bandwidth of the photodiode is very important when designing a photonic 5G C-RAN to coexist within radio astronomy areas without introducing RFI. For example, if the bandwidth of the used photodiode is not carefully characterized. During RFI, the system could be tuned to an RF signal outside the bandwidth of the photodiode. This signal will be small in power to be detected as an RFI by the RFI detector. But it can severely affect the radio astronomer. Therefore, it is important to know the correct bandwidth of the photodiode so that the 5G C-RAN is operated within this bandwidth.

9.1.2 Experimental setup of the heterodyning-based 5G C-RAN in radio astronomy

The conceptual diagram is given in figure 9.3. The radio astronomy area acts as the central station where all the BBUs and radio equipment controller (REC) are centralized, hence the name C-RAN (see figure 3.5). The REC assigns radio resources to the RRH, in this case the matching circuit and the passive antenna unit. The frequency at which the astronomer is observing is monitored by the RF detector. When this frequency collides with the frequency at which the 5G C-RAN is operating, interference occurs. The control algorithm instantly detects and corrects for such an RFI, consequently avoiding it. The 5G C-RAN can be extended to support surrounding areas with the required 5G services by pulling optical fiber cables, acting as fronthaul links to those locations. The centralization of the REC and DU at the astronomy site ensures that the network hardware and software are used to supply 5G services to both the radio astronomer and the surrounding community, thereby effectively using the network infrastructure.

Figure 9.3 shows the experimental setup. Incoming baseband optical data is converted to electrical format by photodiode 2 (PD 2 on figure 9.3). The two continuous-wave, free-running lasers were used to create a heterodyne-based RF carrier signal by combining them at the optical coupler and allowing them to beat at the photodiode (PD 1).

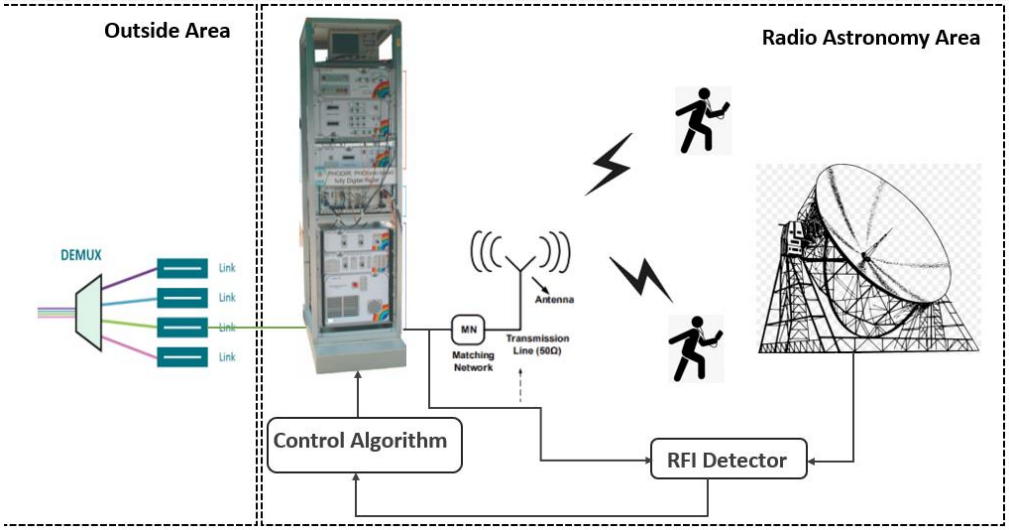

Figure 9.3 Conceptual diagram of 5G services within a radio astronomy area.

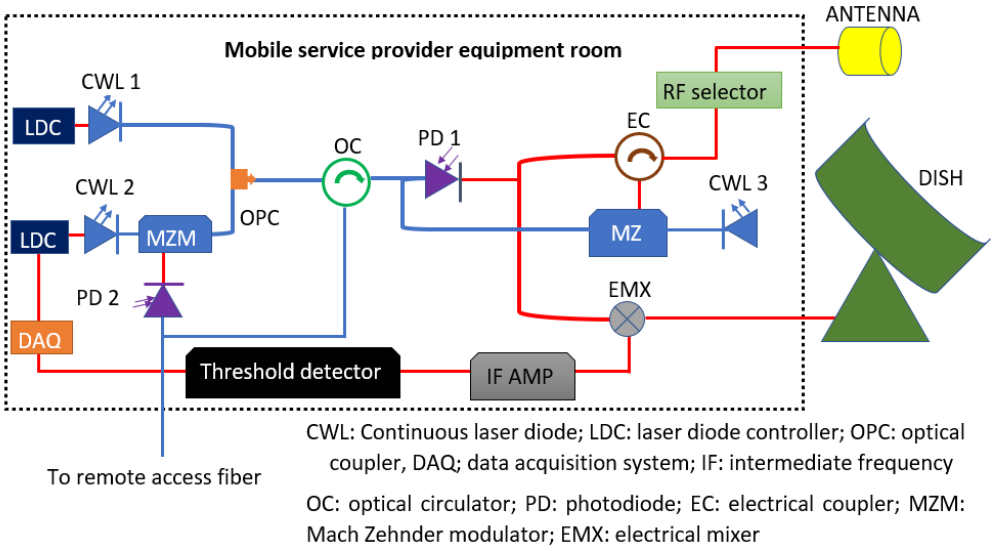

Figure 9.4 Experimental configuration of the proposed C-RAN with RFI mitigation capability.

We adopted distributed feedback (DFB) lasers to improve both the signal-to-noise ratio [201] and the phase noise [202,203] of the generated RF carrier signals. The thermal instabilities and the absence of thermal control board for our VCSEL rendered them unsuitable for this application. However, VCSELs are power-efficient optical sources which are relatively cheaper to purchase. With the right stabilization equipment, VCSELs could have been excellent light sources to be used in this experimental demonstration.

The wavelength for DFB laser 1 was fixed to 1550.0 nm with 3.1-dBm optical power, while the wavelength for DFB laser 2 was automatically tuned whenever the generated RF signal matched that at which the telescope dish was observing. The power for DFB laser 2 was fixed to 4.1-dBm. The MZM, optical coupler (OC), electrical coupler (EC), RF selector, continuous wave laser 3 (CWL 3), and the antenna were included in figure 9.3 to show how a complete photonic 5G C-RAN system can be configured in a practical setup to allow full-duplex transmission. In this demonstration, no data modulation and transmission were carried out. The data transmission performance for this 5G C-RAN was dementated earlier in chapter 5. The main aim for this chapter is to demonstrate how RFI caused by two colliding RF sources could be avoided using this architecture. This will consequently allow two systems to operate within the same spectral band. This will be the case when these 5G C-RANs are adopted within radio astronomy areas where the descopes do not observe at their full frequency bands at all times.

The resultant unmodulated RF carrier signals were measured using an electrical spectrum analyzer (ESA) after the photodiode (PD 1). The dish was represented by our 20-GHz RF source. A recent report suggested the frequency range under which the SKA telescope will operate on [204]. The other frequencies are also given in table 1. With these frequency ranges in mind, the interfering source, in this case our 20-GHz RF generator representing the SKA dish, was automatically tuned to generate these interfering frequencies.

To monitor any collision between the unmodulated RF carrier from the photodiode (PD 1) and the interfering signal from the 20-GHz RF sources, an electrical mixer with intermediate frequency (IF) bandwidth from DC to 4 GHz was used as the primary RFI detector. An electrical mixer is a simple passive electrical device that generates an IF frequency at its IF port. The IF signal frequency equals the different in frequency between the local oscillator port and the RF port of the mixer. When the two frequencies at the local oscillator and RF ports are the same, the signal at the IF port matches the bandwidth of the IF port of the electrical mixer. This signal can therefore pass through to the control circuit, in this case the threshold detector,

and is used to trigger the control circuit. However, when the signal frequencies at the local oscillator and RF ports of the mixer are completely far from each other, a high-frequency RF signal, outside the bandwidth of the IF port of the mixer is generated. This frequency is blocked by the IF port of the mixer as it does not match its bandwidth. Therefore, it does not trigger the threshold detector, leaving the 5G C-RAN system undisturbed. It is interesting to note that the bandwidth of the IF port of the electrical mixer determines the bandwidth of the 5G C-RAN.

For the control circuit, we used a data acquisition board (DAQ) from our lab. When the DAQ is interfaced, it can detect signals at its input ports and send signals at its output ports. So, the detected signal passed by the IF port of the mixer is send to the DAQ. The DAQ then sends a predetermined electrical signal to the laser diode controller (LDC in figure 9.3). The LDC works by shifting the bias current of the laser when it detects a certain voltage at its eternal port. It also stabilizes the cavity of the laser through thermal control. The shift in bias current results into a shift in the wavelength of the second DFB laser (CWL 2). As a result, the beating frequency at the photodiode generated through the optical heterodyning of the two lasers, with the second laser now having a new wavelength, results into a new RF carrier signal generated. This will be the new frequency at which the 5G C-RAN will operate on. At this instant, the difference in frequency between the local oscillator port and the RF port of the mixer is at high frequency. This high-frequency RF signal is blocked by the IF port of the mixer. Therefore, it does not trigger the control circuits. The 5G C-RAN system then remains at the new RF frequency. The process repeats again when a change in frequency occurs at the 20-GHz RF source (the telescope dish) such that its frequency matches the frequency at which the 5G C-RAN is operating.

We designed our own IF amplifier and threshold detector. The amplification of the IF signal from the IF port of the mixer is necessary to avoid using low resistor value to set a low reference voltage at the threshold detector. It also avoids ambient noise from triggering the system. This was achieved by setting the reference signal of the comparator (threshold detector) circuit to 2 volts (2 V). The incoming error signal is amplified by the IF amplifier. The resultant amplified signal is then sent to the comparator (threshold detector). The threshold detector circuit had a rectification part. This was necessary to generate a constant control DC signal which can be send to the control circuit. This control DC signal was constant, determined by the components of the threshold detector circuit. This in turn gave a very good system stability for RFI control and mitigation.

9.1.3 RFI mitigation results and discussion

Figure 9.5 shows the IF signal from the mixer before and after amplification by the IF amplifier. The IF signal (error signal) was not a complete DC as it is expected when two exact frequencies interfere. This is avoided because if the interfering signal should collide completely with the information signal before correcting for RFIs, both the radio astronomy data and the 5G data will be affected. To avoid this, the system was designed to correct itself as soon as the interfering signal is within a specified bandwidth of the information signal. As highlighted above, this bandwidth is determined by the spectral bandwidth of the IF port of the mixer. Thus, it is expected that the IF signal will not be a complete DC signal as can be seen in figure 9.5.

From figure 9.5, we can see that our designed IF amplifier was able to amplify the error signal from 500 mV to 6 V. Remarkably, the linearity of the error signal is maintained across the entire signal duration. The amplified signal was rectified to allow the system to be interfaced with any DC systems. However, in our design, it was not necessary to use the DC signal from the IF amplifier because we rectified the IF signal after the threshold detector circuit. Depending on electronic circuit available and the preference of the system designer, rectification can be done either after the IF amplifier or after the threshold detector circuit. The amplified IF signal was then passed on to the threshold detector circuit.

The operation of the threshold circuit is as follows. When the IF signal amplitude is above 2 V, the output goes to the positive bias voltage of 5 V. However, when the input IF signal amplitude is below 2 V, the output of the comparator goes to -5 V. These results are given in figure 9.6. It becomes obvious from the signal pattern in figure 9.6 that the average DC value for the comparator output signal will be 0 V. This signal will not be detected by the input port of the DAQ systems and therefore will not trigger the system to correct for RFI. This is why a rectifier circuit immediately after the comparator circuit was needed. The signal was then rectified by using a simple silicon diode device that will only allow the positive cycle of the signal to pass, while blocking the negative cycle. At this point, the output of the comparator is a fixed DC value, determined by the average of the positive cycles of the rectifier output.

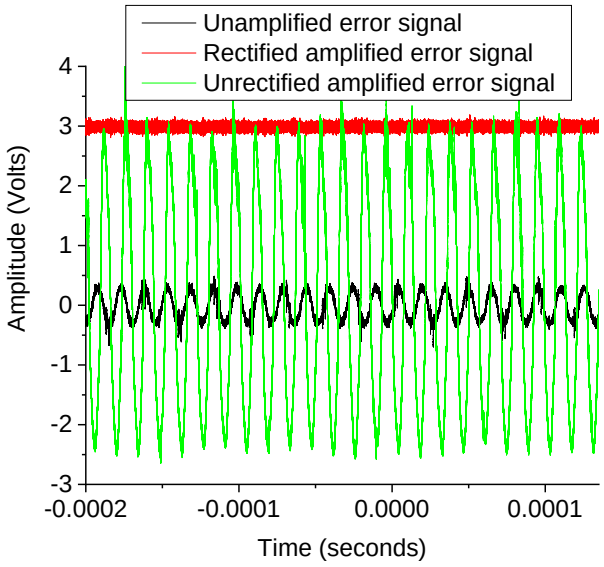

Figure 9.5 The unamplified and amplified error/IF signal used to trigger the threshold detector

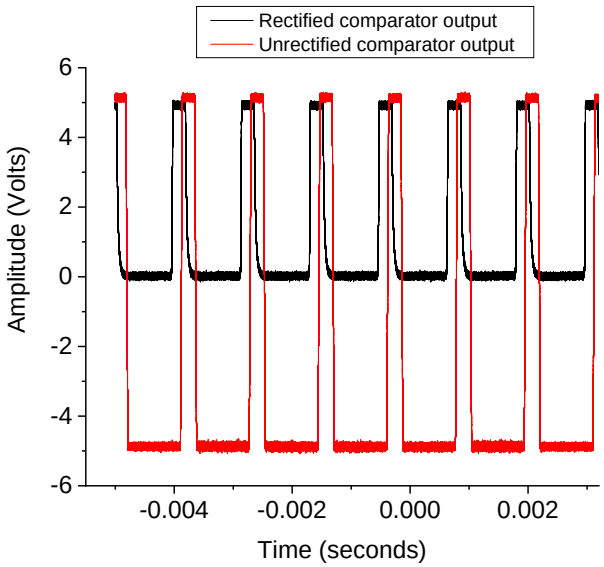

Figure 9.6 The unamplified and amplified error/IF signal used to trigger the threshold detector

We used two DFB lasers due to the availability of their temperature stabilization boards in our laboratory. The DFB lasers were wavelength-tuneable through the LDC. When the output of the comparator, a fixed DC value determined by the average of the positive cycles of the rectifier output, is applied to the LDC, the bias current can be changed. This change in bias current will then shift the wavelength of the DFB. The detail discussion on DFB laser and their wavelength tunability and flexibility is given in section 4.1.3. When tuning the wavelength of one DFB laser while keeping that of the other DFB laser constant while allowing them to beat a photodiode, different RF frequency can be generated.

Figure 9.7 shows some of the RF spectrums generated by the DFB laser-based heterodyning scheme. The photonically-generated RF spectrums can be extended to other high frequencies, normally limited by the bandwidth of the photodiode. In figure 9.7, we can see that the adopted photonic RF transmitter system could generate both spectral lines that co-exist around the SKA-SA frequency bands as given in table 1. Open transmission RF frequencies where the telescope does not observe would include: 850- to 900-MHz, 1670- to 1750-MHz, and above 3500-MHz. The flex-spectrum photonic RF transmitter system can then be tuned to the unused in-band telescope frequencies during times when the telescope is not measuring at all the three bands concurrently. This further allows the applicability of 5G C-RAN in future radio astronomy areas to realize mobile communication services without RFI.

Photonic RF synthesizers such as optical heterodyning have advantages over the current electronic synthesizers. Electronic synthesizers work at low frequencies below 5-GHz [26]. Future 5G C-RANs are expected to work at frequencies well above the current limits of electronic synthesizers. The optical heterodyning scheme adopted here can support these high frequency requirements. The heterodyning scheme have several other advantages. Firstly, it is easy to implement and achieving RF flexibility is relatively easy and straight forward. This reduces the frequency control/tuning algorithm. As a result, the CAPEX and OPEX of the network can be reduced. The generated spectrum is in the gigahertz ranges, supporting future 5G RANs which require high frequency RF carriers to achieve the eMBB requirement. The RF transmitter is optical, supporting future 5G RANs which will mostly use optical fiber to distribute RF signals to RRHs as demonstrated in chapters 5,7 and 8.

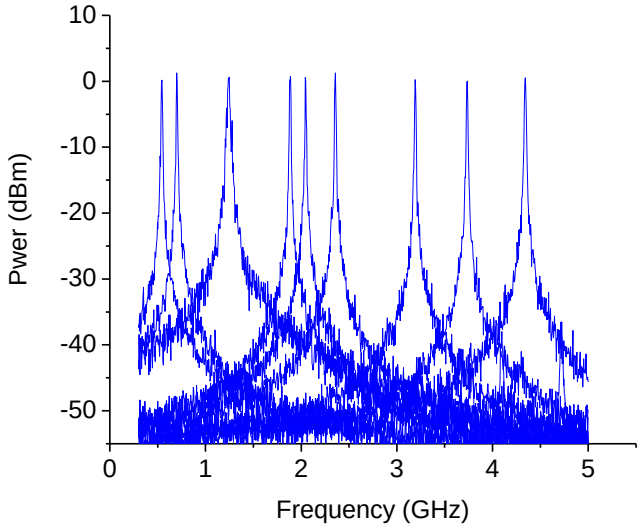

Figure 9.7 RF flexibility of the heterodyning DFB continuous wave lasers used

It is worth mentioning that the choice of the photonic RF transmitter to be implemented within radio astronomy areas will depend on the application and performance requirements of the 5G C-RAN. For example, in application systems where narrow spectral bands have to be exploited to maximize spectrum efficiency, while also avoiding RF interference, the optical heterodyning scheme reported here can be improved to generated low phase noise RF carriers. This can be achieved through phase-locking mechanisms [120]. Other proposed photonic techniques discussed in section 4.2 of this thesis can be adopted to meet the intended system requirements.

Figure 9.8 is the results showing how the system responded when an interfering frequency is detected. In figure 9.8, the RF carrier frequency (the RF frequency at which the 5G C-RAN is operating) is initially set at 4 GHz. The interfering frequency (representing a frequency at which the telescope is observing at that particular time) is automatically varied from 0 GHz (it can start at any frequency) towards the frequency of the RF carrier. When the interfering frequency is within the forbidden bandwidth of the 5G C-RAN (in this case close to the 4 GHz frequency at which the 5G C-RAN is operating), the system detected a large error signal, alarming the presences of an RFI. The value of this error signal is fixed by the threshold detector circuit to 2.01 V. At this instant, the RF frequency of the 5G C-RAN is shifted to a new RF frequency to operate on. In this example on figure 9.8, this new frequency is around 4.8 GHz. At the same time, the error signal goes off, showing that danger is cleared and no RFI is present. The 5G C-RAN then stays at this new RF frequency until other system (or until the telescope shift and observe at this new frequency) comes and interferes with it. It will then shift to a new RF frequency to operate on, leaving the other system (in this case the telescope) to occupy the previous spectrum of the 5G C-RAN. Noteworthy in figure 9.8 is how spectrally-rich the system is. When carefully analysing figure 9.8 (blue curve), we can see that the shift in RF carrier frequency is small. The adopted photonic RF transmitter system could generate RF carrier frequencies in steps of less than 1 GHz. For instance, in our previous example, the shift was only 0.8 GHz. This shows that the adopted RF transmitter can achieves coexistence and high spectral efficiency by exploiting narrow gaps in the ambient spectrum.

Additionally, we analysed how the wavelength difference of the two lasers shift when an RFI is detected. The results are given in figure 9.9. The RF carrier frequency is set at 4 GHz initially. The interfering frequency is automatically varied from 0 GHz towards the frequency of the RF carrier. When the interfering frequency is within the forbidden bandwidth of the 5G C-RAN, the system detected a large error signal, showing that a different system is interfering with it. At this instant, the wavelength for the DFB laser (CWL 1 on figure 9.3) is shifted to a new wavelength. At the same time, the error signal goes off, showing that no RFI is present. The system then stays at this new wavelength until another system comes and interferes with it. It will then shift to a new wavelength to operate on.

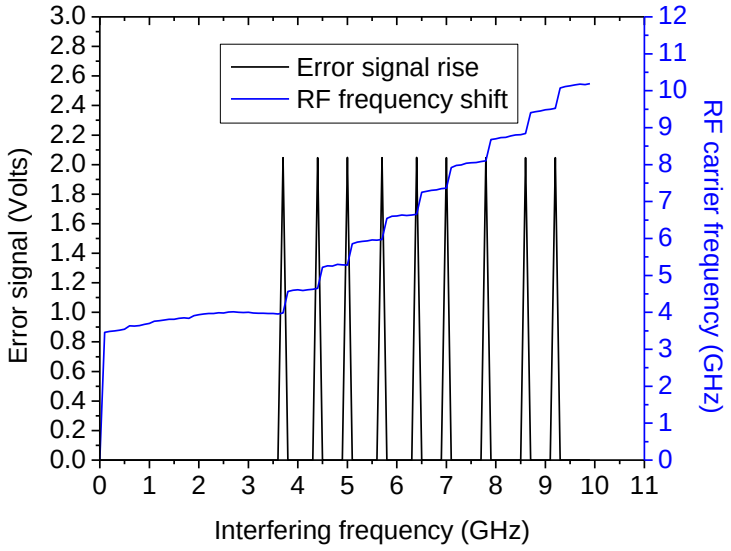

Figure 9.8 Shift in RF carrier frequency for C-RAN when RFI is detected

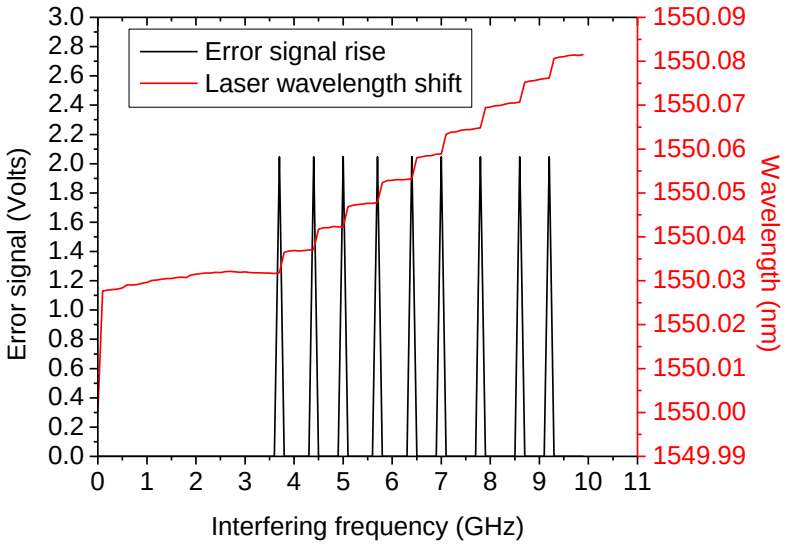

Figure 9.9 Shift in CWL 2 wavelength for C-RAN when RFI is detected

Figure 9.10 shows how the RF carrier frequency and the wavelength shift when an interfering frequency collides with the operating frequency of the 5G C-RAN. We can see that both the wavelength and the RF carrier frequency shift instantly when the system detects an interfering frequency. It is worth noting that the wavelength value on figures 9.9 and 9.10 is not the shift in wavelength for CWL 2, but rather it is the difference in wavelength that results when CWL 2 is shifted by the system or trigger by the threshold detector circuit. We can see that when RFI occurs, the wavelength difference between CWL 1 and CWL 2 increases. This increase in wavelength difference corresponds to a new RF carrier frequency generated at which the 5G C-RAN can now operate. For example, when the RF carrier collides with an intruding RF signal at 6 GHz, the wavelength difference becomes 1550.06 nm, corresponding to a heterodyning RF frequency of about 7 GHz.

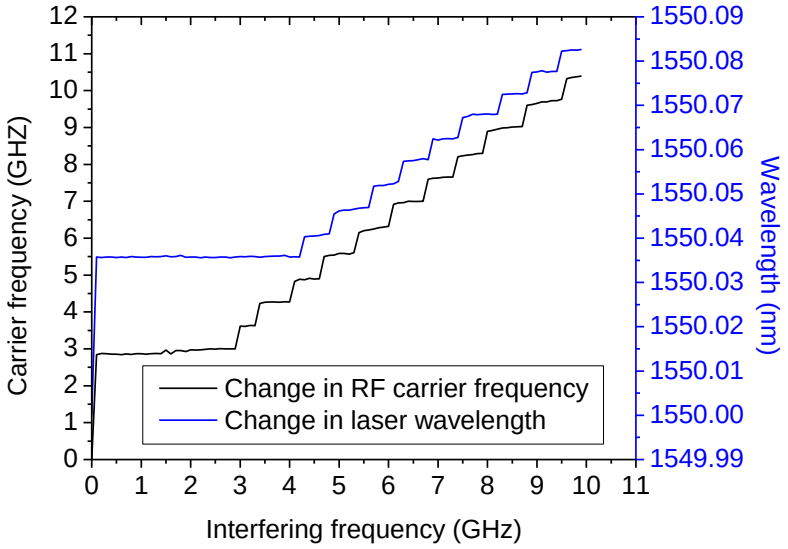

Figure 9.10 Shift in CWL 2 wavelength and RF carrier for the C-RAN when RFI is detected

For the proposed 5G C-RAN system to operate effectively without compromising, the reaction time for the system to RFIs is very important. The system should correct for RFIs as fast as possible without any compromise on both the transmitted data for the 5G C-RAN and the observed astronomical data. We have measured the time response of our proposed system. Figure 9.11 summarizes these findings. In figure 9.11, we measured the time when the error signal rises and when it falls. The time when the error signal rises symbolize the presence of an RFI. When it falls, it symbolizes the absence of an RFI. The difference in time is the system's response time. When this time was measured for our systems, we found that the system was able to correct for RFI within a time frame of about 3 microseconds. This means that when the system detects an RFI, it is able to correct for that interference within 3 microseconds.

The time response of our network is recommendable when considering the data rates these 5G C-RANs are expected to achieve. For example, a 5G C-RAN using the mid-band frequencies between 1 and 6 GHz is expected to transmit at the download and upload speed of 100 Mbps and 50 Mbps, respectively [205]. This means that within a fraction of a second, before another 50 megabits are transmitted, our 5G C-RAN system should has already corrected itself, and the new data to be transmitted will not be affected. Since the RFI mitigation algorithm is implemented at the photonic RF transmitter, the 5G user will have to tolerate for a transmission delay of around 3 milliseconds while the network is correcting for an RFI. In fact, the most crucial part is that the newly generated RF frequency should also be a 5G signal to accommodate the next data to be transmitted. This is the case when we look at figures 9.8. These results clearly demonstrate the applicability of our proposed solution for RFI mitigation when two networks are sharing the same RF spectrum for different applications.

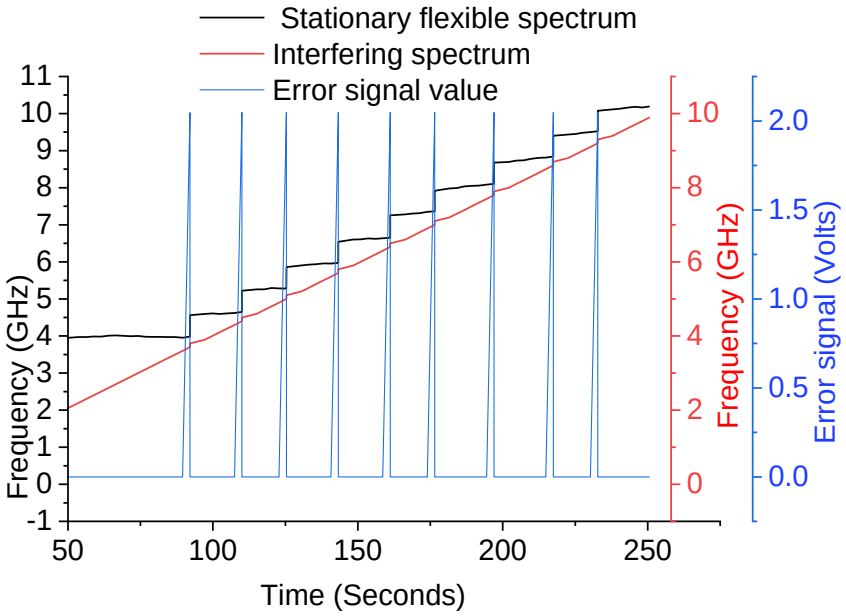

Figure 9.11 Time response of the system when RFI is detected

Chapter Summary

Chapter 9 experimentally demonstrated the flexibility of a photonic RF transmitter based on optical heterodyning of two DFB laser in mitigating RFI due to frequency collisions. This demonstration will find application in future converged networks where different telco services are expected to share spectrum resources. When this system is used within radio astronomy to realize mobile communication without the consequences of RFI, it was found that the photonic RF transmitter is able to respond to interference within 3 milliseconds. This fast response time was achieved by designing a network that flexibly shift the wavelength of one of the heterodyning lasers in order to generate a new beating RF carrier signal at the photodiode. The system proved to be spectrally rich by generating RF carriers in steps of less than 1 GHz when the network shift from one RF carrier to the next at the time of interference. This means our photonic RF transmitter can be find application in tightly-park spectral bands to realize effective utilization of radio frequency resources.

Chapter 10: Conclusions

Radio astronomy research in Africa is growing rapidly. South Africa and other SKA partner countries such as Ghana have taken a keen interest in radio astronomy research. The unprecedented interest for radio astronomy research is due to the overall undeniable benefits that these big data science projects have in overall economy of a partaking country. These benefits include job creation, advanced infrastructure development, and the creation of technically-skilled societies.

In a parallel manner, 5G communication systems are also continuously being research and deployed across the African continent. South Africa is also expected to realize 5G mobile services by 2023. The advantages of 5G communication systems are clearly visible, especially when considering the digital revolution that is expected by the 21 century.

Throughout history, the developments in either radio astronomy or radio communication network is known to weigh negatively on each other. For example, radio communication services are known to have negative impact on radio astronomy research.

To that end, different techniques have been proposed to mitigate the radio frequency interference to the radio astronomer due to radio communication networks. Few of these techniques include, but not limited to government regulations, radio quite zones, and design of advanced electronic transmitter solutions. The establishment of proposed techniques such as radio quite zones have resulted into contradicting opinions from the society. In the opinion of the authors, the currently proposed solutions to mitigate radio frequency interference are ineffective, unscalable and creates inconvenient.

Next generation networks will be converged. This means that different telco services will have to share spectrum resource without one application affecting the other. To achieve this, advanced RFI mitigation solutions are needed.

In this thesis, we proposed advanced novel photonic solution to improve the use of the already-scarce radio frequency spectrum. We have proposed for the first, the use of flexible photonic RF transmitter to design 5G radio communication systems within radio astronomy areas without the threat of radio frequency interference to the radio astronomer. This proposed solution will greatly improve the utilization of radio frequency resources by designing networks that share spectrum without affecting one another.

In chapter 5, we developed an experimental photonic 5G communication system based on cost-effective vertical cavity surface emitting semiconductor lasers. These lasers are low-power and have excellent wavelength tenability to enable them for this novel application. Chapter 5 demonstrated how an optical heterodyning scheme use independent VCSELs can be used to achieve flexible 5G network that offer high data rate to the radio astronomer. Advanced modulation and demodulation techniques were implemented to achieve the unprecedent network performance. In the same chapter, we demonstrated a novel 5G photonic transmitter system by gain-switching a VCSEL laser to generate multichannel optical source. The resultant coherent optical lines were used to transmit high data rates to the radio astronomer. The flexibility for the novel transmitter to achieve RFI-free applications in radio astronomy was also highlighted and discussed.

In chapter 6, we numerically analyzed the effects of optical power ratio between two heterodyning optical signals on the generated RF carrier signal and the baseband signal. Recommendation based on the findings were given to help 5G network designer realize simple photonic RF transmitters. The finding for chapter 6 will help 5G network designers realize simplified 5G photonic RF transmitters without compromising on the data transmission

performance of the network.

Chapter 7 demonstrated the novel use of a single vertical cavity surface emitting laser to transmit both reference clock signals and data signals in radio astronomy networks. Wavelength division multiplexing technique was used to maximize the use of the enormous bandwidths of optical fibers. A 30-Gbps network was demonstrated. In our demonstration, both the clock and the data signals were received error-free. For the transmitted data, bit error rate of 10^{-9} were achieved for the three transmitted channels. This technique is expected to assist radio astronomers by avoiding the use of independent lasers to transmit both clock and data signals. Using independent laser sources makes the network costly and difficult to manage.

Future radio astronomy facilities will require the presence of both fixed and wireless network. The radio astronomer will require these advanced telco services without compromising on the issue of radio frequency interference. In chapter 8, we developed a novel 5G network that simultaneously provide fixed and wireless communication services to an astronomer. In our demonstration, a single low-power and low-cost vertical cavity laser was used for the first time to achieve this hybrid application. Up to 28 Gbps error-free data were delivered to a wireless user. The fixed user was supported with advanced data rates up to 8.5 Gbps. Both results were realized with a novel photonic transmitter systems that automatically control and mitigate the RFI effects expected from these radio networks.

The intelligence of a photonic RF transmitter to mitigate radio frequency interference was demonstrated for the first in chapter 9. We developed an optical heterodyning-based photonic RF transmuter using DFB lasers to demonstrate the application of these systems in radio astronomy to realize RFI-free radio communication services. The developed photonic transmitter system was able to response and correct for RFI within an impressive time duration of 3 milliseconds.

As network providers seek and continue to research on novel solutions to maximize the spectral efficiency of future 5G communication systems, results reported in this thesis serve as a guide toward that exciting future. Through the findings of this thesis, network designer can look toward a future where telco networks will coexist in harmony without any threat to one another. In this thesis, we have laid a foundation toward a network revolution where low-cost optical devices such as VCSELs and photodiodes are used to achieve radio communication service within areas where these systems are otherwise known to be avoided.

Appendix A: Research out in peer reviewed journals and conferences

Year 2021 Peer Reviewed Journal Publications

R. S. Karembera, K. Nfanyana, G. M. Isoe & T. B. Gibbon (2021) Experimental investigation of VCSEL-based optical heterodyning with PAM 4 and envelop detection for 5G fronthaul systems, Journal of Modern Optics, DOI: 10.1080/09500340.2021.1999516

Reinhard Karembera and Tim Gibbon, "Coherent 16-QAM bidirectional fiber-wireless hybrid access network with optimal use of the optical local oscillator signal," *Optics Communications,* vol. 501, no. 127367, 2021.

Reinhard Karembera, Ketshabile Nfanyana, and Tim Gibbon, "Simultaneous transmission of clock and data signals in photonic-assisted WDM passive optical networks," *J. Opt. Soc. Am. B*, vol. 38, Issue 2, pp. 914-921, 2021.

Reinhard Karembera and Tim Gibbon, "Effects of optical local oscillator power on the network bit error rate in optical heterodyning of comb lines from a gain-switched VCSEL comb," *Optics & Laser Technology*, vol. 139, pp. 106-955, 2021.

Year 2020 Peer Reviewed Journal Publications

Reinhard Karembera, Chrispine Censur, and Tim Gibbon, "Sub-60-GHz power-efficient fronthaul system of up to 16-Gbps using RF carriers generated from a gain-switched VCSEL," *OSA Continuum*, vol. 3, Issue 12, pp. 3482-3496, 2020.

Reinhard Karembera, Shukree Wassin, George Isoe, Ketshabile Nfanyana, and Tim Gibbon, "All-optical flexible 5G signal generation and transmission for spectrum resource optimization," *J. Opt. Soc. Am. B*, vol. 37, Issue 11, pp. pp. A324-A330, 2020.

Ketshabile Nfanyana, Shukree Wassin, **Reinhard Karembera**, James Jena, and Tim Gibbon, "All-photonic 20-MHz clock for latency monitoring in a 5G network at 10 Gbps over optical fiber," *J. Opt. Soc. Am. B*, vol. 37, Issue 11, pp. A202-A206, 2020.

George Isoe, **Reinhard Karembera**, and Tim Gibbon, "Advanced VCSEL photonics: Multi-level PAM for spectral efficient 5G wireless transport network," *Optics Communications*, vol. 461, pp. 125-273, 2020

Year 2019 Peer Reviewed Conference Publications

Reinhard Karembera, S Wassin, J Jena, G Isoe, TB Gibbon, "Flexible Photonic-based RF Signals Generation and Data Modulation for Emerging 5GWireless Communication," Proceedings of Southern African Telecommunication Networks and Application Conference (SATNAC), Kwa-Zulu Natal, South Africa (1-4 September 2019), pp. 2-3. [Work in Progress Paper]

Year 2019 Non-Reviewed Conference Publications

Reinhard Karembera, T.B. Gibbon, “Flexible Photonic-based Generation of 5G RF Carriers to Co-Exist with SKA Frequency Spectrum”, SKA Student Conference, Durban, 2-6 Dec 2019.

References

[1] P.W.W Fuller, "An introduction to high speed photography and photonics," *The Imaging Science Journal*, Vol 57, No. 6, pp. 293-302, 2009, DOI: 10.1179/136821909X12490326247524.

[2] Bland-Hawthorn J, Leon-Saval SG, "Astrophotonics: molding the flow of light in astronomical instruments," *Opt Express*, Vol. 25, No. 15549, 2017, https://doi.org/10.1364/OE.25.015549. arXiv:1706.05132.

[3] Romina Diener, Jan Tepper, Lucas Labadie, Thomas Pertsch, Stefan Nolte, and Stefano Minardi," Towards 3D-photonic, multi-telescope beam combiners for mid-infrared astrointerferometry," *Opt. Express* Vol 25, No. 16, pp. 19262-19274, 2017.

[4] P.G. Kryukov, "Laser optical frequency combs and their applications in optical fibre communication systems and astrophysics," *Quantum Electron*., Vol. 49, No. 10, 2019.

[5] N. Cvetojevic, N. Jovanovic, J. Lawrence *et al*., "Developing arrayed waveguide grating spectrographs for multi-object astronomical spectroscopy," *Optics express*, Vol. 20, No. (3), pp. 2062, 2012, doi:10.1364/oe.20.002062.

[6] N. Anugu, K.M. Morzinski, J. Eisner *et al*., "Betelgeuse scope: Single-mode-fibers-assisted optical interferometer design for dedicated stellar activity monitoring," *Proceedings of SPIE - The International Society for Optical Engineering*, Vol. 11490. SPIE. https://doi.org/10.1117/12.2568900.

[7] R. Siebrits *et al*., "Dissemination of Reference Signals for a Next Generation Radio Telescope," *2018 IEEE International Frequency Control Symposium (IFCS)*, pp.1-6, 2018, doi: 10.1109/FCS.2018.8597492.

[8] K.M Hampson, R. Turcotte, D.T Miller et al., "Adaptive optics for high-resolution imaging," *Nat Rev Methods Primers* Vol. 1, No. 68, 2021, https://doi.org/10.1038/s43586-021-00066-7.

[9] S. Srikanth, "An Examination of Radio Telescope Parameters and their Significance," *2021 International Conference on Electromagnetics in Advanced Applications (ICEAA)*, pp. 205-205, 2021, doi: 10.1109/ICEAA52647.2021.9539636.

[10] David Mandaha, "Celebrating 30 years of Space Geodesy," in *Science and Technology*, Volume 68, 2016.

[11] P. Thavasimani and A. Scaife, "Square Kilometre Array: Processing Voluminous MeerKAT data on IRIS," *Cornell University, Astrophysics: Instrumentation and Methods for Astrophysics*, 2021.

[12] Helgavan der Merwe, "Vegetation of the Square Kilometre Array (SKA), South Africa: A baseline to measure local and global change," South African Journal of Botany, Vol. 132, pp. 22-29, 2020, https://doi.org/10.1016/j.sajb.2020.03.025.

[13] D. Crichton, M. Aich, A. Amara *et al*., "The Hydrogen Intensity and Real-time Analysis eXperiment: 256-Element Array Status and Overview," *Cornell University, Astrophysics: Instrumentation and Methods for Astrophysics*, 2021.

[14] B D Sabered, M J Gaylard, C Horellou, H Winkler, and T Jarrett, “Radio astronomy in Africa: the case of Ghana,” *Scientific Report*, Vol. 6, April 2015.

[15] G. Barb and M. Otesteanu, “4G/5G: A Comparative Study and Overview on What to Expect from 5G,” *2020 43rd International Conference on Telecommunications and Signal Processing (TSP)*, pp. 37-40, 2020, doi: 10.1109/TSP49548.2020.9163402.

[16] R. Somanah and U. Shankar, “Astrophysical results of the Mauritius radio telescope” *Astrophy. & Space Sci*., pp 282 57-67, 2002.

[17] Baldwin J E et al., “The 6C survey of radio sources – I. Declination zone δ>+80,” *Monthly Notices of the Royal Astronomical Society*, Vol. 217, No. 4, pp. 717-730, 1985, https://doi.org/10.1093/mnras/217.4.717.

[18] P. A Woudt, R. P Fender, R. P Armstrong, and C. Carignan, “Early science with the Karoo Array Telescope test array KAT-7,” *South African Journal of Science*. Vol. 109 No. (7/8), 2013.

[19] B. D. Asabere, M. Gaylard, C. Horellou, H. Winkler, and T. Jarrett, “Radio astronomy in Africa: the case of Ghana,” *Cornell University*, *Astrophysics: Instrumentation and Methods for Astrophysics*, Vol 2, 2015.

[20] African radio astronomy ready for takeoff, Aerospace Technology, 2015. Available online: https://www.aerospace-technology.com/features/featureafrican-radio-astronomy-ready-for-takeoff/

[21] J. G. B. de Vaate and A. J. Faulkner, “Aperture arrays for the Square Kilometre Array,” *2012 International Conference on Electromagnetics in Advanced Applications*, pp. 618-621, 2012, doi: 10.1109/ICEAA.2012.6328700.

[22] R. T. Schilizzi, E. F. P Dewdney, T. W. J Lazio “The square kilometre array”, *Proc. SPIE 7733, Ground-based and Airborne Telescopes III*, No. 773318, 2010, https://doi.org/10.1117/12.856344.

[23] P. E. Dewdney, P. J. Hall, R. T. Schilizzi and T. J. L. W. Lazio, “The Square Kilometre Array,” *in Proceedings of the IEEE*, Vol. 97, No. 8, pp. 1482-1496, 2009, doi: 10.1109/JPROC.2009.2021005.

[24] Cherryl Walker and Davide Chinigò, “Disassembling the Square Kilometre Array: astronomy and development in South Africa,” *Third World Quarterly*, Vol. 39, No. 10, 2018.

[25] R. N. Ghose, “Interference Mitigation: Theory and Application,” New York, IEEE Press, 1996.

[26] http://www.itu.int/pub/R-REC/en.

[27] J. Cohen, T. Spoelstra, R. Ambrosini, and Wim van Diel, “CRAF Handbook for Radio Astronomy,” *European Science Foundation*, Vol. 3, Strasbourg, France, 2005.

[28] International Telecommunication Union, “ITU-R Handbook on Radio Astronomy,” *ITU-R Radiocommunications Bureau*, Geneva, Switzerland, 2003.

[29] RECOMMENDATION ITU-R RA.769-2, “Protection criteria used for radio astronomical measurements,” *The ITU Radiocommunication Assembly*, Available online: https://www.itu.int/dms_pubrec/itu-r/rec/ra/R-REC-RA.769-2-200305-I!!PDF-E.pdf.

[30] M. Kesteven, “The Current Status of RFI Mitigation in Radioastronomy,” available online: https://www.gb.nrao.edu/~sheather/SAVI/iau_rfi-1.pdf.

[31] Wiid, P. Gideon, “Lightning Protection and Radio Frequency Interference Mitigation for the Karoo array telescope,” *Thesis (PhD (Electrical and Electronic Engineering)), University of Stellenbosch*, 2010. Available online: http://scholar.sun.ac.za/handle/10019.1/4009.

[32] A. W. Hotan, J. D. Bunton, A. P. Chippendale *et al*., “Australian square kilometre array pathfinder: I. system description,” *Publications of the Astronomical Society of Australia*, Vol. 38, 2021, DOI: https://doi.org/10.1017/pasa.2021.1

[33] W. van Driel, “Radio quiet, please! – protecting radio astronomy from interference,” *Published online by Cambridge University Press*, 2011. Available online https://www.cambridge.org/core/journals/proceedings-of-the-international-astronomical-union/article/radio-quiet-please-protecting-radio-astronomy-from-interference/AE8E2F8CDF8B29FAF7890BAD24F4691F

[34] D. R. DeBoer, A. R. Parsons1, J. E. Aguirre *et al.*, “Astronomical Instrumentation, Telescopes, Observatories, and Site Characterization,” *Astronomical Society of the Pacific*, Vol. 129, No. 974, 2017.

[35] J. J. Sun, M. P. Chang, and P. R. Prucnal, “Demonstration of Over-the-Air RF Self-Interference Cancellation Using an Optical System,” *in IEEE Photonics Technology Letters*, vol. 29, no. 4, pp. 397-400, 2017, doi: 10.1109/LPT.2017.2651589.

[36] V. Clerc, R. Weber, L. Denis, and C. Rosolen, “High Performance Receiver for RFI Mitigation in Radio Astronomy: Application at Decameter Wavelengths,” EUSPICO'02, Toulouse, France, 2002.

[37] R. Weber, V. Clerc, L. Denis, and C. Rosolen, “Robust Receiver for RFI Mitigation in Radio Astronomy,” Proceedings of the XXVII General Assembly of the International Union of Radio Science, Maastricht, The Netherlands, 2002.

[38] G. Tuccari, A. Caddemi, G. Nicotra, and F. Consoli, “Cryogenic Filters for RFI Mitigation in Radioastronomy,” Proc. 7th European VLBI Network Symposium, Toledo, Spain, 2004.

[39] N. Niamsuwan, J. T. Johnson, and S. W. Ellingsen, “Examination of a Simple Pulse-Blanking Technique for Radio Frequency Interference Mitigation,” Radio Science, 50, 5, 2005, RS5S03.

[40] S. W. Ellingson and G. A. Hampson, “Mitigation of Radar Interference in L-Band Radio Astronomy,” Atrophys. J Suppl. Ser., 147,2003, pp 167-176.

[41] W. A. Baan, P. A. Fridman, and R. P. Millenaar, “Radio Frequency Interference Mitigation at the Westerbork Synthesis Array: Algorithms, Test Observations and System Implementation,” Astronomical Journal, 128,2004, pp. 993-949.

[42] Ch. Yang, T. Nguyen, E. Blasch et al., "Post-correlation semi-coherent integration for high-dynamic and weak GPS signal acquisition," *2008 IEEE/ION Position, Location and Navigation Symposium*, pp. 1341-1349, 2008, doi: 10.1109/PLANS.2008.4570122.

[43] Simon Haykin, Adaptive Filter Theory, New York, Prentice Hall, 1986.

[44] R. Finger, F. Curotto, R. Fuentes *et al*., "A FPGA-based Fast Converging Digital Adaptive Filter for Real-time RFI Mitigation on Ground Based Radio Telescopes," Astronomical Society of the Pacific, Vol. 130, No. 984, 2017.

[45] R. Weber, L. Denis, and S. Bretteil, "DSP enabled radio astronomy in highly corruptive environment," *IEEE Colloquium on DSP enabled Radio*, pp. 1-6, 2003, doi: 10.1049/ic.2003.0336.

[46] K. D. Buch, "RFI Excision in Radiometers: A Radio Astronomy Perspective," *IGARSS 2019 - 2019 IEEE International Geoscience and Remote Sensing Symposium*, pp. 4535-4538, 2019, doi: 10.1109/IGARSS.2019.8898589.

[47] T. S Rappaport, A. Annamalai, R. M. Buehrer, and W. H Trante, "Wireless Communications: Past Events and a Future Perspective," *IEEE Communications Magazine*, Vol. 40, No. 5, pp. 148-161, 2015, DOI:10.1109/MCOM.2002.1006984.

[48] J. Rendon, F. Casadevall, L. Garcia and R. Jimenez, "Characterization of the GPRS radio interface by means of a statistical model," *IEEE VTS 53rd Vehicular Technology Conference*, Vol. 4 pp. 2392-2396, 2001, doi: 10.1109/VETECS.2001.944029.

[49] A. Furuskär, S. Mazur, F. Müller, and H. Olofsson, "EDGE: Enhanced data rates for GSM and TDMA/136 evolution," *IEEE Pers. Commun*., vol. 6, pp. 56-66, 1999.

[50] H. Holma and A. Toskala, "WCDMA for UMTS: Radio Access for Third Generation Mobile Communications," New York, NY, USA: Wiley, 2001.

[51] H. Holma and A. Toskala, "WCDMA for UMTS: HSPA Evolution and LTE," New York, NY, USA: Wiley, 2007.

[52] H. Honkasalo, K. Pehkonen, M. T. Niemi and A. T. Leino, "WCDMA and WLAN for 3G and beyond," *in IEEE Wireless Communications*, Vol. 9, No. 2, pp. 14-18, 2002, doi: 10.1109/MWC.2002.998520.

[53] H. Holma and A. Toskala, "WCDMA for UMTS: Radio Access for Third Generation Mobile Communications," New York, NY, USA: Wiley, 2001.

[54] F. Hillebrand, "The creation of standards for global mobile communication: GSM and UMTS standardization from 1982 to 2000*," in IEEE Wireless Communications*, Vol. 20, No. 5, pp. 24-33, 2013, doi: 10.1109/MWC.2013.6664470.

[55] Ivan B. Djordjevic, "Advanced Optical and Wireless Communications Systems," *Springer International Publishing AG*, 2018.

[56] M. H Reddy1, S. Jaswanth, and N. V. Pramod, "Evolution of Mobile Networks: From 1G TO 4G," Advanced Research in Electrical and Electronic Engineering, Vol. 3, No. 4, pp. 307-310, 2016.

[57] Ivan B. Djordjevic, "Advanced Optical and Wireless Communications Systems," 1st Ed. USA: Springer, Cham, 2018, https://doi.org/10.1007/978-3-319-63151-6.

[58] M. Döttling, W. Mohr, A. Osseiran, “Radio Technologies and Concepts for IMT-Advanced,” John Wiley & Sons, 2009.

[59] M. Njikam, S. Nanna, S. Shahrin, M. F Othman, “High speed internet development in Africa using 4G-LTE technology-a review,” *Bulletin of Electrical Engineering and Informatics*, Vol.8, No.2, pp. 577~585, 2019, DOI: 10.11591/eei.v8i2.684.

[60] Z. Abichar, Y. Peng, and J. M. Chang, “WiMax: The Emergence of Wireless Broadband,” *in IT Professional*, vol. 8, no. 4, pp. 44-48, 2006, doi: 10.1109/MITP.2006.99.

[61] Evolved Universal Terrestrial Radio Access (E-UTRA) and Evolved Uni- versal Terrestrial Radio Access Network (E-UTRAN); Overall Description, document TS 36.300, 3GPP, Release 8, 2006.

[62] Evolved Universal Terrestrial Radio Access (E-UTRA) and Evolved Uni- versal Terrestrial Radio Access Network (E-UTRAN); Overall Description, document TS 36.300, 3GPP, Release 9, 2006.

[63] T. Ali-Yahiya, Understanding LTE and Its Performance. Berlin, Germany: Springer, 2011.

[64] Alcatel. (2009). The LTE Network Architecture: A Comprehensive Tutorial. Accessed: Sep. 19, 2018. [Online]. Available: http://www.cse.unt.edu/~rdantu/FALL_2013_WIRELESS_NETWORKS/LTE_ Alcatel_White_Paper.pdf

[65] Technical Specification Group Services & System Aspects, “TS 23.402: Architecture enhancements for non-3GPP accesses (Release 8),” 3GPP, Tech. Rep. v8.1.1, March 2008.

[66] E. Dahlman, “3G Evolution: HSPA LTE for Mobile Broadband,” Amsterdam, The Netherlands: Elsevier, 2010.

[67] A. Checko, H. L. Christiansen, Y. Yan, L. Scolari, G. Kardaras, M. S. Berger, and L. Dittmann, “Cloud RAN for mobile networks: A technology overview,” *IEEE Commun. Surveys Tuts*., vol. 17, no. 1, pp. 405-426, 2015.

[68] The Path to 5G Requires a Strong Optical Network: From C-RAN to Cloud-RAN, Expo, Houston, TX, USA, 2017.

[69] J. Gozalvez, “5G Tests and Demonstrations [Mobile Radio],” in *IEEE Vehicular Technology Magazine*, vol. 10, no. 2, pp. 16-25, 2015, doi: 10.1109/MVT.2015.2414831.

[70] J. Gozalvez, “5G Worldwide Developments [Mobile Radio],” in *IEEE Vehicular Technology Magazine*, vol. 12, no. 1, pp. 4-11, March 2017, doi: 10.1109/MVT.2016.2641138.

[71] G. Kardaras and C. Lanzani, “Advanced multimode radio for wireless & Mobile broadband communication,” in *Proc. Eur. Wireless Technol. Conf*., Rome, Italy, 2009, pp. 132-135.

[72] C-RAN the Road Towards Green RAN-White Paper, China Mobile Res. Inst., China Mobile, Beijing, China, Oct. 2011.

[73] Y. Lin, L. Shao, Z. Zhu, Q. Wang, and R. K. Sabhikhi, "Wireless network cloud: Architecture and system requirements," *IBM J. Res. Develop*., vol. 54, no. 1, pp. 4:14:12, 2010.

[74] C. I, J. Huang, R. Duan, C. Cui, J. Jiang and L. Li, "Recent Progress on C-RAN Centralization and Cloudification," in *IEEE Access*, vol. 2, pp. 1030-1039, 2014, doi: 10.1109/ACCESS.2014.2351411.

[75] M. A. Habibi *et al.*, A Comprehensive Survey of RAN Architectures Toward 5G Mobile Communication System, IEEE Access, Vol. 17, 2019.

[76] M. Fiorani, S. Tombaz, J. Mårtensson, B. Skubic, L. Wosinska, and P. Monti, "Energy performance of C-RAN with 5G-NX radio networks and optical transport," *2016 IEEE International Conference on Communications (ICC)*, pp. 1-6, 2016, doi: 10.1109/ICC.2016.7510717.

[77] R. Waterhouse *et al*., "RF over fiber distribution schemes for 60 GHz wireless personal area networks (WPANs)," in *Proc. Asia-Pac. Microw. Conf.*, Melbourne, Australia, pp. 1714–1717, 2011.

[78] N. Al-Falahy and O. Y. Alani, "Technologies for 5G Networks: Challenges and Opportunities," in *IT Professional*, vol. 19, no. 1, pp. 12-20, 2017, doi: 10.1109/MITP.2017.9.

[79] J. An, K. Yang, J. Wu, N. Ye, S. Guo, and Z. Liao, "Achieving Sustainable Ultra-Dense Heterogeneous Networks for 5G," in *IEEE Communications Magazine*, vol. 55, no. 12, pp. 84-90, 2017, doi: 10.1109/MCOM.2017.1700410.

[80] J. Kim *et al.*, "MIMO-Supporting Radio-Over-Fiber System and its Application in mmWave-Based Indoor 5G Mobile Network," in *Journal of Lightwave Technology*, Vol. 38, No. 1, pp. 101-111, 2020, doi: 10.1109/JLT.2019.2931318.

[81] A. Sukarno, A. Hikmaturokhman, and D. Rachmawaty, "Comparison of 5G NR Planning in Mid-Band and High-Band in Jababeka Industrial Estate," *2020 IEEE International Conference on Communication, Networks and Satellite (Comnetsat)*, pp. 12-17, 2020, doi: 10.1109/Comnetsat50391.2020.9329000.

[82] Osseiran A, Boccardi F, Braun V, Kusume K, Marsch P, Maternia M, Queseth O, Schellmann M, Schotten H (2014) Scenarios for 5G mobile and wireless communications: the vision of the METIS project. IEEE Commun Mag 52(5):26–35

[83] Osseiran A, Monserrat JF, Marsch P (2016) 5G mobile and wireless communications technology. Cambridge University Press, Cambridge, MA.

[84] J. G. Andrews et al., "What will 5G be?" IEEE J. Sel. Areas Commun., vol. 32, no. 6, pp. 1065–1082, 2014.

[85] E. Gustafsson and A. Jonsson, "Always best connected," IEEE Wireless Commun., vol. 10, no. 1, pp. 49–55, 2003.

[86] F. Lu, L. Cheng, M. Xu, J. Wang, S. Shen, and G. K. Chang, "Orthogonal and sparse chirp division multiplexing for MMW fiber-wireless integrated systems," IEEE Photon. Technol. Lett., vol. 29, no. 16, pp. 1316–1319, 2017.

[87] J. Poirson, F. Bretenaker, M. Vallet, and A. L Floch, "Analytical and experimental study of ringing effects in a Fabry–Perot cavity. Application to the measurement of high finesses," J. *Opt. Soc. Am. B* Vol. 14, pp. 2811-2817, 1997.

[88] B. Mroziewicz, "Physics of Semiconductor Lasers," pp. 348 - 364. 1991.

[89] S. Fu, W. Shi, Y. Feng *et al*., "Review of recent progress on single-frequency fiber lasers [Invited]," J. *Opt. Soc. Am. B* Vol. 34, pp. A49-A62, 2017.

[90] S. Zhang, Y. Li, and X. Zong. "Progress in Dual Frequency HeNe Laser and Application."

[91] D. J Potgieter and T. C du Plessis, *Standard Encyclopedia of Southern Africa*, Vol. 6. pp. 306–307. Nasou, Cape Town, 1972.

[92] I. M. Jauncey, L. Reekie, J. E. Townsend et al., "Single-longitudinal-mode operation of an Nd3+-doped fibre laser," *Electron. Lett.* Vol. 24, pp. 24–26, 1988.

[93] L. Dong, W. H. Loh, J. E. Caplen, et al., "Efficient single-frequency fiber lasers with novel photosensitive Er/Yb optical fibers," *Opt. Lett.* Vol. 22, pp. 694–696, 1997.

[94] J. Shi, S. Alam, and M. Ibsen, "Sub-watt threshold, kilohertz linewidth Raman distributed-feedback fiber laser," *Opt. Lett*. Vol. 37, pp. 1544–1546 , 2012.

[95] G. A. Ball, W. W. Morey, and W. H. Glenn, "Standing-wave monomode erbium fiber laser," *IEEE Photon. Technol. Lett*. Vol 3, pp. 613–615, 1991.

[96] C. P. Spiegelberg, "Compact 100 mW fiber laser with 2 kHz linewidth," in *Optical Fiber Communication Conference*, OSA Technical Digest (Optical Society of America, 2003), paper PD45.

[97] Z. Meng, G. Stewart, and G. Whitenett, "Stable single-mode operation of a narrow-linewidth, linearly polarized, erbium-fiber ring laser using a saturable absorber," *J. Lightwave Technol.* Vol 24, pp. 2179–2183, 2006.

[98] S. Feng, Q. Mao, Y. Tian, Y. Ma, W. Li, and L. Wei, "Widely tunable single longitudinal mode fiber laser with cascaded fiber-ring secondary cavity," *IEEE Photon. Technol. Lett.*, Vol 25, pp. 323–326, 2013.

[99] X. Liu, "A Novel Dual-Wavelength DFB Fiber Laser Based on Symmetrical FBG Structure," *IEEE Photonics techno. Lett*., Vol. 19, No. 9, 2007.

[100] J. Geng, S. Staines, and S. Jiang, "Dual-frequency Brillouin fiber laser for optical generation of tunable low-noise radio frequency/microwave frequency," *Opt. Lett*. Vol. 33, pp. 16-18, 2008.

[101] Z. Wu, Q. Shen, L. Zhan *et a*l., "Optical Generation of Stable Microwave Signal Using a Dual-Wavelength Brillouin Fiber Laser," in *IEEE Photonics Technology Letters*, Vol. 22, No. 8, pp. 568-570, 2010, doi: 10.1109/LPT.2010.2042803.

[102] M. Dasan, F. Francis, K. T Sarath, E. Dipin, and T. Srinivas, “Optically Multiplexed Systems: Wavelength Division Multiplexing,” *Open access peer-reviewed chapter*, 2009, DOI: 10.5772/intechopen.88086.

[103] P. W. Smith, “Mode selection in lasers,” in *Proceedings of the IEEE*, vol. 60, no. 4, pp. 422-440, 1972, doi: 10.1109/PROC.1972.8649.

[104] A. Schülzgen *et al*., “Distributed feedback fiber laser pumped by multimode laser diodes”, *Opt. Lett*. Vol. 33, No. 6, pp. 614, 2008, doi:10.1364/OL.33.000614.

[105] D. F. Welch, “A brief history of high-power semiconductor lasers,” in *IEEE Journal of Selected Topics in Quantum Electronics*, Vol. 6, No. 6, pp. 1470-1477, 2000, doi: 10.1109/2944.902203.

[106] T. Kunii and Y. Matsui, “Narrow spectral linewidth semiconductor lasers,” *Opt Quant Electron*, Vol. 24, pp. 719–735, 1992, https://doi.org/10.1007/BF00620152.

[107] H. Liu, S. Arahira, T. Kunii, and Y. Ogawa, “Tuning characteristics of monolithic passively mode-locked distributed Bragg reflector semiconductor lasers,” in *IEEE Journal of Quantum Electronics*, Vol. 32, No. 11, pp. 1965-1975, 1996, doi: 10.1109/3.541683.

[108] Y. Zhang *et al*., “Experimental Demonstration of the Distributed Feedback Semiconductor Laser With S-Bent Waveguide and Sampled Grating,” in *IEEE Photonics Journal*, vol. 9, no. 5, pp. 1-11, 2017, doi: 10.1109/JPHOT.2017.2751573.

[109] T. Jung, H. Sung, M.C. Wu et al., “Demonstration of monolithic optical injection locking using a two section DFB laser,” *Conference on Lasers and Electro-Optics*, paper CThC4, 2003.

[110] H. Sung, E. K. Lau, and M. C Wu, “Large-signal analog modulation response of monolithic optical injection-locked DFB lasers,” *Conference on Lasers and Electro-Optics*, paper CTuV7, 2005.

[111] D. Liu, C. Sun, B. Xiong, and Y. Luo, “Suppression of chaos in integrated twin DFB lasers for millimeter-wave generation,” *Opt. Express*, Vol 21, pp. 2444–2451, 2013.

[112] D. Liu, C. Sun, B. Xiong, and Y. Luo, “Nonlinear dynamics in integrated coupled DFB lasers with ultra-short delay,” *Opt. Express*, Vol. 22, pp. 5614–5622, 2014.

[113] K. Iga, T. Kambayashi, K. Wakao *et al*., “GaInAsP/InP double-heterostructure planar LED’s,” *IEEE Trans. Electron Devices*, Vol. ED-26, No. 8, pp. 1227–1230, 1979.

[114] H. Soda, K. Iga, C. Kitahara, and Y. Suematsu, “GaInAsP/InP surface emitting injection lasers,” *Jpn. J. Appl. Phys*., Vol. 8, No. 12, pp. 2329–2330, 1979.

[115] K. Iga, S. Kinoshita, and F. Koyama, “Microcavity GaAlAs/GaAs surface emitting laser with Ith ¼ 6 mA,” *Electron. Lett*., Vol. 23, No. 3, pp. 134–136, 1987.

[116] T. Sakaguchi, F. Koyama, and K. Iga, “Vertical cavity surface emitting laser with an AlGaAs/AlAs Bragg reflector,” *Electron. Lett*., Vol. 24, No. 15, pp. 928–929, 1988.

[117] K. Iga, F. Koyama, and S. Kinoshita, “Surface emitting semiconductor lasers,” *IEEE J. Quantum Electron*., Vol. QE24, No. 9, pp. 1845–1855, 1988.

[118] D. L. Huffaker, Z. Zou, and D. G. Deppe, “Reduced cavity loss for ultra-low threshold vertical cavity surface emitting lasers,” *1999 IEEE LEOS Annual Meeting Conference Proceedings. LEOS'99. 12th Annual Meeting. IEEE Lasers and Electro-Optics Society 1999 Annual Meeting (Cat. No.99CH37009)*, Vol. 2, pp. 391-392, 1999, doi: 10.1109/LEOS.1999.811763.

[119] K. Iga, “Vertical-Cavity Surface-Emitting Laser (VCSEL),” *Proceedings of the IEEE*, Vol. 101, No. 10, 2013.

[120] J. Yao, “Microwave photonics,” *J. of Lightw. Technology*, Vol. 27, No. 3, 2009.

[121] D. Wake, “Optoelectronics for millimetre-wave radio over fibre systems” in Analogue Optical Fibre Communications, B. Wilson, Z. Ghassemlooy, and I. Darwazeh, ed. (The Institute of Electrical Engineers, London, 1995).

[122] A. Giesberts, “Receiver Design for a Radio over Polymer Optical Fiber System”, (M.Sc. Thesis, Eindhoven University of Technology, Eindhoven, 2003.

[123] H. J. Kbashi, V. Sharma, and S. Sergeyev, “Phase-stable millimeter-wave generation using switchable dual-wavelength fiber laser,” *Optics and Lasers in Engineering*, Vol. 137, No. 106390, 2021.

[124] I. Aldaya, G. Campuzano, C. Gosset, and G. Castañón, “Phase-Insensitive RF Envelope Detection Allows Optical Heterodyning of MHz-Linewidth Signals,” in *IEEE Photonics Technology Letters*, vol. 25, no. 22, pp. 2193-2196, 2013, doi: 10.1109/LPT.2013.2282627.

[125] G. R. Olbright, R. P. Bryan, W. S. Fu *at al*., “Linewidth, tunability, and VHF-millimeter wave frequency synthesis of vertical-cavity GaAs quantum-well surface-emitting laser diode arrays,” in *IEEE Photonics Technology Letters*, vol. 3, no. 9, pp. 779-781, 1991, doi: 10.1109/68.84490.

[126] P. Dowd, I. H. White, M. R. T. Tan et al., “Linewidth narrowed vertical-cavity surface-emitting lasers for millimeter-wave generation by optical heterodyning,” in *IEEE Journal of Selected Topics in Quantum Electronics*, vol. 3, no. 2, pp. 405-408, 1997, doi: 10.1109/2944.605685.

[127] G.M. Isoe, R.S. Karembera, and T.B. Gibbon, “Advanced VCSEL photonics: Multi-level PAM for spectral efficient 5G wireless transport network,” *J. Opti. Communications*, Vol. 461, 2020.

[128] M. Alemohammad, Y. Li, and P. Herczfeld, “Design and Dynamics of Multiloop Optical Frequency Locked Loop,” in *Journal of Lightwave Technology*, vol. 31, no. 22, pp. 3453-3459, 2013, doi: 10.1109/JLT.2013.2283470.

[129] U. Gliese et al., “A wideband heterodyne optical phase-locked loop for generation of 3-18 GHz microwave carriers,” in *IEEE Photonics Technology Letters*, vol. 4, no. 8, pp. 936-938, 1992, doi: 10.1109/68.149915.

[130] Q. Tang et al., “25 Gb/s Directly Modulated Widely Tunable 1.3 μm Dual Wavelength DFB Laser for THz Communication,” in *IEEE Photonics Technology Letters*, vol. 32, no. 7, pp. 410-413, 2020, doi: 10.1109/LPT.2020.2976569.

[131] Y. Zhang *et al*., “A stable dual-wavelength DFB semiconductor laser with equivalent chirped sampled grating,” in *IEEE Journal of Quantum Electronics*, doi: 10.1109/JQE.2021.3126447.

[132] H. J. Kbashi, V. Sharma, and S. Sergeyev, “Phase-stable millimeter-wave generation using switchable dual-wavelength fiber laser,” *Optics and Lasers in Engineering*, Vol. 137, No. 106390, 2021.

[133] B. Nakarmi, H. Chen, and S. Pan, “Microwave comb generation using single-mode Fabry-Perot laser diode,” SPIE digital library, Vol. 10917, 2019, https://doi.org/10.1117/12.2511211.

[134] H. -Y. Wang, C. -H. Cheng, B. Su et al., “QAM-GFDM of Dual-Mode VCSEL Mixed 28-GHz MMW Carrier for Fiber-Wireless Link,” in *Journal of Lightwave Technology*, vol. 39, no. 19, pp. 6076-6084, 2021, doi: 10.1109/JLT.2021.3096246.

[135] W. -Y. Yang *et al*., “Experimental Investigation on Wideband Optical Frequency Comb Generation Based on a Gain-Switched 1550 nm Multi-Transverse Mode Vertical-Cavity Surface-Emitting Laser Subject to Dual Optical Injection,” in *IEEE Access*, vol. 8, pp. 170203-170210, 2020, doi: 10.1109/ACCESS.2020.3023965.

[136] Y. Li et al., “Optical comb generator with flat-topped spectral response using one electroabsorption-modulated laser and one phase modulator,” *Optical Engineering*, Vol. 59, No. 1, 2020, https://doi.org/10.1117/1.OE.59.1.016112.

[137] P. D. Lakshmijayasimha *et al*., “Tunable mm-wave A-RoF transmission scheme employing an optical frequency comb and dual-stage active demultiplexer,” in *Journal of Lightwave Technology*, doi: 10.1109/JLT.2021.3098949.

[138] P. Shen et al., “High-Purity Millimetre-Wave Photonic Local Oscillator Generation and Delivery”, in *Proceedings of the International Topical Meeting on Microwave Photonics (MWP 2003)*, pp. 189-192, 2003.

[139] A. Rosado, “Experimental study of optical frequency comb generation in gain-switched semiconductor lasers,” Optics & Laser Technology, Vol. 108, pp.542-550, 2018.

[140] J. J. O’Reilly, P. M. Lane, and M. H. Capstick , “Optical Generation and Delivery of Modulated mm-waves for Mobile Communications”, in *Analogue Optical Fibre Communications*, B. Wilson, Z. Ghassemlooy, and I. Darwazeh, ed. (The Institute of Electrical Engineers, London, 1995).

[141] G. Jain *et al*., “Experimental Investigation of External Optical Injection and its Application in Gain-Switched Wavelength Tunable Optical Frequency Comb Generation,” in *Journal of Lightwave Technology*, Vol. 39, No. 18, pp. 5884-5895, 2021, doi: 10.1109/JLT.2021.3091956.

[142] A. Ng'Oma, "Radio-over-fibre technology for broadband wireless communication systems," *Technische Universiteit Eindhoven*, Eindhoven, 2005, DOI: 10.6100/IR592332.

[143] P. M. Anandarajah, S. P. Ó Dúill, R. Zho *et al*, "Enhanced Optical Comb Generation by Gain-Switching a Single-Mode Semiconductor Laser Close to Its Relaxation Oscillation Frequency," in *IEEE Journal of Selected Topics in Quantum Electronics*, Vol. 21, No. 6, pp. 592-600, 2015, Art no. 1801609, doi: 10.1109/JSTQE.2015.2456751.

[144] E. P. Cano *et al*, "Experimental Study of VCSEL-Based Optical Frequency Comb Generators," in *IEEE Photonics Technology Letters*, Vol. 26, No. 21, pp. 2118-2121, 2014, doi: 10.1109/LPT.2014.2348594.

[145] H. Ren, L. Fan, N. Liu *et al*., "Generation of Broadband Optical Frequency Comb Based on a Gain-Switching 1550 nm Vertical-Cavity Surface-Emitting Laser under Optical Injection," *Photonics*, Vol. 7, No. 95, 2020, https://doi.org/10.3390/photonics7040095.

[146] J. O'Reilly and P. Lane, "Remote Delivery of Video Services Using mm-Waves and Optics", *JLT*, Vol. 12, No. 2, pp. 369-375, 1994.

[147] Du, Wenbo *et al*. "Experimental study of SBS suppression with phase-modulation in all-fiber amplifier." *International Symposium on Photoelectronic Detection and Imaging 2011: Laser Sensing and Imaging; and Biological and Medical Applications of Photonics Sensing and Imaging*, Vol. 8192, 2011.

[148] C. K Singh, R. Bhatia, and A. Raghuvanshi, "Generation and transmission of 60-GHz mmWave emitted by VCSEL, DFB–EAM over RoF," *Int. j. inf. tecnol*. Vol. 13, pp. 83-87, 2021, https://doi.org/10.1007/s41870-020-00521-w.

[149] H. Zhang *et al*, "A Novel Radio-Over-Fiber System Based on Carrier Suppressed Frequency Eightfold Millimeter Wave Generation," in *IEEE Photonics Journal*, vol. 9, no. 5, pp. 1-6, 2017, Art no. 7203506, doi: 10.1109/JPHOT.2017.2731620.

[150] X. Foukas, G. Patounas, A. Elmokashfi, and M. K. Marina, "Network Slicing in 5G: Survey and Challenges," in *IEEE Communications Magazine*, Vol. 55, No. 5, pp. 94-100, 2017, doi: 10.1109/MCOM.2017.1600951.

[151] P. Rost *et al*., "Network Slicing to Enable Scalability and Flexibility in 5G Mobile Networks," in *IEEE Communications Magazine*, Vol. 55, No. 5, pp. 72-79, 2017, doi: 10.1109/MCOM.2017.1600920.

]152] S. M. Usha and K. R. Nataraj, "Analysis and mitigation of adjacent and co-channel interference on AWGN channel using 8-PSK modulation for data communication," *2016 International Conference on Wireless Communications, Signal Processing and Networking (WiSPNET)*, pp. 922-926, 2016, doi: 10.1109/WiSPNET.2016.7566268.

[153] Spectrum Policy Task Force, Nov. 2002.

[154] J. Mitola and G. Q. Maguire, "Cognitive radio: Making software radios more personal," *IEEE Pers. Commun*., Vol. 6, No. 4, pp. 13-18, 1999.

[155] S. Haykin, “Cognitive radio: Brain-empowered wireless communications,” *IEEE J. Sel. Areas Commun*., Vol. 23, No. 2, pp. 201-220, 2005.

[156] W. Xu, R. Qiu and J. Cheng, “Fair Optimal Resource Allocation in Cognitive Radio Networks With Co-Channel Interference Mitigation,” in *IEEE Access*, Vol. 6, pp. 37418-37429, 2018, doi: 10.1109/ACCESS.2018.2845460.

[157] V. Chandrasekhar, J. Andrews, and A. Gatherer, “Femtocell Networks: A Survey,” *IEEE Comms. Mag*., Vol. 46, No. 9, pp. 59-67, 2008.

[158] Y. Loong Lee, T. Chee Cuah, J. Loo, and A. Vinel, “Recent advances in Radio Resource Management for Heterogeneous LTE/LTE-A Networks,” *IEEE Comm. Surveys and Tut*., Vol. 16, No. 4, pp. 153-159, 2014.

[159] S. Hung, S. Lien, and K. Chen, “Stochastic Topology Cognition in Heterogeneous Networks,” *IEEE Coop. and Het. Cellular Networks*, pp. 194-199, 2013.

[160] M. Adedoyin and O. Falowo, “Self-organizing radio resource management for next generation heterogeneous wireless networks,” *2016 IEEE International Conference on Communications (ICC)*, pp. 1-6, 2016, doi: 10.1109/ICC.2016.7511561.

[161] P. Gao, D. Chen, M. Feng, D. Qu *et al*., “On the interference avoidance method in two-tier LTE networks with Femtocells,” *IEEE WCNC*, pp. 3538-3590, 2013.

[162] C. Herranz, V. Osa, J. Monserrat *et al*., “Cognitive radio enabling Opportunistic Spectrum Access in LTE-Advanced femtocells,” *IEEE ICC*, pp. 5593-5597, 2012.

[163] W. Chung, C. Chang, and C. Ye, “A Cognitive Priority-based resource management scheme for cognitive Femtocells in LTE systems,” *IEEE ICC*, pp. 6220-6224, Jun. 2013.

[164] G. Carpintero *et al*., “Photonic Integrated Circuits for Terahertz Communication: The Hybrid Integrated Microwave Photonic approach,” *2021 Optical Fiber Communications Conference and Exhibition (OFC)*, pp. 1-2, 2021.

[165] B. Nakarmi, S. Pan, and Y. H. Won, “Simultaneous Generation of Multiband Signals Using External Cavity-Based Fabry–Perot Laser Diode,” in *IEEE Transactions on Microwave Theory and Techniques*, Vol. 66, No. 1, pp. 606-617, 2018, doi: 10.1109/TMTT.2017.2735410.

[166] F. van Dijk *et al*., “Integrated InP heterodyne millimeter wave transmitter,” *IEEE Photon. Technol. Lett*, Vol. 26, No. 10, pp. 965-968, 2014.

[167] X. S. Yao and L. Maleki, “Ultralow phase noise dual-loop optoelectronic oscillator,” in *Optical Fiber Communication Conference and Exhibit*, pp. 353-354, 1998.

[168] Z. Zhang, L. Wu, Y. Zhan *et al*., “Method to improve the signal-to-noise ratio of photon-counting chirped amplitude modulation ladar,” *Appl. Opt*., Vol. 52, pp. 274-279, 2013.

[169] K. Szczerba, P. Westbergh, M. Karlsson *et al*., “60 Gbits error-free 4-PAM operation with 850 nm VCSEL,” *Electronic Lett*. Vol. 49, No. 15, pp. 953-955, 2013.

[170] R. Karembera, T. Yamaguchi, and H. Toda, "Output power enhancement in photonic-based RF generation by optical pulse compression with a dispersion managed highly-nonlinear fiber," in *2018 International Topical Meeting on Microwave Photonics (MWP)*, pp. 1-4, 2018.

[171] E. Hugues-Salas, R. P. Giddings, X. Q. Jin, *et al*., "Real-time experimental demonstration of low-cost VCSEL intensity-modulated 11.25 Gb/s optical OFDM signal transmission over 25 km PON systems," *Opt. Exp*., Vol. 19, No. 4, pp. 2979–2988, 2011.

[172] K. Szczerba, P. Westbergh, J. Karout *et al*., "30 Gbps 4-PAM transmission over 200 m of MMF using an 850 nm VCSEL," *Opt. Express*, Vol. 19, pp. B203-B208, 2011.

[173] R. Rodes, N. Cheng, J. B. Jensen *et al*, "10 Gb/s real-time all-VCSEL low complexity coherent scheme for PONs," *Optical Fiber Communication Conference, Optical Society of America*, pp. 1-3, 2012.

[174] G. Isoe, R. Karembera, and T. Gibbon, "Advanced VCSEL photonics: Multi-level PAM for spectral efficient 5G wireless transport network," *Optics Communications*, 2020, DOI:10.1016/j.optcom.2020.125273.

[175] D. Y. C. Lie, J. C. Mayeda, and J. Lopez, "Highly efficient 5G linear power amplifiers (PA) design challenges," in *2017 International Symposium on VLSI Design, Automation and Test (VLSI-DAT)*, Hsinchu, pp. 1-3, 2017.

[176] J. Pertessis, S. Datta, and Abhay Joshi, "56 Gbaud PAM4 real time optical Datacom link," *Proc. SPIE 11308, Metro and Data Center Optical Networks and Short-Reach Links III, 113080B*, 2020, https://doi.org/10.1117/12.2546767.

[177] Keysight Technologies, "86105C 9 GHz Optical/20 GHz Electrical Sampling Module 750 to 1650 nm-SMF and MMF," Accessed on: September 17, 2020. [Online]. Available: https://www.keysight.com/en/pdx-x202239-pn-86105C/9-ghz-optical-20-ghz-electrical-sampling-module-750-to-1650-nm-smf-and-mmf?cc=CZ&lc=eng&lsrch=true&searchT=86105C.

[178] X. Yu, W. Jin, M. Sui et al., "Evaluation of Forward Error Correction Scheme for Underwater Wireless Optical Communication," *2011 Third International Conference on Communications and Mobile Computing*, pp. 527-530, 2011, doi: 10.1109/CMC.2011.49.

[179] A.R.C.B Serrano, D. C Fernandez, E. P Cano *et al*, "VCSEL-Based Optical Frequency Combs: Toward Efficient Single-Device Comb Generation," *IEEE Photonics Technology Letters*, Vol. 25, No. 20, 2013.

[180] A. Quirce, C. de Dios, A. Valle *et al*, "VCSEL-Based Optical Frequency Combs Expansion Induced by Polarized Optical Injection," *presented at the 2019 21st International Conference on Transparent Optical Networks (ICTON),* Angers, France, pp. 1-4.

[181] Kimmitt et al. "Control of an Optical Modulator for Desired Basing of Data and Pulse Modulators," U.S. patent 7,394,992 B2, 2008.

[182] G. K. M. Hasanuzzaman, H. Shams, C. C. Renaud *et al*., "Tunable THz Signal Generation and Radio-Over-Fiber Link Based on an Optoelectronic Oscillator-Driven Optical Frequency Comb," in *Journal of Lightwave Technology*, Vol. 38, No. 19, pp. 5240-5247, 2020, doi: 10.1109/JLT.2019.2953070.

[183] L. Maleki, A. B. Matsko, A. Savchenkov *et al*., "Low-noise RF oscillation and optical comb generation based on nonlinear optical resonator," U.S. patent 1,117,22 B1, 2009.

[184] C. Chenab, C. Zhangac, We. Zhanga *et al*., "Scalable and reconfigurable generation of flat optical comb for WDM-based next-generation broadband optical access networks", *Optics Communication*, Vol. 321, 2014.

[185] P. Shen, N. J. Gomes, P. A. Davies et al., "Generation of 2 THz Span Optical Comb in a Tunable Fiber Ring Based Optical Frequency Comb Generator," presented *at the 2007 International Topical Meeting on Microwave Photonics*, Victoria, BC, pp. 46-49, 2007.

[186] X. Pang, M. Beltrán, J. Sánchez *et al*., "Centralized Optical-Frequency-Comb-Based RF Carrier Generator for DWDM Fiber-Wireless Access Systems," *J. Opt. Commun. Netw*. Vol. 6, pp. 1-7, 2014.

[187] Yu Xiang, N. Jiang, C. Chen *et al*., "Wired/wireless access integrated RoF-PON with scalable generation of multi-frequency MMWs enabled by tunable optical frequency comb," *Opt. Express*, Vol. 21, pp. 19762-19767, 2013.

[188] R. Siebrits *et al*., "Dissemination of Reference Signals for a Next Generation Radio Telescope," *2018 IEEE International Frequency Control Symposium (IFCS)*, pp. 1-6, 2018, doi: 10.1109/FCS.2018.8597492.

[189] Antennas-Amplifiers, "50 - 51 MHz Low Loss Receiving Band-pass Filter. 6 Meter band.," https://www.antennas-amplifiers.com/6-meter-bandpass-filter-50mhz-bpf.

[190] P. P. Iannone, K. C. Reichmann, and N. J. Frigo, "High-speed point-to-point and multiple broadcast services delivered over a WDM passive optical network," in *IEEE Photonics Technology Letters*, Vol. 10, No. 9, pp. 1328-1330, 1998, doi: 10.1109/68.705632.

[191] K. Nfanyana, S. Wassin, R. Karembera *et al*, "All-photonic 20-MHz clock for latency monitoring in a 5G network at 10 Gbps over optical fiber," *J. Opt. Soc. Am. B* Vol. 37, pp. A202-A206, 2020.

[192] T. Peng, Y. Wang, A. G. Burr et al., "Physical Layer Network Coding in Network MIMO: A New Design for 5G and Beyond," in *IEEE Transactions on Communications*, Vol. 67, No. 3, pp. 2024-2035, 2019, doi: 10.1109/TCOMM.2018.2886184.

[193] C. Browning et al., "Converged wired and wireless services in next generation optical access networks," *2017 19th International Conference on Transparent Optical Networks (ICTON)*, pp. 1-3, 2017, doi: 10.1109/ICTON.2017.8025032.

[194] G. M. Isoe, S. Wassin, and T. B. Gibbon, “VCSEL wavelength reuse for intrinsically bidirectional data traffics in next generation GPONs,” *Optoelectronics Letters*, Vol. 15 No.5, 2019.

[195] S. Wassin, G. M. Isoe, A. W. R. Leitch *et al*, “All-optical wavelength reservation for flexible spectrum networks using amplifier saturation and VCSEL injection,” *Opt. Eng*. Vol. 58, No. 4, 2019, doi: 10.1117/1.OE.58.4.046110.

[196] A. Singh and K. Singh, “Demonstration of a Bidirectional WDM-PON with 10 Gb/s Downstream DQPSK and 5 Gb/s Upstream Re-modulated OOK Data Based on Reflective Semiconductor Optical Amplifier,” *IJISET - International Journal of Innovative Science, Engineering & Technology*, Vol. 1, No. 4, 2014.

[197] Z. Jia, J. Yu, G. Ellinas *at al.*, “Key Enabling Technologies for Optical–Wireless Networks: Optical Millimeter-Wave Generation, Wavelength Reuse, and Architecture,” *J. Lightwave Technol*. Vol. 25, pp. 3452-3471, 2007.

[198] Y. Gao, X. Chen, G. Chen *et al.*, “1 × 25 LCOS-based wavelength selective switch with flexible passbands and channel selection,” *Optical Fiber Technology*, Vol. 45, Pages 29-34, 2018, https://doi.org/10.1016/j.yofte.2018.05.008.

[199] F. Fuochi, M. U. Hadi, J. Nanni *et al.*, “Digital predistortion technique for the compensation of nonlinear effects in radio over fiber links,” *2016 IEEE 2nd International Forum on Research and Technologies for Society and Industry Leveraging a better tomorrow (RTSI)*, pp. 1-6, 2016, doi: 10.1109/RTSI.2016.7740562.

[200] M. Fuentes et al., ”5G New Radio Evaluation Against IMT-2020 Key Performance Indicators,” in *IEEE Access*, Vol. 8, pp. 110880-110896, 2020, doi: 10.1109/ACCESS.2020.3001641.

[201] H. Soda, H. Ishikawa and H. Imai, “Design of DFB lasers for high-power single-mode operation,” *Electronics Letters*, Vol. 22, No. 20, 1986.

[202] X. Pang, A. Lebedev, J. J. V. Olmos *et al.*, “Performance evaluation for DFB and VCSEL-based 60 GHz radio-over-fiber system,” presented *at the 17th International Conference on Optical Networking Design and Modeling (ONDM)*, Brest, 2013.

[203] K. K. Lee and H. F. Taylor, “Comparison of fiber Fabry-Perot interferometer sensor using 850nm VCSEL vs 1300nm DFB laser as light source,” *Proc. SPIE 6351*, 635125, 2006.

[204] P. Hall, R. Schillizzi, P. Dewdney *et al.*, “The square kilometer array (SKA) radio telescope: Progress and technical directions,” *International Union of Radio Science URSI*, Vol. 236, pp.4-19, 2008.

[205] G. Ancansa, V. Bobrovsa, A. Ancans et al., “Spectrum Considerations for 5G Mobile Communication Systems,” Procedia Computer Science, Vol. 104, pp. 509-516, 2017.